Modelling, optimization, and control for hydrogen refuelling stations

Shang, Xinxin; Wang, Yunli; Shi, Yang; Zhang, Lincheng; Decès-Petit, Cyrille

Modelling, Optimization, and Control

for Hydrogen Refuelling Stations

Non-sensitive

Volume 1
Report No 56888
June 27 2025

Xinxin Shang, Yunli Wang, Yang Shi, Lincheng Zhang, and Cyrille Decès-Petit

National Research Council Canada
Conseil national de recherches Canada
Canada

PDF: catalogue number NRC-CEI-56888

Table of contents

List of Figures

List of Tables

Acronyms

FCEVs	Hydrogen Fuel Cell Electric Vehicles
HRSs	Hydrogen Refuelling Stations
SAE	Society of Automotive Engineers
HRSC	Hydrogen Refuelling Station Controller
MINLP	Mixed Integer Nonlinear Programming
MPC	Model Predictive Control
LB	Low Pressure Buffer/Large Buffer
MB	Medium Pressure Buffer/ Medium Buffer
HB	High Pressure Buffer
SB	Small Buffer

Introduction

This section presents the background and significance of this project. Then, the key challenges and difficulties are analyzed. Finally, the objectives of this project are outlined.

Project Background

Global efforts to combat climate change have underscored the urgent need for reducing carbon emissions, with transportation being one of the largest contributors to greenhouse gas emissions. Transitioning to sustainable energy is essential to reducing carbon emissions. Hydrogen, as one of the key sustainable energies, has emerged as a promising solution to decarbonize the transportation sector.

Hydrogen stands out due to its high energy density and ability to produce zero-emission energy through fuel cell technology. These characteristics have driven significant advancements in hydrogen-powered mobility, with Fuel Cell Electric Vehicles (FCEVs) emerging as a leading application. As FCEVs gain traction globally, the development of Hydrogen Refuelling Stations (HRSs) has become critical. Consequently, Canada, along with many other countries, is actively developing HRSs to ensure efficient and reliable hydrogen supply.

Overview of Hydrogen Refuelling Stations

An HRS consists of power cubes (low pressure storage), a compressor, cascade high pressure buffers, a precooler, and a dispenser. The schematic diagram of the HRS with components and their connections is shown in Figure 1.1.

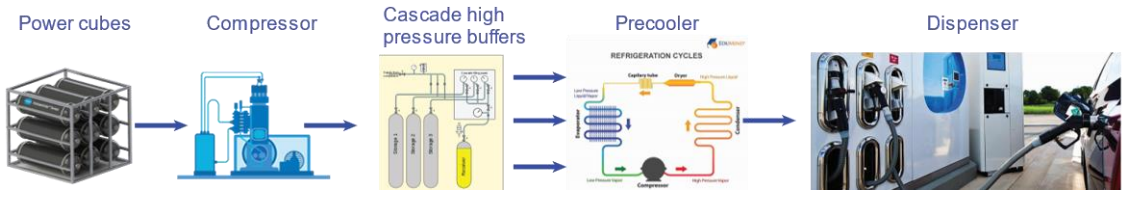

Figure 1.1 Schematic diagram of the HRS: Components and their connections.

(1) Power cubes

Power cubes are used to store hydrogen produced by electrolysers. Commonly, they are designed to be modular and scalable. This design allows for flexible installation and expansion of HRSs to meet increasing demand.

(2) Compressor

A compressor is responsible for compressing the low-pressure hydrogen from the power cubes into high pressure hydrogen. Hydrogen is compressed to be at the required pressure for fast and efficient refuelling for vehicles.

(3) Cascade high pressure buffers

Cascade high pressure buffers, also known as high pressure storage tanks, are used to store hydrogen at high pressures. These buffers store hydrogen at different pressure levels, which can deliver hydrogen at various flow rates. By coordinating the hydrogen from different buffers, HRSs ensure a stable and consistent supply during the hydrogenation process to meet different needs while maintaining the pressure required for efficient operation.

(4) Precooler

A precooler is used to decrease the temperature of hydrogen before it is dispensed into vehicles. It is necessary because the rapid compression and expansion of hydrogen lead to significant temperature increases due to the Joule-Thomson effect and adiabatic compression [1], potentially causing safety concerns and reducing the refuelling efficiency.

(5) Dispenser

The dispenser is the interface between HRSs and FCEVs. It is responsible for transferring hydrogen from cascade high pressure buffers to the vehicle's onboard storage tank. The dispenser typically includes a nozzle, pressure sensors, flow meters, and safety shutoff valves to ensure that hydrogen is dispensed accurately, efficiently, and safely. It is designed to handle the high-pressure hydrogen and ensure that the refuelling process is completed quickly, usually within a few minutes, to provide the vehicle with sufficient fuel for extended travel.

HRSs achieve efficient and safe hydrogen refuelling by coordinating five key components. Hydrogen is initially stored in modular power cubes, providing flexible storage capacity. The compressor increases the pressure of low to medium pressure hydrogen to high levels, meeting the refuelling pressure requirements of vehicles. Subsequently, the hydrogen is stored in cascade high pressure buffers at different pressure levels to balance supply-demand fluctuations and ensure flow stability. To prevent temperature rise caused by the rapid compression of gas during refuelling, the precooler cools the hydrogen to an appropriate range. Finally, the hydrogen is dispensed to FCEVs through the dispenser at precise flow rates, completing the refuelling process. It is important to note that the flow rate of hydrogen

through the dispenser is affected by cascade high pressure buffers at different pressure levels. Therefore, the control of cascade high pressure buffers is crucial for the entire refuelling process.

Challenges in HRSs

Despite the eco-friendly benefits of hydrogen, the widespread adoption of HRSs must meet the requirements of safety, economy, and efficiency.

To enhance the safety of hydrogen refuelling, the Society of Automotive Engineers (SAE) fuel cell standards committee interface working group collaborated with experts from gas companies, fuel suppliers, and the automotive industry to develop the SAE J2601 Standard [2]. All HRSs mentioned in this report follow this protocol. The SAE J2601 protocol specifies the hydrogen fuelling protocols and process limitations for FCEVs, including restrictions on fuel delivery temperature, maximum fuel flow rate, pressure ramp rate, and termination pressure. These limitations are influenced by factors such as ambient temperature, fuel delivery temperature, and the initial pressure in the vehicle's compressed hydrogen storage system. To comply with these limitations, HRSs typically need to control the flow rate of hydrogen dispensed into the vehicles.

To compete with traditional fossil fuel-powered vehicles, the price of hydrogen for FCEVs needs to be reduced to below $7 per kilogram at HRSs. For a standard gaseous hydrogen station operating at a $70\ MPa$ pressure level and with a daily refuelling volume of $250\ kg$, the estimated levelized cost already exceeds $3 per kilogram; adding the costs of hydrogen production and transportation, achieving a price below $7 becomes a significant challenge. Figure 1.2 illustrates the operational energy demand of two types of HRSs. The operational costs of gaseous hydrogen HRSs are significantly lower than those of liquid hydrogen HRSs. Moreover, in the case of gaseous hydrogen, the distribution, and dispensing costs account for a substantial portion of energy consumption.

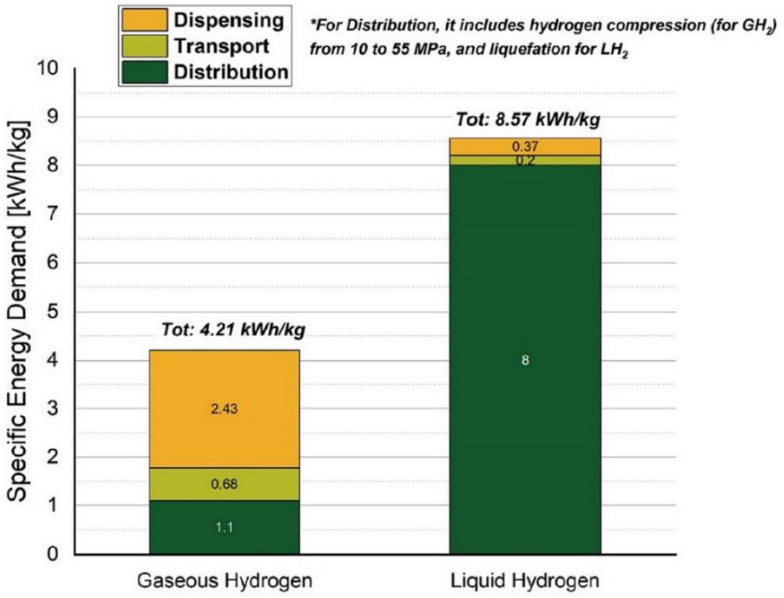

Figure 1.1 Energy demand for gaseous hydrogen and liquid hydrogen, from production to dispensing [3].

As the number of HRS users increases, hydrogen refuelling efficiency becomes a key factor affecting the user experience. Hydrogen refuelling efficiency means the speed and efficiency with which hydrogen is dispensed into a vehicle. Inefficiency leads to long waiting times, which not only wastes users' time but also leads to congestion at gas stations, which in turn affects the quality of service.

Additionally, the refuelling time of FCEVs is highly uncertain, with demand potentially concentrated at specific times or spread out. This results in a distinctly dynamic characteristic of the hydrogen demand for HRSs. When the demand is high, such as multiple FCEVs arriving at the refuelling station simultaneously, it is essential to manage the hydrogen flow efficiently to reduce waiting time and ensure that the refuelling process is completed as quickly as possible. In contrast, during low-demand periods, HRSs need to ensure a steady hydrogen supply while minimizing operational costs.

In summary, the primary challenge faced by HRSs is optimizing hydrogen flow based on fluctuating demands to ensure efficient and cost-effective refuelling for FCEVs.

Project Objectives

To address this challenge, advanced modelling and optimization technologies are crucial. Modelling techniques simulate the dynamic changes of the various components and key variables involved in the hydrogen refuelling process. Optimization techniques calculate the

hydrogen flow required to meet fluctuating demands. The two work together: modelling provides the necessary data and context for the optimization process, while optimization generates specific operational strategies and adjustment plans based on the modelling results. This collaboration improves refuelling efficiency and reduces costs, ensuring that the hydrogen refuelling needs of FCEVs are met efficiently. Based on a comprehensive literature review and analysis, there exist some technical difficulties in modelling and optimization.

Based on a comprehensive literature review and analysis, there exist some technical difficulties for modelling and optimization.

- When designing the simulators for HRSs, mathematical models of some components might be inaccurate due to the inherent difficulty in establishing good models of components of the HRSs. In addition, to characterize and simulate practical features of real HRSs and the control performance, it is desirable to model the nonlinearity, uncertainties, parameters drifting or variations, and unmodelled dynamics in the simulator. This is quite essential yet particularly challenging in simulator development.

- Due to the complex and dynamically changing requirements of HRSs, it is necessary to use simulators to predict the results of different control methods and evaluate their performance. This requires the simulator to be adapted to different control methods.

- The existing control methods are based on logic control. This control method typically relies on preset rules and conditions for decision-making. When the system faces complex or dynamic changes, logic control may not be able to adjust its strategy in time, resulting in poor adaptability.

This project aims to develop innovative modelling and optimization techniques for HRSs to enhance their efficiency, reduce operational costs, and support the transition to a sustainable hydrogen-based transportation system. To achieve this goal, the main objectives are listed in the following.

- To build a customized simulator that can imitate the dynamic state changing of HRSs. Meanwhile, this customized simulator can conveniently implement novel control methods.

- To test the adaptability of the developed simulator, it is tested by existing representative logic controllers.

- To propose and design an optimal controller that can optimize energy consumption.

Summary

This section begins by emphasizing the importance of HRSs in supporting the transition to hydrogen-powered transportation. It then describes the key components of HRSs and their operational mechanisms. The challenges faced by HRSs are highlighted, including fluctuating demand, safety concerns, and cost issues under dynamic demand conditions. Next, the need for advanced modelling and optimization techniques is discussed to improve refuelling efficiency, reduce costs, and ensure the sustainable operation of HRSs. Finally, the project aims are presented, including the development of a customized simulator, the evaluation of control methods, and the design of an optimal controller. Through these efforts, the project promotes the widespread adoption of hydrogen as a sustainable and clean energy source while reducing carbon emissions.

The Design of HRS Simulators

This section provides a brief introduction to two existing HRS simulators. The development and features of the proposed Hydrogen Refuelling Station Controller (HRSC) simulator are then presented. Finally, the simulation results are presented to demonstrate the effectiveness and reliability of the HRSC simulator.

Overview of HRS Simulators

The design and operation of HRSs can benefit from simulators, which allow for the testing and optimization of various components and processes before implementation. HRS simulators simulate the entire replenishing and refuelling processes, from power cubes to vehicle dispensing, enabling engineers to evaluate system performance and ensure efficiency and safety. An HRS simulator typically includes various components, such as compressors, buffers, and dispensers.

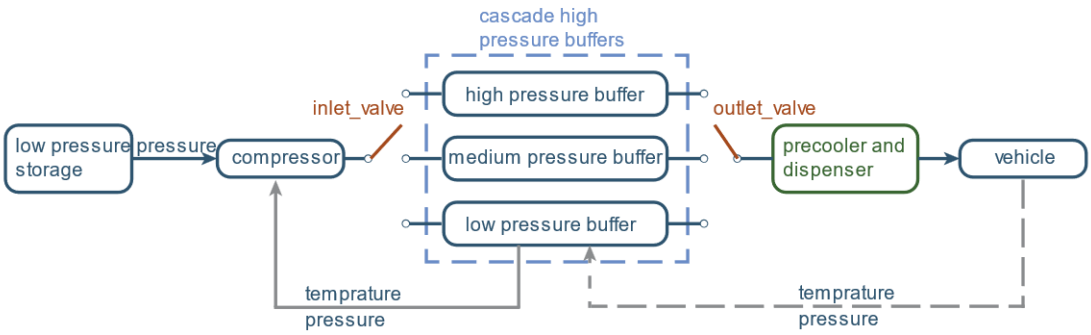

Figure 2.1 HRS simulator structure.

The HRS simulator structure considered in this project is shown in Figure 2.1. Hydrogen is delivered from low pressure storage (power cubes) to the compressor. The compressor delivers hydrogen to one of the cascade buffers, either low, medium, or high pressure, depending on the actual requirements. Once stored in the appropriate buffer, hydrogen flows through the outlet valve to the precooler and dispenser. At the final stage, the dispenser fuels a vehicle.

Throughout the process, the pressure of the HRS is continuously monitored at all stages, while the temperature is measured specifically in the buffers and the vehicles. The continuous monitoring supports effective system control. The states to be monitored and controlled in the

HRS simulator include: 1) The pressure of each buffer and the vehicles, 2) the delivery flow rate of each component, and 3) the temperature of hydrogen in the buffers and vehicles.

The gray solid line in Figure 2.1 represents the feedback loop between the buffers and the compressor, enabling the measured pressure and temperature data to be sent to the compressor for regulating buffer replenishment. The compressor plays a critical role in this process, replenishing the buffers whenever their pressure approaches the lower limit to maintain uninterrupted refuelling. Notably, the compressor is a significant energy consumer, accounting for over 50% of the total energy consumption in the HRS. Then, the dispensing process can occur with or without communication between the vehicle and the HRS. If there is no direct communication, as indicated by the gray dashed line in Figure 2.1, the pressure and temperature of the vehicle are only monitored at the beginning of dispensing.

Finally, a controller uses the pressure and temperature data, along with the states of the inlet and outlet valves, to dynamically decide when and how to switch between three buffers, ensuring efficient hydrogen flow and safe operation. Considering three buffers located between the compressor and dispenser, the inlet and outlet valves of buffers can be designed as two three-way switches, as indicated by the red valves in Figure 2.1.

In summary, the HRS simulator provides a comprehensive platform for analyzing and optimizing the replenishing and refuelling processes by incorporating key components such as compressors, buffers, and dispensers. Through continuous monitoring and control of pressure, temperature, and flow rates, the simulator enables efficient system operation and enhances safety. The integration of dynamic control strategies, including buffer switching and energy management, ensures the reliable and energy-saving operation of HRSs.

Preliminaries of HRS simulators

This project considers several preliminaries and assumptions for all HRS controllers. They are listed below for a clearer understanding.

1. **Environmental temperature is a constant value $25°C$.**

   This assumption is made for simplification, as this project does not focus on the impact of environmental factors on energy usage. This topic can be further explored in future research.
2. **The hydrogen considered in this project is assumed to be the ideal gas.**

   This assumption is made for simplification, as the project does not focus on the thermal and pressure behavior of hydrogen. A more precise representation is possible but would significantly increase computational costs.

3. **The maximum flow rate of the dispenser is $60\ g/s$** [4]**.**

   Section 6.4.2 of [4] proposes that the design of the fuelling protocols should not exceed a maximum $60\ g/s$.
4. **The threshold of the pressure difference between buffers and vehicles during refuelling process should be greater than $100\ bars$.**

   This value is used to ensure a sufficient pressure differential exists between the buffers and the vehicle to ensure a speedy refuelling process according to SAE J2601 fueling protocol.
5. **The maximum temperature of hydrogen in vehicles and buffers is set to $80°C$ to follow safety restrictions.**

   In [4], the temperature of the hydrogen in the storage tank must be less than $85°C$. For safety reasons, in this project, this constraint is set into $80°C$ to comply with the safety restriction.
6. **Only one of the inlet valves and one of the outlet valves can be opened at the same time; for one buffer, its inlet and outlet valves cannot be opened together.**

   This assumption is based on the realistic conditions of HRSs.
7. **The initial and maximum pressure of the unrefueled vehicles are $100\ bars$ and $700\ bars$, respectively.**

   The three types of hydrogen vehicles considered in this project follow this protocol.
8. **The inlet valve threshold of buffers is set to $800\ bars$.**

   The inlet valve is designed to open only when the buffer pressure falls below 800 bars. This threshold prevents short and frequent refuels that would occur if the valve responded to minor pressure deviations. Based on this design, it is expected the system would reduce the valves' wear and minimize the compressor energy consumption by reducing the compressor's duty cycle.

Existing HRS Simulators

In the following, two representative simulators are briefly introduced. The first one is the general HRS simulator, and the second one is the Hydrogen Filling Simulation (H2FillS). Both are developed in Simulink.

General HRS Simulator

The general HRS simulator models the operation of an HRS based on the SAE refuelling protocol SAE J2601 [4]. The general HRS simulator in Simulink is depicted in Figure 2.2. It simulates a three-stage, intercooled compressor that fuels high ($950\ bar$), medium ($650\ bar$),

and low ($450\ bar$) pressure buffers (cascade structure) from low pressure storage (power cubes). It is desirable to optimize energy usage by dispensing hydrogen from the buffer with the lowest pressure exceeding the vehicle's pressure. The priority of valves manages the switch between buffers, while a reduction valve and precooler ensure that hydrogen is cooled to $-40\ °C$ and safely delivered to vehicles at up to $700\ bar$. It is of paramount importance to prevent excessive temperature increases [5].

In this simulator, a logic control strategy is implemented, as shown in Figure 2.3. This simulator is developed based on the toolbox Stateflow [6]. This toolbox is designed for modelling and simulating complex systems through state machines and flow charts, supporting conditional logic, time-driven behaviors, and event-driven operations.

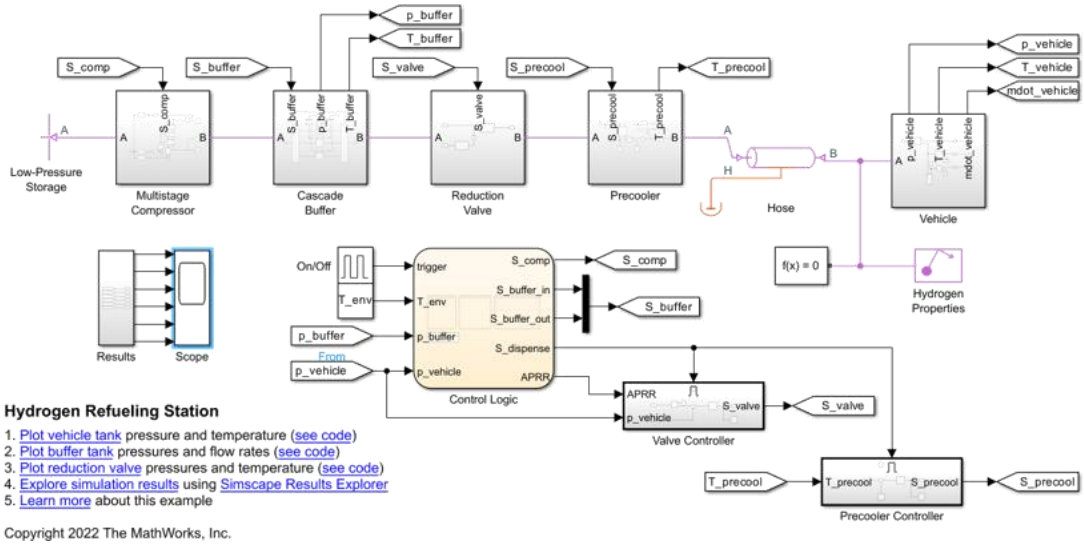

Figure 2.1 General HRS simulator in Simulink.

The control logic illustrated in Figure 2.3 has been widely adopted for the HRS. The red circles indicate the control decision following a deterministic prior order. In general, the replenishment of buffers obeys the priority High → Medium → Low pressure, while the refuelling of buffers followed by the priority Low → Medium →High pressure. Meanwhile, switches among high, medium, and low-pressure buffers are decided by different thresholds (green rectangles). The pressure difference between the vehicle and the buffers determines whether a buffer can refuel the vehicle. Also, for each buffer, there is a pressure threshold for it to be replenished by the compressor.

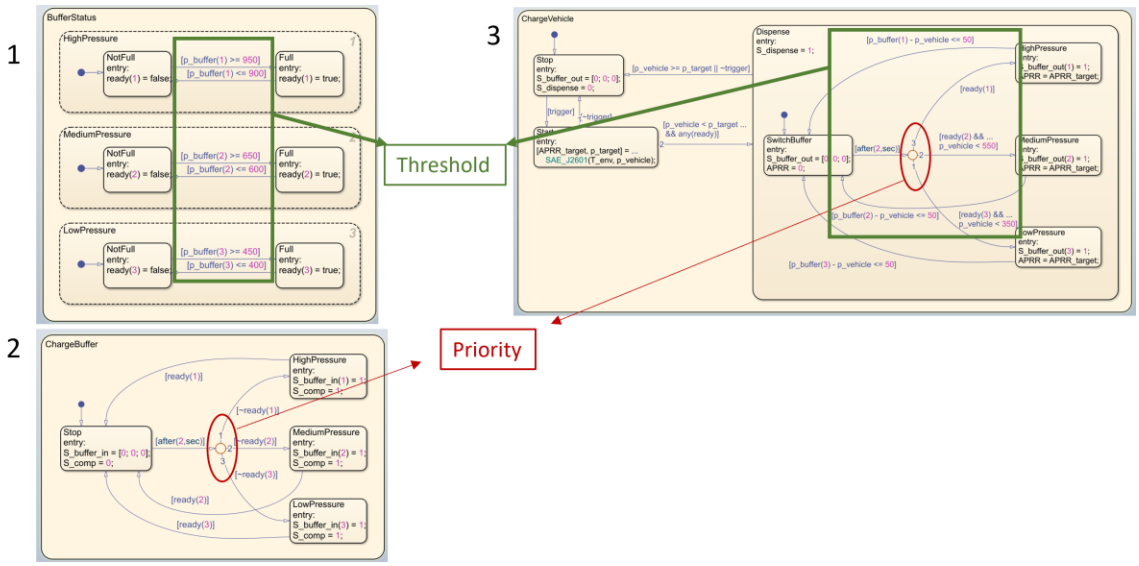

Figure 2.2 Logic control of the general HRS simulator.

The simulation results by running the general HRS simulator are shown in Figure 2.4. All buffers start from the pressure $200\ bar$ and are replenished by the compressor one by one. Then, one vehicle arrives at the HRS and starts to be refueled. The pressure change of buffers during the refuelling process are shown in Figure 2.4(a) and can be well approximated by linear functions. However, the temperature change is highly nonlinear. Hence, it is not easy to find a linear function to model it.

In 2.4(a) and (b), it is interesting to look into the different parts of the curves: (1) The increasing parts of the curves represent that three buffers are replenished from $200\ bar$ to the full level, at corresponding time instants (e.g., around $800\ s$, $1300\ s$, $1600\ s$, respectively); (2) during the refuelling process in Figure 2.4(a), a sudden yet little drop of the magnitude on the flat curve means that a vehicle is refueled at about $2500\ s$; (3) the decreasing parts of the curves from $2450\ s$ to $2650\ s$ in temperature plot show that the buffers are being used for vehicle refuelling in Figure 2.4(b); (4) in 2.4(c) and (d), the sharp increase of both pressure and temperature occurs when the vehicle is being refueled.

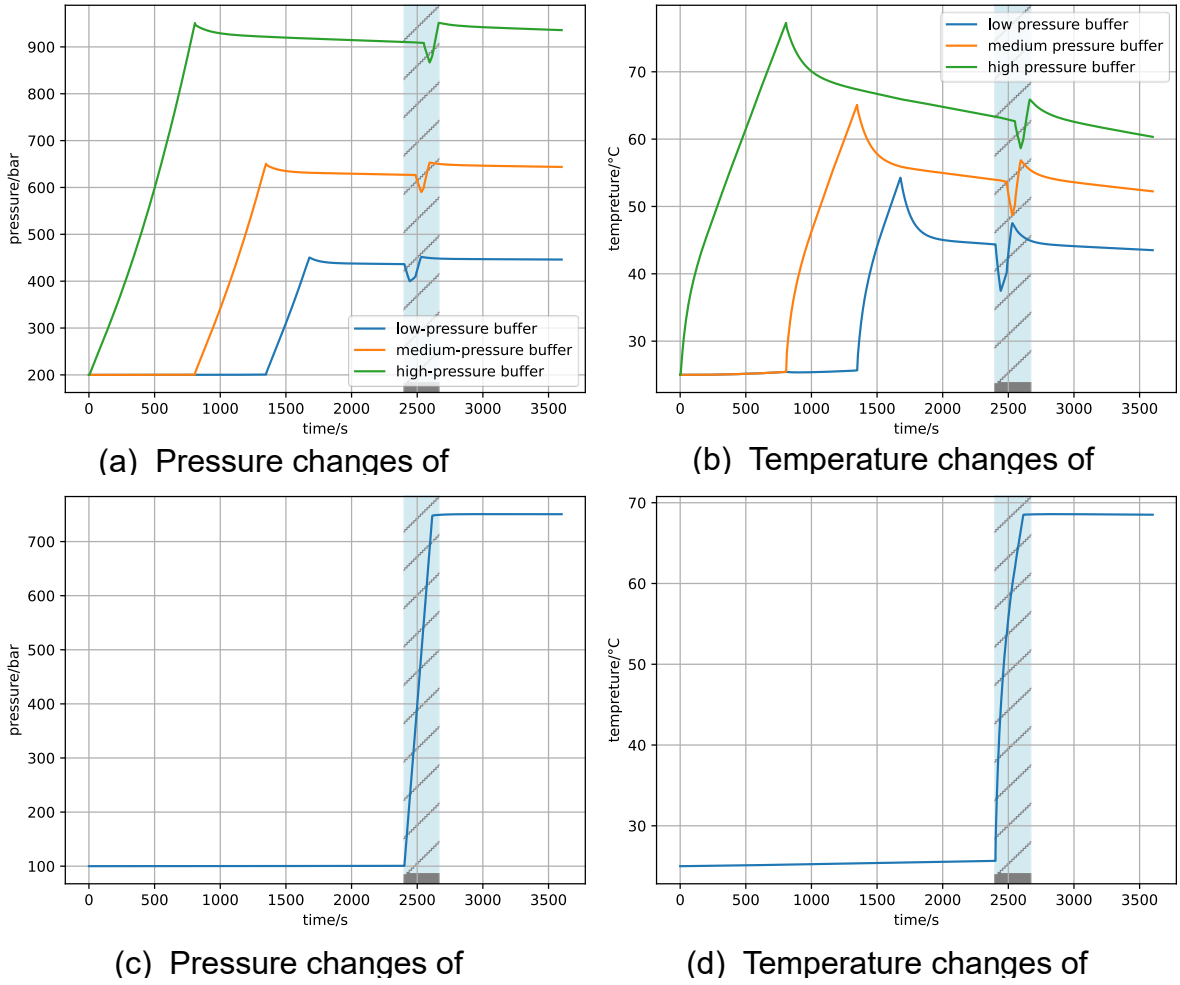

(a) Pressure changes of (b) Temperature changes of

(c) Pressure changes of (d) Temperature changes of

Figure 2.3 Simulation results of the general HRS

Hydrogen Fuelling Simulation

Another commercial simulator is the H2FillS. The H2FillS serves as a thermodynamic model that captures and reports the transient variations in temperature, pressure, and flow rate of hydrogen during the process of refuelling vehicles. Figure 2.5 shows an example of the H2FillS which is presented in [7].

This simulator models the hydrogen gas flow from the HRSs to the vehicles, employing empirical data sets from actual refuelling events. It has been rigorously validated across a spectrum of refuelling conditions to reflect the typical refuelling profiles of light-duty FCEVs accurately. H2FillS offers substantial advantages to the market for light-duty vehicle refuelling by bridging the knowledge gaps regarding the dynamics between the HRS and an FCEV [7].

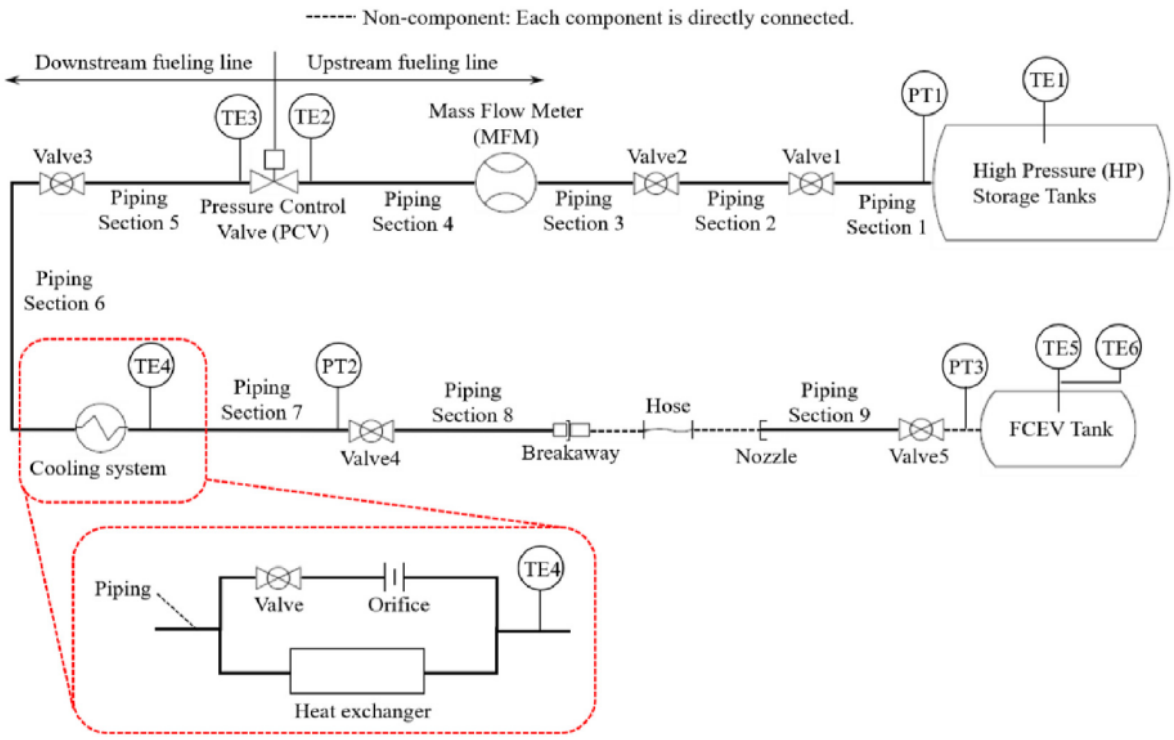

Figure 2.4 Schematic diagram example of H2Fills [10].

There are several advantages of this simulator including the flexibility of parameter modification for each component and user-friendliness due to the clear structure of the simulated refuelling process. However, this simulator is designed to research the thermodynamic changes in the HRS but does not have the inlet/outlet valves for the control strategy. It reveals the processes of the system but does not elaborate on the control of the compressors and the dispenser in the HRS simulator. As a result, this simulator cannot be utilized in our project.

HRSC Simulator

The above simulators embedded in Simulink cannot be directly used in this project because their embedded design prevents us from accessing, modifying, or distributing them. Additionally, MATLAB, as a proprietary platform, has licensing requirements and associated costs that can pose significant barriers, especially for individual researchers. As a result, these simulators cannot be used to simulate the control process of the HRS in this project, making it urgent to develop an independent simulator to ensure the feasibility for this project. Therefore, an HRSC simulator using Python is developed to provide an effective simulation platform for the validation of the HRS control process.

The structure of the designed HRSC simulator is shown in Figure 2.6. The simulator consists of four modules. Module 1 processes data offline to get the vehicle arrival patterns, the system model of HRS, and its control logic. The other three modules are used online. Module 2 and Module 3 simulate two classes of hardware: Cascade high pressure buffers and vehicles. Module 4 is the system controller that needs to be designed and tested in this project.

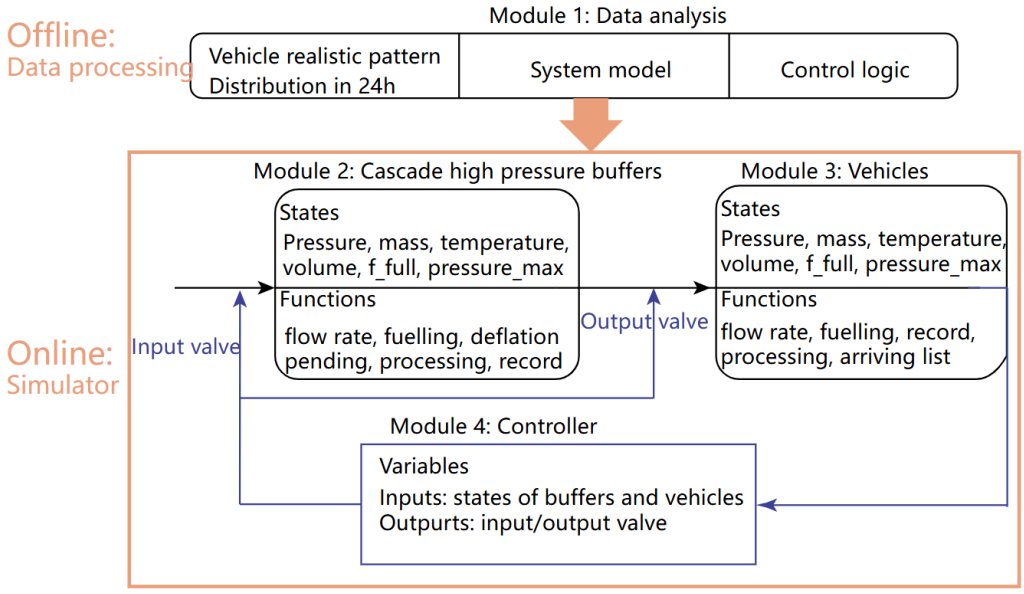

Figure 2.1 Structure of the designed HRSC simulator.

(1) Module 1: Data analysis

This module is an isolated module from the simulator. It is an offline module that helps build the system model and recognize the pattern of vehicle arriving. With the data from four HRSs, valuable information can be extracted to verify the system model and control logic. At the same time, the pattern of vehicle arriving can show the conditions that the HRS has faced over the past years.

(2) Module 2: Cascade high pressure buffers

This module represents the class of three buffers. It contains all the properties of the buffers, including pressure, mass of hydrogen, temperature, volume, state of full or not, and the maximum pressure of the buffer. It also consists of the functions for the buffers to simulate the replenishing and refuelling processes. The function "*flow rate*" is designed to describe the relationship between the pressure and the flow rate of the valve. Three functions, "*refuelling*," "*deflation*," and "*dispending*," describe the evolution of the buffer states. The functions "*processing*" and "*record*" are used to simulate the state transition and record the buffer states.

In the general HRS simulator, the difference between different buffers is that the pressure is different, but their volume is the same, so "*high*, *medium*, *and low-pressure buffers*" are used to name them. However, in the HRSC simulator, the difference between different buffers lies in their volumes, with the same pressures. "*Large, medium*, *and small buffers*" are used to name them.

(3) Module 3: Vehicles

This module describes the class of a sequence of vehicles to be refueled. Similar to Module 2, this module includes all the properties of vehicles. It also includes several similar functions to simulate the refuelling process. One special function, "*arriving list*," is designed to generate a list of the time of coming vehicles in a simulation period.

(4) Module 4: Controller

The control inputs are system states, including pressure, temperature, and the history of inlet/outlet valves. Then, the control inputs for the buffers and vehicles (inlet/outlet valves) are generated based on the control methods.

Validation Results of HRSC Simulator

To evaluate the performance and accuracy of the HRSC simulator, simulations are conducted with a single vehicle being refueled at the HRS. The goal of these simulations is to verify whether the HRSC simulator can accurately replicate the dynamics of a real system. In the HRSs considered in this project, the pressure hydrogen in the power cubes is $450\ bar$ [8]. This pressure level is insufficient for refuelling a vehicle, as the required fuelling pressure is $700\ bar$ [9]. Therefore, the pressure of hydrogen is increased to $875\ bar$ through compression, after which it is stored in cascade high-pressure buffers.

The simulation adopts the similar initial condition used in the general HRS simulator shown in Figure 2.4. The buffer setup (with all three buffers at $875\ bar$ but with different volumes) corresponds to the actual configuration of four HRSs. Although this setup slightly differs from that of a typical HRS, the real data on the states (e.g., buffer pressures and running time) provide valuable insights into the actual conditions of a real-world HRS. As a result, all simulations and controller designs are based on this setup.

In this simulation, a specific case is considered where all three buffers share the same maximum pressure of $875\ bar$, but their volumes are in a ratio of $1{:}\ 2{:}\ 3$ with varying numbers of hydrogen cylinders. When applying controllers, the buffers in this case are mapped one-to-one to those in general configurations, as shown in Table 2.1. All simulations start with the initial condition where the buffers are at $100\ bar$, and their temperatures match the ambient temperature.

Table 0.1 HRSC setup in the simulation compared with the general HRS simulator.

	Name of cascade high pressure hydrogen buffers		
General HRS Simulator	Low Pressure Buffer (LB)	Medium Pressure Buffer (MB)	High Pressure Buffer (HB)
	$450\ bar$	$650\ bar$	$875\ bar$
Simulation scenario	Large Buffer (LB)	Medium Buffer (MB)	Small Buffer (SB)
	$875\ bar$ (3 cylinders)	$875\ bar$ (2 cylinders)	$875\ bar$ (1 cylinder)

The simulation results of a single vehicle refuelling process using the HRSC simulator are shown in Figure 2.7. It is observed that the buffers are replenished first. When a vehicle arrives, the buffers refuel the vehicle following the same control sequence illustrated in Figure 2.3. The results demonstrate that the effect of HRSC simulator aligns closely with those of the Simulink simulator under similar initial conditions.

By comparing the pressure and temperature variations of the buffers from the Simulink simulator (Figures 2.2 and 2.4) and HRSC simulator (Figure 2.7), the overall results are found to be comparable. Although some nonlinear aspects, particularly nonlinear temperature variations evident in Figure 2.4(b) are not fully reflected in the HRSC results (Figure 2.7(b)), the overall performance of the HRSC simulator is acceptable. These findings confirm its utility as a viable tool for the development and refinement of HRS controllers.

Several differences are evident between the two simulation results, which can be explained as follows:

1. The pressurization rate in HRSC decreases as the buffer refuels (Figure 2.7(a)), contrasting with the trend in Figure 2.4(a). This difference may stem from the HRSC simulator's assumption of hydrogen as an ideal gas. Since the internal model in the Simulink simulator is not fully transparent, the exact cause of the slope reduction remains uncertain. However, the observed slope variations are minimal, indicating a linear relationship. Thus, this discrepancy has a negligible impact on the validity of the simulation results.

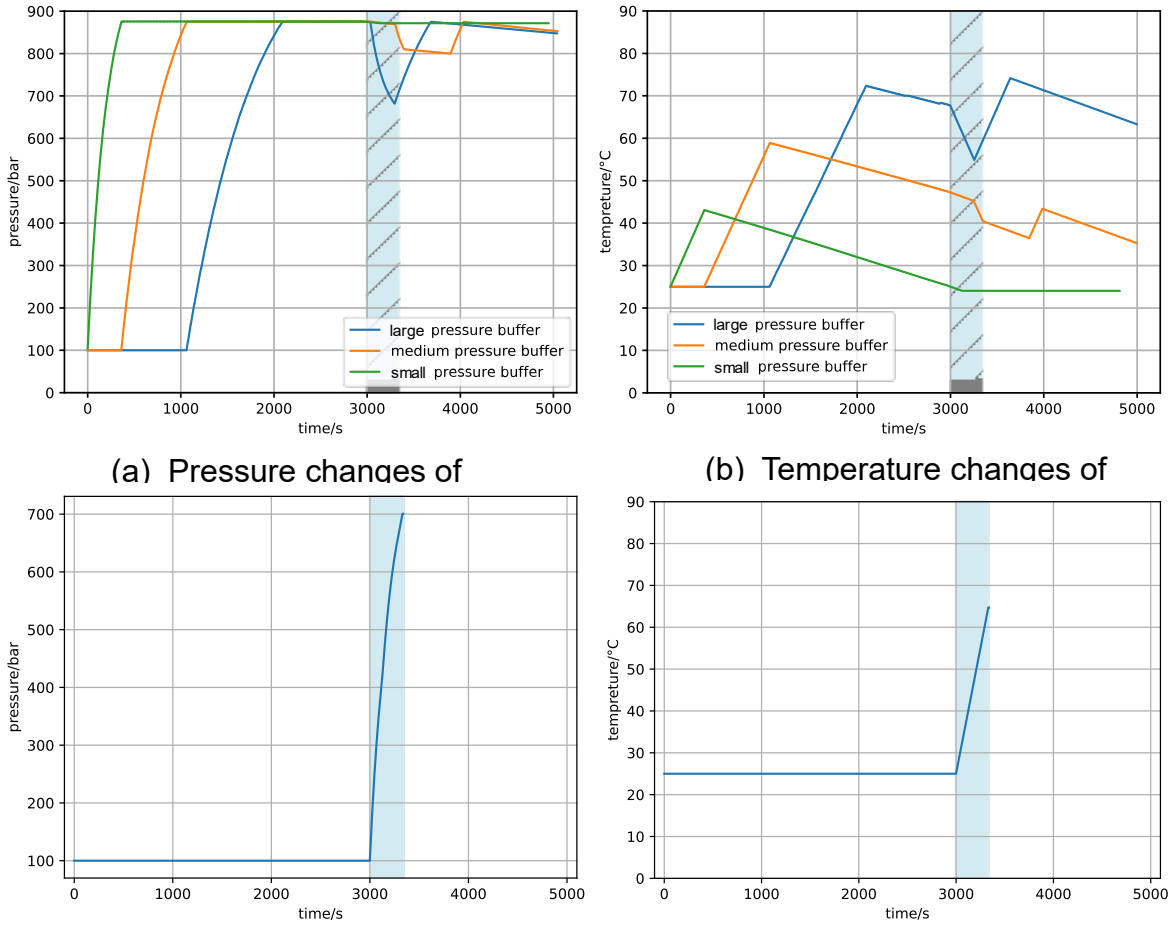

(a) Pressure changes of (b) Temperature changes of

(c) Pressure changes of (d) Temperature changes of

Figure 2.1 Simulation results of single vehicle using HRSC.

2. HRSC utilizes only the LB and MB (as shown in Figure 2.7(a)), unlike the Simulink simulator, which employs all three buffers (LB, MB, and SB). This difference arises from their distinct configurations.

   In the Simulink simulator, the LB operates at a lower initial pressure. Consequently, the pressure difference between the LB and the vehicle tank drops rapidly, limiting gas transfer and requiring additional supply from the MB and SB.

   In contrast, HRSC adopts a real-world HRS model (as shown in Table 2.1) where the LB has a larger volume. This allows the LB to deliver most of the required hydrogen during the initial stage, minimizing the need for the MB and SB.

3. The MB of HRSC is only pressurized later in the simulation (~3800s) when the temperature drop causes the pressure to fall below the threshold of 800 bars.

Summary

This section introduces the design and validation of HRS simulators, beginning with a review of two existing simulators developed in MATLAB. These simulators, while useful for studying HRS behavior, are limited by proprietary restrictions, lack of control system features, and limited accessibility. Such limitations make them unsuitable for projects requiring control strategy development.

To address these challenges, this project proposes an HRSC simulator developed using Python. The HRSC simulator features a modular design, including offline data processing, hardware simulation for buffers and vehicles, and a flexible controller testing environment. It demonstrates excellent adaptability and scalability, supporting the customization of system parameters and control strategies. Validation results show that the HRSC simulator maintains high fidelity in replicating the dynamics of real-world HRSs, with outcomes aligned to MATLAB-based simulators, while offering improved flexibility and usability for future HRS development and testing.

Logic Control for HRSs

This section validates the effectiveness of the HRSC simulator in evaluating two existing control methods: Logic 1 Control (LC-1), which uses a priority-based approach, and Logic 2 Control (LC-2), which uses a pressure-based approach. The performance of these methods is tested under four scenarios with vehicle arrival patterns based on uniform and normal distributions.

Overview of Logic Control

Logic control is a fundamental method in automation systems, where decisions are made based on logical rules derived from system inputs. Unlike complex mathematical models, this approach relies on simpler binary conditions such as "on/off" or "true/false," making it particularly effective in systems that prioritize reliability and simplicity. Logic control finds extensive application in areas such as industrial automation, energy management, and process control, where it evaluates inputs against predefined rules to determine appropriate actions. A key advantage of logic control lies in its ability to optimize resource management under diverse operational scenarios and ensure system stability even in rapidly changing environments. Common logic control methods include priority-based control and state-machine-based logic, both of which are invaluable in systems requiring efficient resource utilization under dynamic conditions, such as HRSs.

In HRSs, logic control is instrumental in streamlining refuelling processes, managing buffers, and ensuring safe and efficient vehicle refuelling. Two widely adopted control method, LC-1 and LC-2, meet these critical requirements. LC-1 employs a priority-based buffer control strategy, buffers sequentially based on predetermined criteria such as pressure and availability. On the other hand, LC-2, as presented in [10], adopts a pressure-priority strategy, dynamically adjusting the refuelling sequence in response to buffer pressure levels. These methods not only optimize operational efficiency but also play a crucial role in minimizing energy consumption and ensuring quick refuelling times, which are vital for maintaining user satisfaction and system reliability.

The controller module of the existing control methods in the HRSC simulator is illustrated in Figure 3.1. The HRSC simulator integrates both LC-1 and LC-2 methods to manage inlet and outlet valves during the refuelling process. These logic control methods operate based on the established logical rules, guiding the system to meet operational requirements effectively while maintaining flexibility to adapt to varying conditions. The following parts delve into the

implementation and evaluation of LC-1 and LC-2 methods within the HRSC simulator, offering a comprehensive analysis of their performance and contributions to system efficiency.

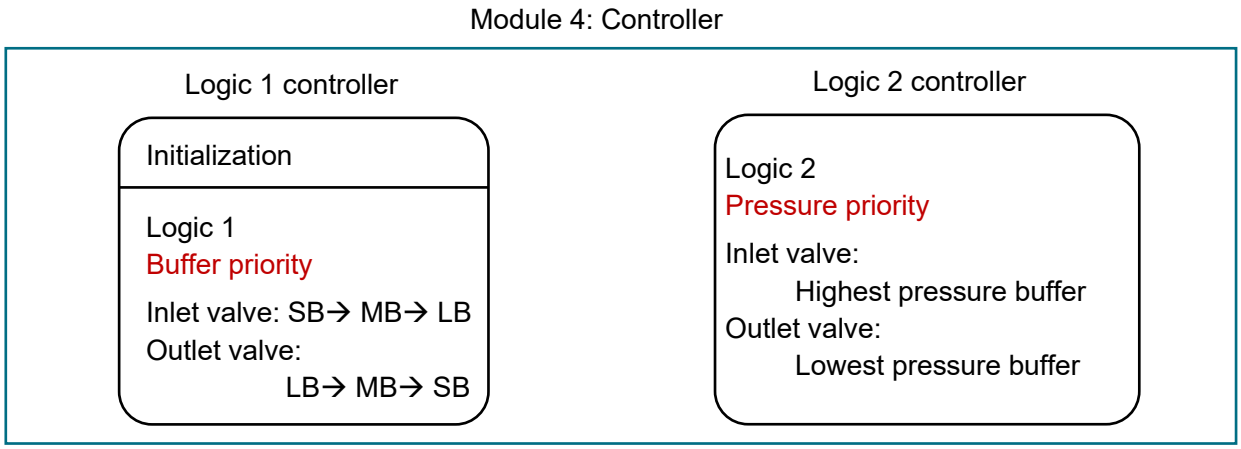

Figure 3.1 The controller module of existing logic controllers in the HRSC simulator.

Logic 1 Control

LC-1 is a priority-based buffer control method used for HRSs. The control logic of LC-1 is implemented in inlet valve and outlet valve control.

Inlet valve control: The compressor replenishes buffers in the order of small buffer, medium buffer, and large buffer. It means the compressor replenishes the small buffer first if it is not full and not occupied by the outlet valve; if it is full or occupied, the compressor tries to replenish the medium buffer. The switch from medium buffer to large buffer follows the same rule. Meanwhile, the pressurizing condition of buffers is the pressure of buffers under $800\ bar$ and the outlet valves of buffers closed.

Outlet valve control: The vehicle is refueled from the buffers in the order of large buffer, medium buffer, and small buffer. It means the vehicle can be refueled by the large buffer first as long as it satisfies the minimum refuelling pressure threshold; otherwise, the medium buffer is used. The same rule is applied when switching from the medium buffer to the small buffer. Additionally, this threshold pressure is defined as p_{dref}.

It is worth noting that, in Logic 1, the dispenser is prioritized over buffer refuelling operations. This design prevents a potential operational deadlock: Consider a scenario where both the pressure of the large and medium buffers falls below the vehicle tank pressure during refuelling while the small buffer is being replenished (with its pressure above the minimum refuelling threshold but still below 800 bars absolute pressure). In such cases, the control logic ensures immediate vehicle refuelling using the small buffer instead of waiting idly.

LC-1 is a widely used and foundational control method in current HRSs, known for its reliability and effectiveness in managing buffer systems. Currently, there is no theoretical analysis about which way is the optimal way to control HRSs. The control logic is adapted from existing literature, as no specific control method has been developed for this kind of station configuration. Moreover, by observing the data from the BC stations, the control logic applied right now is the LC-1.

Given its practicality and relevance, it is employed in this simulation as the **baseline** for comparison with other control methods, providing a consistent and meaningful reference point.

Logic 2 Control

The other control method, LC-2, is a pressure-priority-based logic control method introduced in [10]. Similar to LC-1, it also includes both inlet and outlet valve control strategies. However, LC-2 distinguishes itself by employing a different control logic in managing the buffer system, prioritizing pressure levels over buffer refuelling order. This variation in control method provides an alternative approach to buffer management compared to LC-1, offering potential advantages in specific operational scenarios.

For the convenience of notation, the pressures of the buffers are denoted as x_{P_s}, x_{P_M}, and x_{P_L} for the small, medium, and large buffers, respectively, and x_{P_V} for the pressure of the vehicle to be refueled. Additionally, the threshold pressure is defined as p_{dref}, as mentioned in Section 3.2, where the relationship between pressures from buffers and the vehicle must satisfy $x_{P_{s/M/L}} - x_{P_V} \geq p_{dref}$.

Inlet valve control: The compressor replenishes the buffers in descending order of pressure, prioritizing the buffer with the highest pressure that is still below its upper limit. For example, if the pressure relationship is $x_{P_s} > x_{P_M} > x_{P_L}$, and the small buffer is full, the compressor will first replenish the medium buffer until it reaches its maximum pressure. Then, the pressure levels are evaluated again, and the process repeats to determine the next buffer for refuelling. Likewise, the pressurizing condition of buffers is the pressure of buffers under $800\ bar$ and the outlet valves of buffers closed

Outlet valve control: Vehicles are refueled from the buffers starting with the one that has the lowest pressure but is still sufficient to meet the required flow rate. For example, if the pressure relationship between the buffers and the vehicle $x_{P_s} > x_{P_M} > x_{P_L} > x_{P_V} + p_{dref}$, the large buffer is used first to refuel the vehicle until its pressure drops below $(x_{P_V} + p_{dref})$. If the flow rate cannot be sustained, the system switches to the next buffer with a higher pressure, repeating this process until the target state is reached.

This method is designed to balance speed and efficiency during refuelling while minimizing energy consumption. As noted in [10], it demonstrates the improved performance by increasing refuelling capacity and optimizing resource utilization, making it an effective control method for simulation.

Simulation Results

This section first introduces the simulation scenarios and evaluation criteria of the simulations in this project. Then, the simulation results of Logic 1 and Logic 2 controller is given.

Scenarios and Evaluation Criteria

(1) Simulation scenarios

One of the most principal factors affecting the critical performance of HRS (e.g., energy consumption and vehicle waiting time) is traffic flow. Traffic flow can be characterized by the number of vehicles and the time instants at which vehicles arrive. For example, the authors in [10] consider a scenario involving 96 vehicles over 24 hours. They assume that the arrival times of vehicles during a 24-hour period follow a normal distribution, as shown in Figure 3.2. However, this scenario does not fully capture all possible traffic flow conditions. To better replicate real-world traffic flow and evaluate the performance of the two logic control methods, simulations are conducted under the following four scenarios.

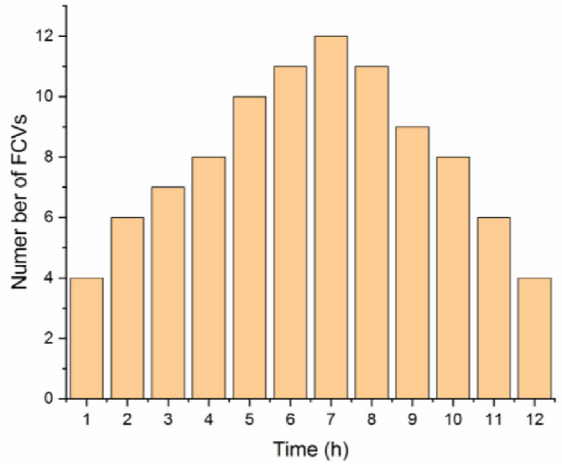

Figure 3.1 Time distribution of 96 vehicles per day.

Four scenarios with vehicle flows following uniform and normal distributions are summarized in Table 3.1. The uniform distribution represents the vehicle traffic with equal intervals over a time-period, while the normal distribution shows peak and off-peak times. Scenarios S1 and S2 are designed to simulate dense vehicle conditions over a brief period,

equivalent to 5 vehicles arriving within 17 minutes. Scenarios S3 and S4 illustrate the daily vehicle conditions of 96 vehicles following uniform distribution and normal distribution over 12 hours. Based on the test scenario presented in [3], scenario S4 is tailored to align with Figure 3.2. To ensure a fair comparison, the simulation is limited to 12 hours, with the remaining 12 hours of the day assumed to have no vehicle charging activity. The subsequent part compares the control performance of the two systems with different distributions under these varying conditions.

Table 0.1 Four simulation scenarios.

		Distribution	
		Uniform	**Normal**
Number of Vehicles/Time Period	$5/1000$ seconds	S1	S2
	$96/12$ hours	S3	S4

The simulation incorporates three vehicle types with identical maximum pressure ratings (700 bars) but varying tank volumes: Type 1 (156L), Type 2 (134L), and Type 3 (122L). To achieve realistic stochastic conditions, a pseudo-random generation algorithm maintains consistent distributions of both vehicle types and arrival intervals across all scenarios. The specific implementation details are as follows.

For S1 and S2, there are five vehicles arrived in 1000 seconds. The specified information of vehicle sequence is shown in Table 3.2.

Table 0.2 Vehicle arrival information for S1 and S2.

Index	1	2	3	4	5
Type	1	3	2	2	2
Arriving time of S1	0	200s	400s	600s	800s
Arriving time of S2	0	109s	405s	538s	782s

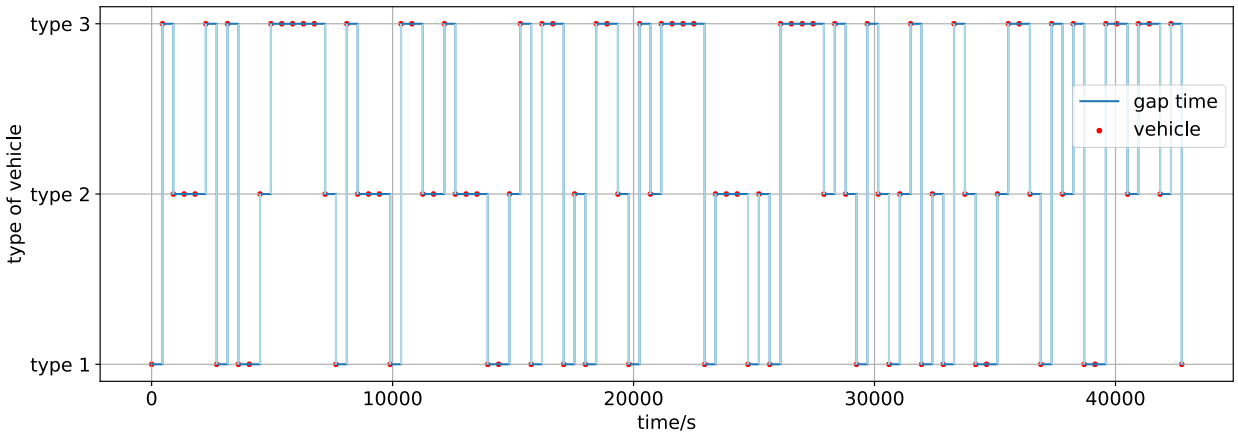

Figure 3.2 Arriving time and gap time of vehicles in S3.

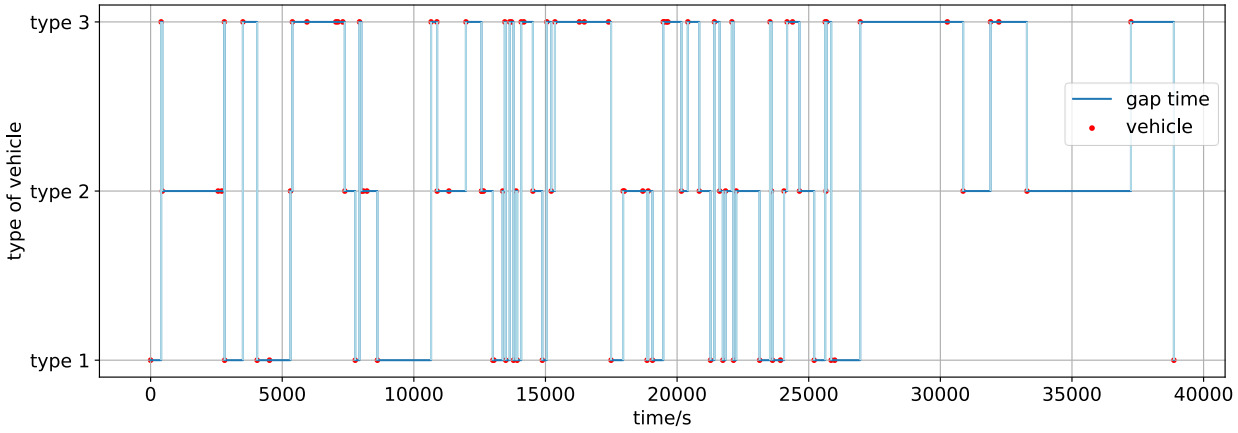

Figure 3.3 Arriving time and gap time of vehicles in S4.

For S3 and S4, 96 random vehicles arrived at the HRS in 12 hours (43200 seconds). S3 consider the uniform distribution which means the gap time between each vehicle are same. On the other hand, the S4 follows the normal distribution, as shown in Figure 3.2. To illustrate the arriving conditions more intuitively, the distribution of time and type of vehicles for S3 and S4 are presented in Figure 3.3 and Figure 3.4, respectively.

(2) Evaluation criteria

Another critical issue to address is the evaluation of the performance of different control logics under the scenarios outlined in Table 3.3, specifically regarding their fuelling efficiency and energy consumption. To facilitate a fair comparison, four key metrics are proposed as shown in Table 3: The total waiting time t_{total} and average waiting time t_{avg} represent the refuelling efficiency, and the compressor runtime t_{comp} and dispenser runtime

t_{dis} serve as indicators for energy consumption. Lower values in performance measures mean shorter waiting times and less energy consumption, which are desirable. Meanwhile, the total waiting time t_{total} and average waiting time t_{avg} exclude the "refuelling time" but only compute the idle time (the new vehicle has arrived, but the dispenser is occupied by the previous vehicle).

Table 0.3 Evaluation measures of simulation results.

$\boldsymbol{t_{total}}$	Total waiting time of all vehicles
$\boldsymbol{t_{avg}}$	Average waiting time of each vehicle
$\boldsymbol{t_{comp}}$	Compressor running time, representing the energy consumption of the compressor
$\boldsymbol{t_{dis}}$	Dispenser runtime, representing the energy consumption of the pre-cooler

It is worth noting that the energy consumption ratio of the compressor is significantly higher than that of the dispenser, and different literature reports varying ratios between the two (ranging from 5:1 to 2:1) depending on the specific base station hardware configurations. This report focuses primarily on analyzing how compressor energy consumption affects overall system energy usage. Future work could include a more detailed comparison of specific energy consumption between these two components.

When setting up the environment, a limitation arises in accurately modeling the power consumption of the compressor and pre-cooler, as it varies over time during operation and may also fluctuate by season due to differences in ambient temperatures. To address this challenge, an indirect estimation approach is adopted, using the operational durations of the input and output valves as proxies to evaluate the energy expended by these components. This approach assumes that the power consumption of each component remains constant throughout its operation. Thus, the amount of time the input and output valves remain open is considered directly proportional to their power usage. Consequently, the total energy consumption of the HRS control system is computed as the sum of the energy consumption of these two components. In Table 3.3, these two indicators are separately delineated and compared to provide a clearer understanding of the energy efficiency and operational dynamics of the HRS under varying scenarios.

In the following subsections, simulations are conducted, and results are analyzed across multiple scenarios using various logic control methods. These results are compared to highlight the impact of each approach on system performance, focusing on energy efficiency, operational effectiveness, and the ability to adapt to varying conditions. This

comparison aims to identify the strengths and limitations of each control method, providing insights into their suitability for different operational requirements.

LC-1 and LC-2 with S1 and S2

The simulation results for LC-1 and LC-2 under scenario S1 are presented in Figure 3.5 and Figure 3.6, respectively. Considering the specific scenario of this project, the initial pressure of all three buffers is the same, but LC-2 makes the control decision in accordance with the pressure. Making control decisions in this special situation will be based on the sequence of buffers (from LB to SB).

By comparing the pressure variation of LC-1 and LC-2 from Figure 3.5(a) and Figure 3.6(a), the differences in control logic between LC-1 and LC-2 can be observed:

1. Both LC-1 and LC-2 demonstrate identical control behavior during the initial period up to approximately 1300 seconds. For outlet valve operations, LC-1 follows a predetermined priority sequence (LB→MB→SB), while LC-2 primarily selects buffers based on ascending pressure levels, defaulting to the same sequence when pressures are equal. Regarding inlet valve operations, both logics exclusively utilize the LB during the first refuelling phase, then shift focus to replenishing the MB after the second refuelling completion.

2. The differences emerge during the later stage of the third refuelling (post-1300s). When the LB becomes insufficient to maintain required pressure differentials, LC-1 continues prioritizing the MB due to its higher priority, whereas LC-2 selects the SB based on its lower pressure state. This divergence clearly illustrates the rigid priority-based approach (LC-1) versus the dynamic pressure-based method (LC-2).

3. The analysis reveals fundamental operational distinctions: LC-1 exhibits preferential usage of the MB throughout the process, reflecting its fixed priority architecture. In contrast, LC-2 demonstrates more balanced buffer utilization by dynamically responding to real-time pressure conditions.

Then, by comparing the buffer pressure (Figure 3.5(a) and Figure 3.6(a), temperature (Figure 3.5(b) and Figure 3.6(b)), and vehicle pressure (Figure 3.5(c) and Figure 3.6(c)), temperature (Figure 3.5(d) and Figure 3.6(d)), it is observed that both methods execute similar control decisions, buffer utilization, and replenishment conditions, with no significant differences. The dots in Figure 3.5(c) and Figure 3.6(c) shows the entering time of each vehicle, so this figure also shows the waiting time of each vehicle.

Additionally, a comparison of Figure 3.5(e), (f), and Figure 3.6(e), (f) depicts the inlet and outlet valves switch buffers. The inlet valve switching among large, medium, and small buffers

represents which buffer is refueled by the compressor, and the inlet valve is closed when the compressor is not used for replenishment. Similarly, the outlet valve shifts buffers show which buffer is utilized by the dispenser to fuel the vehicle, and otherwise, the dispenser is closed. The inlet and outlet valves reflect the decision made by the controller. From these figures, it can be found that under S1, these two control logics have an analogous control execution.

Then the simulation results for these two controllers under scenario S2 are presented in Figure 3.7 and Figure 3.8, respectively. Similarly, with the situation with S1, a comparison of the state changes across these two figures indicates that the trends of the state are analogous which means their executions of control are consistent.

The results of LC-1 and LC-2 for scenarios S1 and S2 are presented in Table 3.4. In S1, it is observed that compared to LC-1, LC-2 has a little longer of waiting times for refuelling and increase about 1.47% of the total refuelling duration for vehicles. This means that LC-1 can save users' time during periods of high-density traffic. However, LC-1 approach also results in longer compressor operating times and higher energy consumption. In the high-density vehicle entry scenario S2, a similar phenomenon is observed: LC-2 increases vehicle waiting times but has less energy consumption. The total refuelling time of S2 is the same as with S1.

Table 0.4 Performance of LC-1 and LC-2 under dense traffic flow scenarios.

Scenario		$t_{total}(s)$		$t_{avg}(s)$		$t_{comp}(s)$		$t_{dis}(s)$	
		Value	Change rate	Value	Change rate	Value	Change rate	Value	Change rate
S1	LC-1 ⇩ LC-2	**1140** ⇩ 1156	**1.40%**	**228** ⇩ 231.2	**1.40%**	1788 ⇩ **1741**	-2.63%	**1763** ⇩ 1789	**1.47%**
S2	LC-1 ⇩ LC-2	**1226** ⇩ 1242	**1.31%**	**245.2** ⇩ 248.4	**1.31%**	1788 ⇩ **1741**	-2.63%	**1763** ⇩ 1789	**1.47%**

The simulation outcomes reveal that when employing LC-2 for controlling the HRS, the usage of the three buffers is more evenly distributed. Contrasted with the control results of LC-1, this strategy ensures a more balanced utilization across all three buffers, leading to more stable temperature variations. However, the performance of these two control methods does not differ significantly, making it difficult to determine which method is better or more energy-saving. Observing the t_{comp} and t_{dis}, it can be found that for the same controller, it has the same values for both S1 and S2 scenarios. The reason is although the vehicles arrived at different times (Figure 3.5(c) and Figure 3.6(c)), they started to be refueled at the same time. Moreover, in the short term, LC-1 and LC-2 demonstrate comparable performance in scenarios S1 and

S2, with identical waiting times (3-second difference on average) and similar energy consumption (-1.27% with a 2:1 ratio between t_{comp} and t_{dis}).

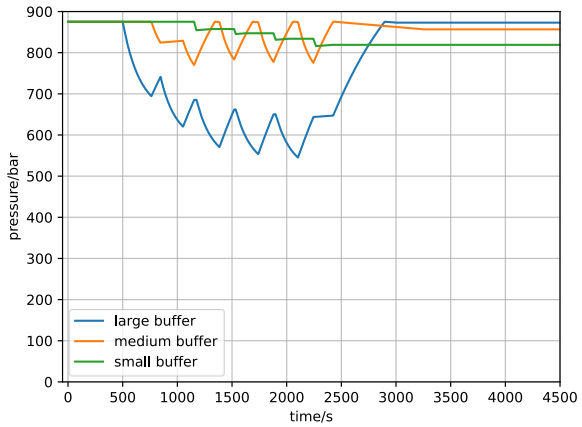

(a) Pressure changes of buffers.

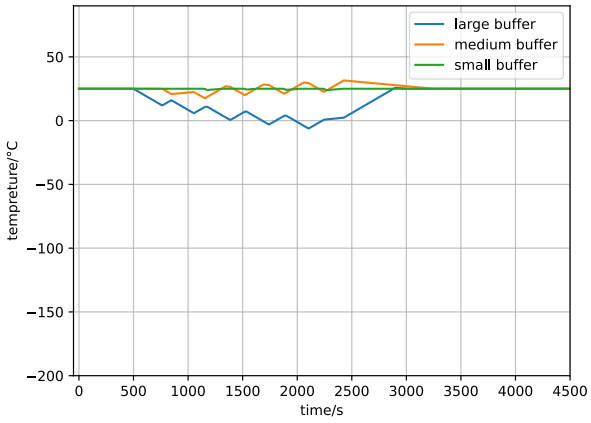

(b) Temperature changes of buffers.

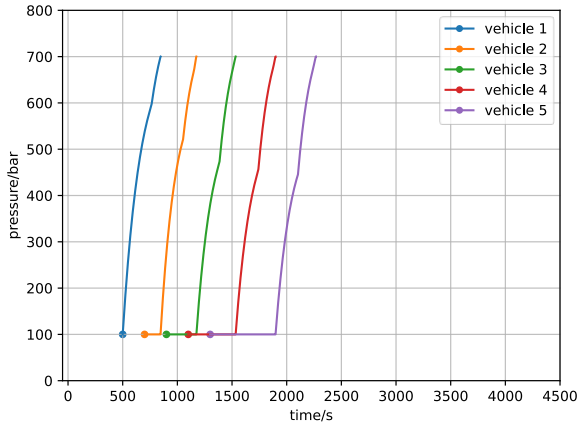

(c) Pressure changes of vehicles. Each colour represents one vehicle.

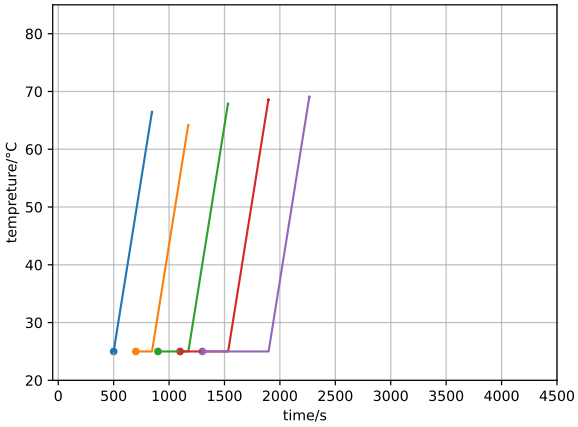

(d) Temperature changes of vehicles. Each colour represents one vehicle.

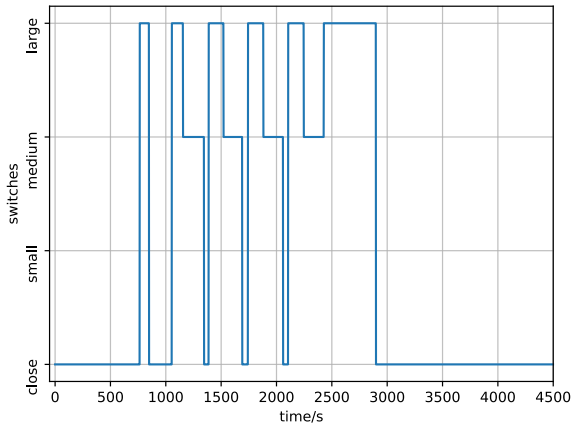

(e) Inlet valve switches buffers.

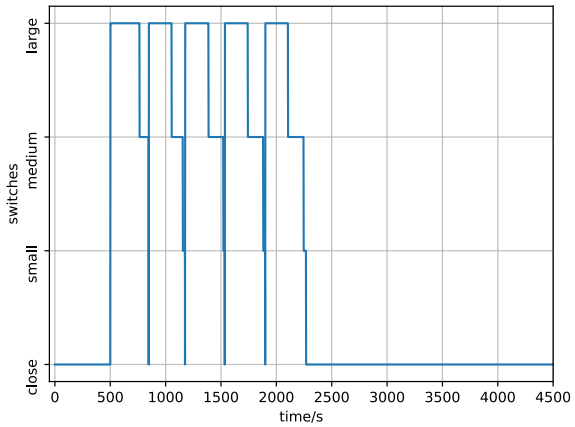

(f) Outlet valve switches buffers.

Figure 3.4 Simulation in S1 using LC-1.

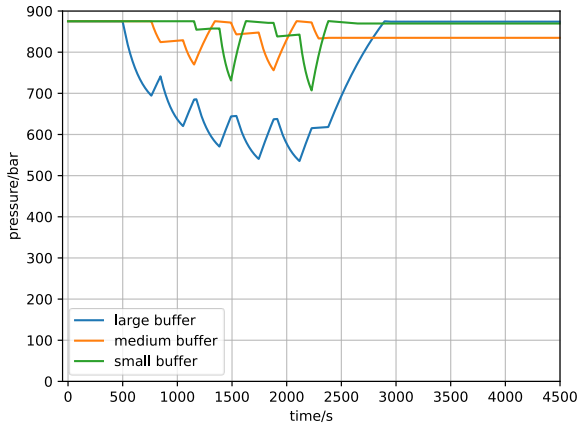

(a) Pressure changes of buffers.

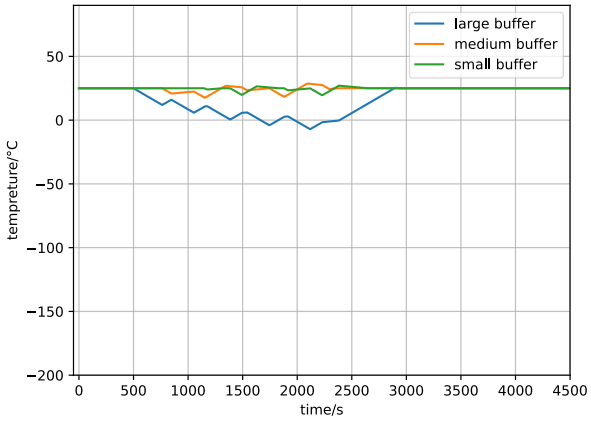

(b) Temperature changes of buffers.

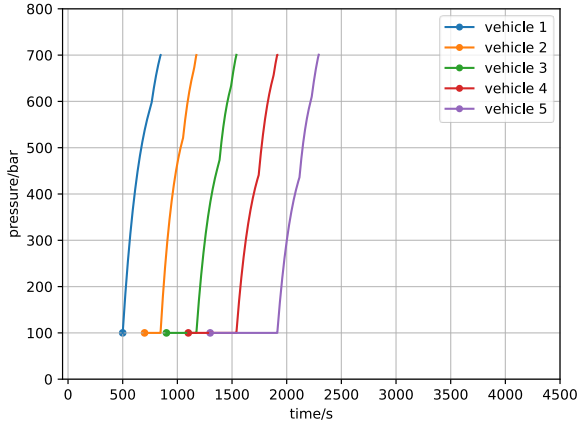

(c) Pressure changes of vehicles. Each color represents one vehicle.

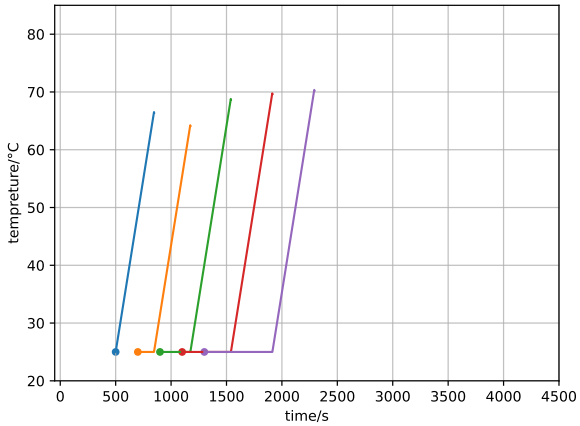

(d) Temperature changes of vehicles. Each color represents one vehicle.

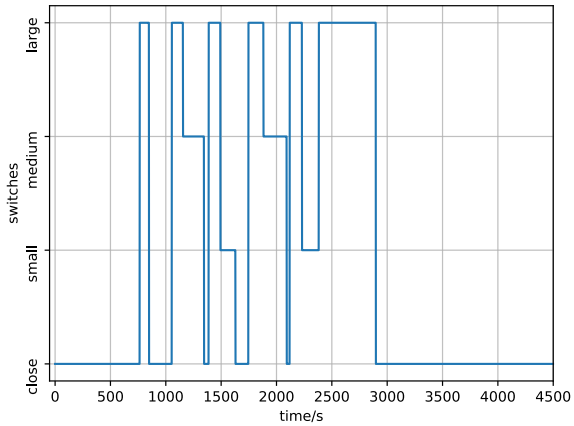

(e) Inlet valve switches buffers.

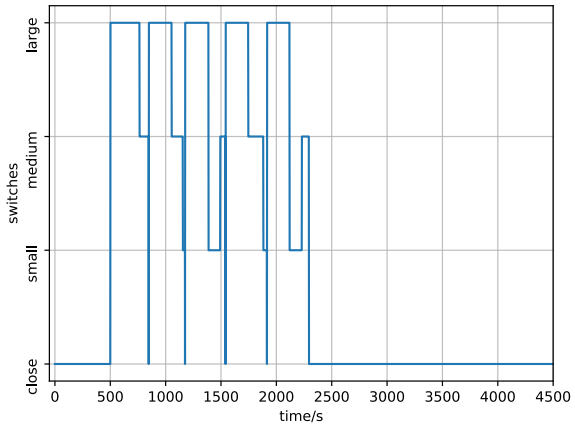

(f) Outlet valve switches buffers.

Figure 3.5 Simulation in S1 using LC-2.

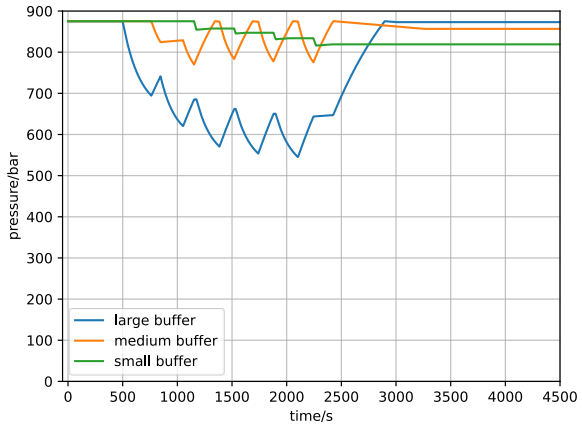

(a) Pressure changes of buffers.

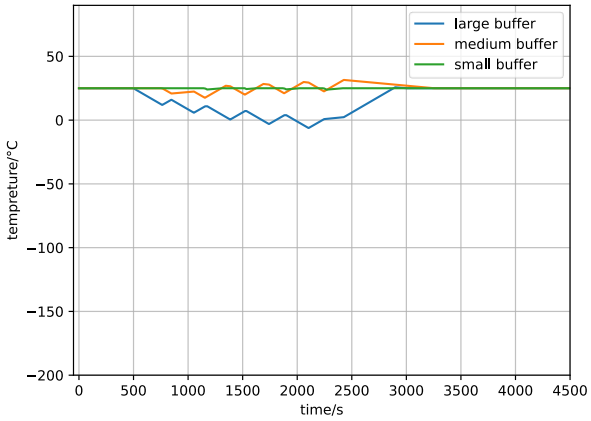

(b) Temperature changes of buffers.

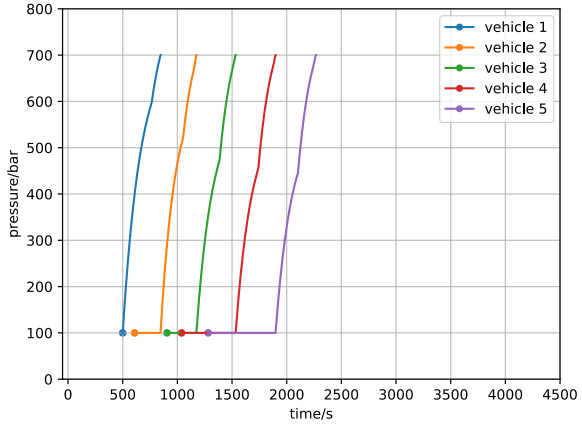

(c) Pressure changes of vehicles.
Each color represents one vehicle.

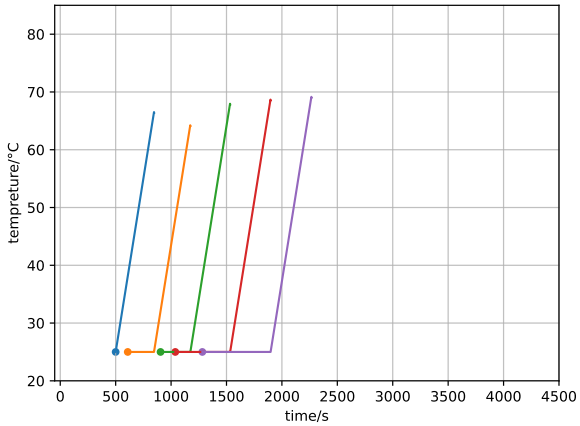

(d) Temperature changes of vehicles.
Each color represents one vehicle.

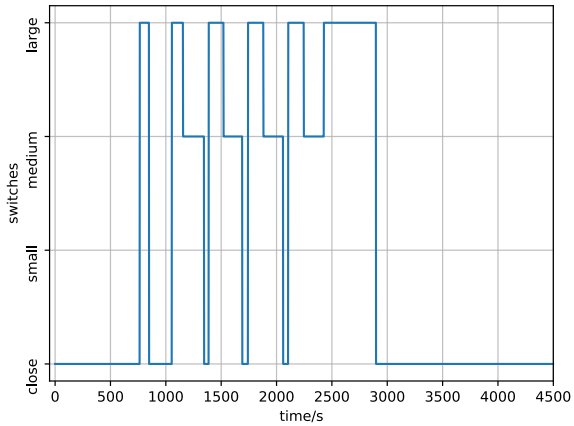

(e) Inlet valve switches buffers.

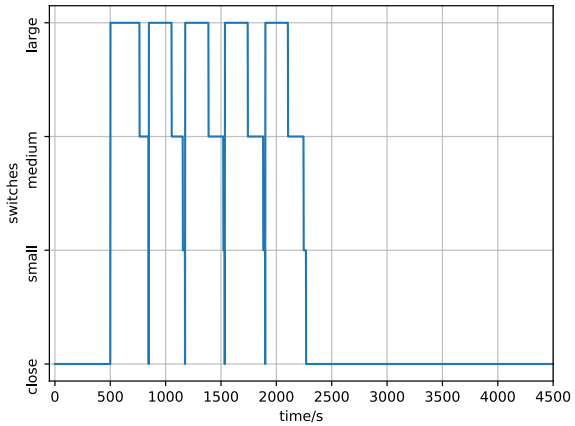

(f) Outlet valve switches buffers.

Figure 3.6 Simulation in S2 using LC-1.

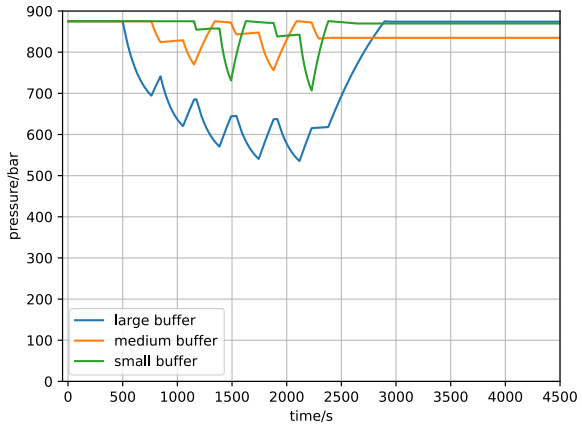

(a) Pressure changes of buffers.

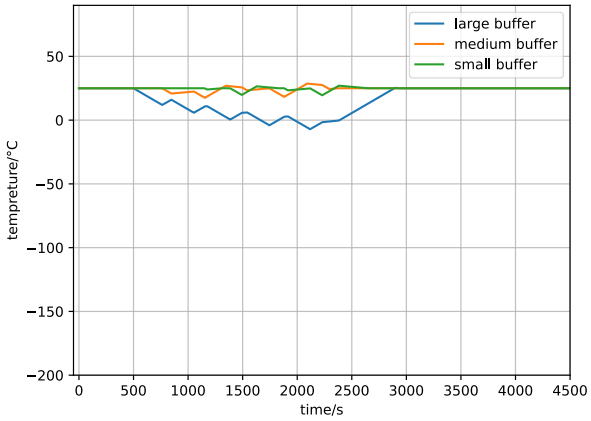

(b) Temperature changes of buffers.

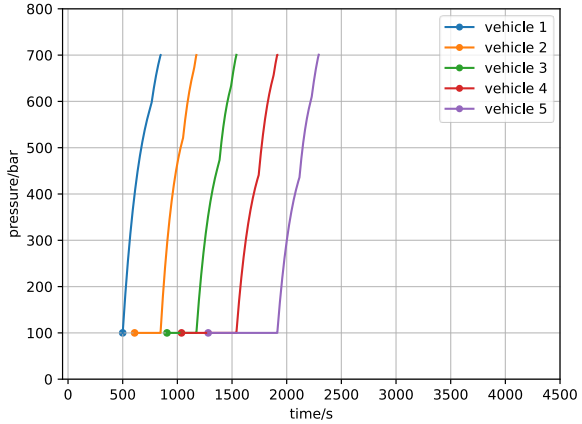

(c) Pressure changes of vehicles.
Each color represents one vehicle.

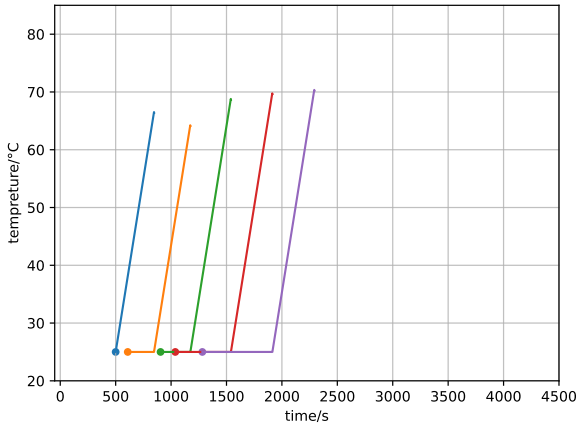

(d) Temperature changes of vehicles.
Each color represents one vehicle.

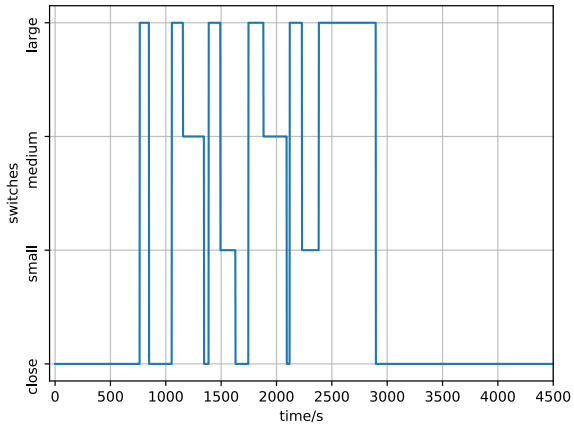

(e) Inlet valve switches buffers.

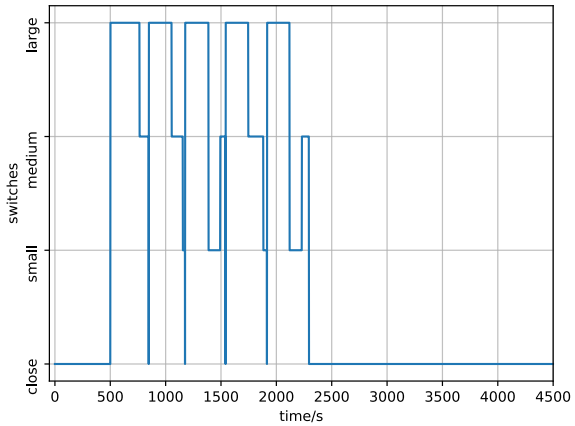

(f) Outlet valve switches buffers.

Figure 3.7 Simulation in S2 using LC-2.

LC-1 and LC-2 with S3 and S4

The simulation results for longer periods are summarized in this subsection. The results of control LC-1 and LC-2 with scenarios S3 and S4 are shown in Figure 3.9-Figure 3.12. The pressure and temperature of vehicles do not violate the limitations of the fuelling protocol. Under a sparse traffic flow condition, all the pressure and temperature of buffers and vehicles are in a moderate range. The simulation outcomes also reveal that when employing LC-2 for controlling the HRS, the usage of the three buffers is more evenly distributed. Comparing the buffer usage in Figures 3.9(a), (b), and Figures 3.10(a), (b), it can be observed these two control logics have similar phenomenon which is the same as those in S1 and S2. The results in Figures 3.9(c), (d), and Figures 3.10(c), (d) show the utilization time of buffers and the percentage time for the inlet or outlet valves which is closed, respectively.

To ensure consistent comparison across all control strategies, we use a fixed simulation duration for all scenarios. However, for some controllers (e.g., LC-1), all vehicles may be fully refueled before the simulation ends. In such cases, the buffers enter an idle state with both inlet and outlet valves closed. While no further compression or refuelling occurs during this period, the associated idle time is included in the statistical results, ensuring a uniform time-scale interpretation across all figures.

Through observation of Figure 3.9(a), Figure 3.10(a), Figure 3.11(a), and Figure 3.12(a), it is noted that the buffer pressure may sometimes exceed 875 bars. When the compressor fills up the buffer with hydrogen, both pressure and temperature increase inside the cylinder. This phenomenon has been experimentally observed and confirmed by thermodynamic simulations [11].

Firstly, by observing Figure 3.9(a) and Figure 3.9(b), a general understanding of the entire S3/S4 workflow can be obtained:

- From Figure 3.9(b), it can be observed that before 20,000 seconds, the temperature of the large buffer continued to decrease until it reached the lower limit of -100°C. This decline is not linear, but a curve with fluctuations. The persistent downward trend is due to more time used to charge than to replenish. During this period, the pressure remains around 600 bars because the system is constantly switching between replenishment and usage. The reason that the pressure stays stable while the temperature keeps decreasing is that the flow rates for gas intake and release differ, requiring varying durations of replenishment and release to maintain stable pressure. Intuitively, it can be observed from simulation results in S1/S2 (e.g. Figure 3.5(a)).

- During the period from 20,000s to 43,000s, the LB maintains a temperature of -100°C because we set -100°C as the safety threshold. Once the temperature reaches this critical value, the system will stop using the LB. The temperature of LB could then rise either through heat exchange with the environment or by replenishment from the compressor. Once the temperature rises above -100°C, it becomes available again. As a result, the temperature of LB fluctuates near the critical threshold throughout this period.
- After 43,000 seconds, all vehicle refuelling tasks are completed, so the pressures in the small and medium buffers show no significant changes. The temperature variations in Figure 3.9(b) during this period are caused by heat exchange between the buffers and the surrounding environment.

Comparative analysis of the four figures reveals distinct buffer utilization patterns between the two control logics. Specifically, LC-2 demonstrates more balanced buffer usage than LC-1. In LC-1 (Figure 3.9(d) and Figure 3.11(d)), the LB exhibits the highest utilization rate. Here, the utilization rate refers to the percentage of running time during which the buffer's outlet valve (dispenser) remains open to a specific storage buffer. This observation aligns with LC-1's priority-based control architecture: the outlet valve is assigned a higher priority, which directly affects the inlet valve operational behavior. Despite this prioritization framework, the inlet valve fails to show an explicitly structured control sequence. This result arises from two factors: (1) the priority between the two valves and (2) their coupled dynamic interactions within the HRS. In addition, it is observed that under both LC-1 and LC-2, the control outcomes for scenarios S3 and S4 are similar.

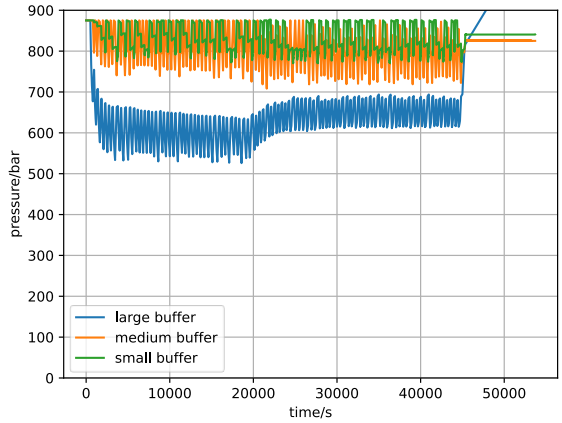

(a) Pressure changes of buffers.

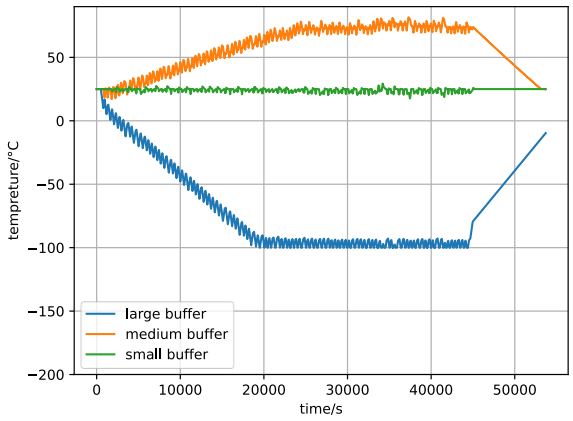

(b) Temperature changes of buffers.

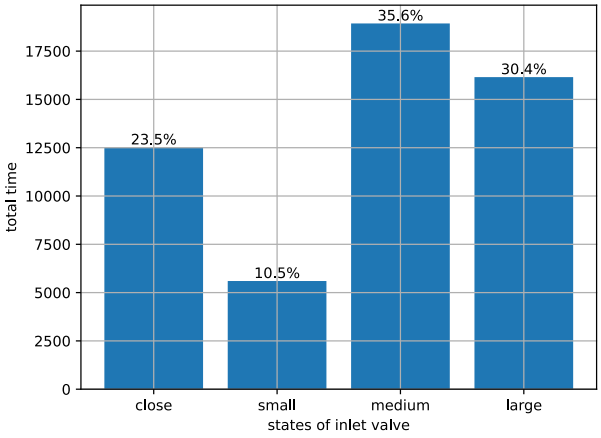

(c) Inlet valve switches buffers.

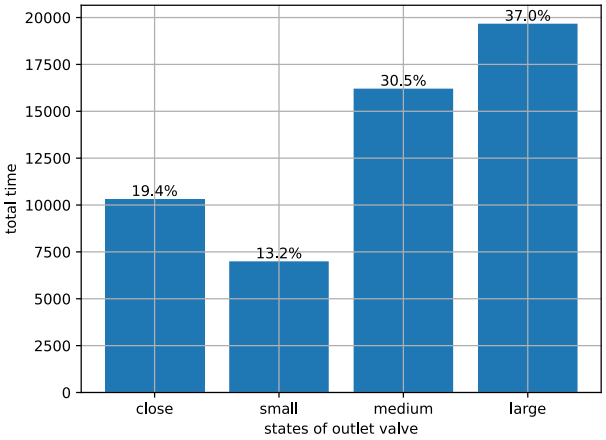

(d) Outlet valve switches buffers.

Figure 3.8 Simulation in S3 using LC-1.

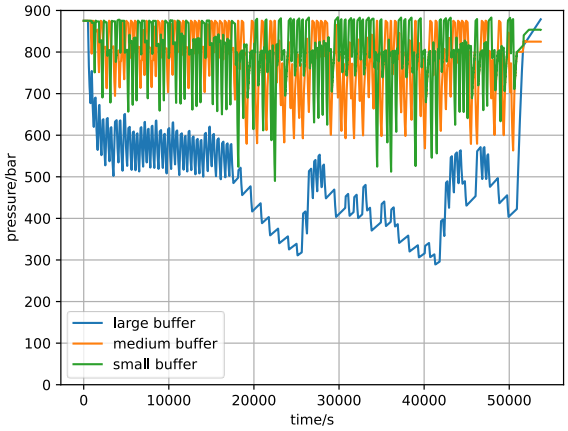

(a) Pressure changes of buffers.

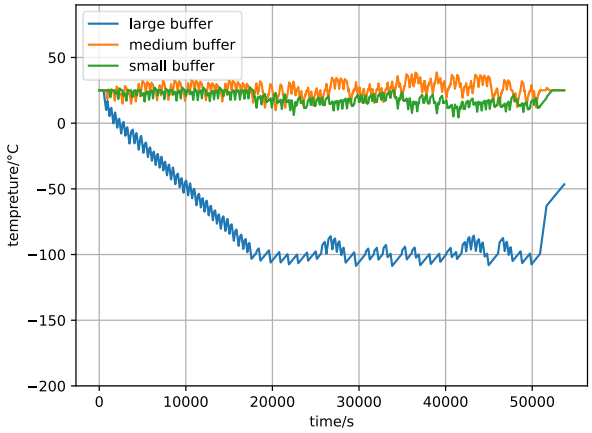

(b) Temperature changes of buffers.

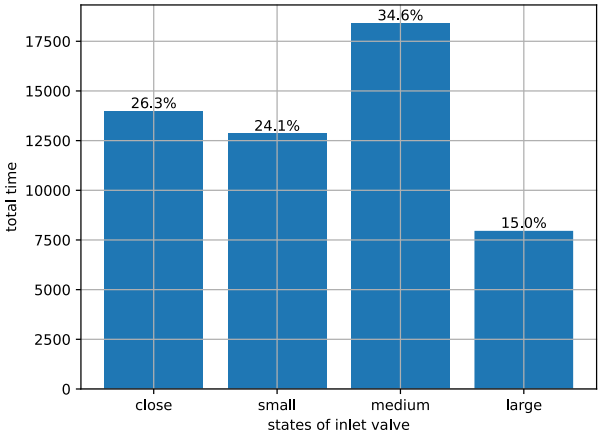

(c) Inlet valve switches buffers.

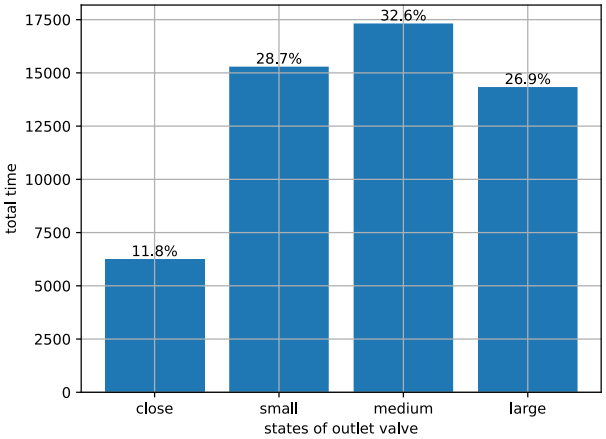

(d) Outlet valve switches buffers.

Figure 3.9 Simulation in S3 using LC-2.

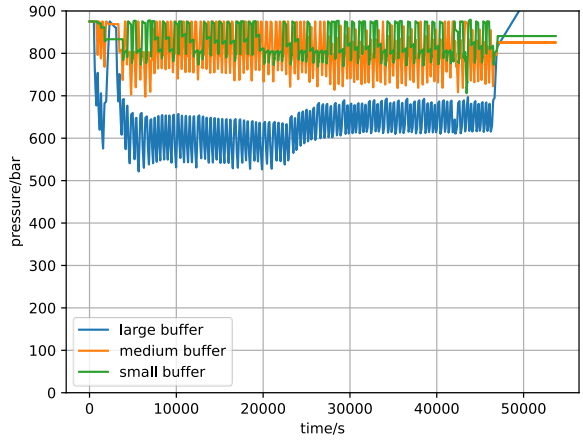

(a) Pressure changes of buffers.

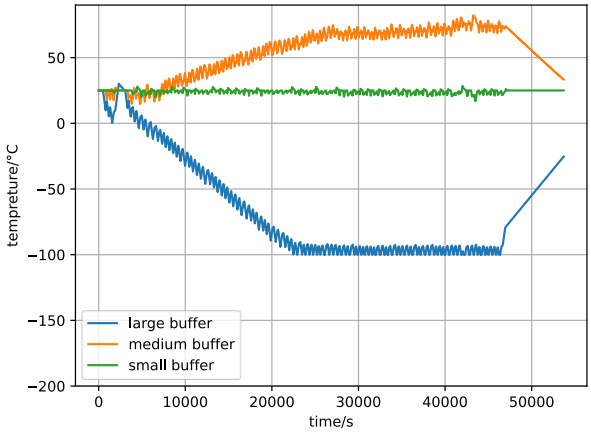

(b) Temperature changes of buffers.

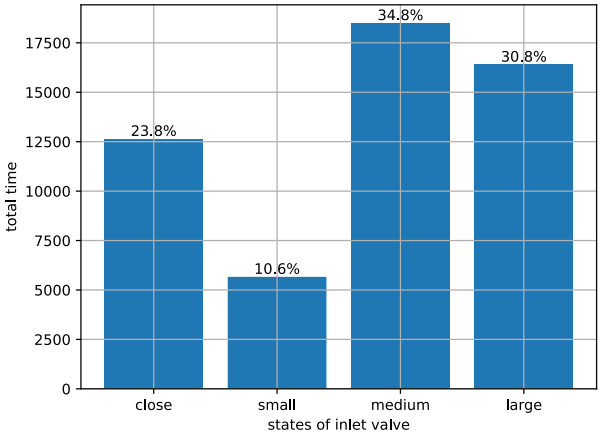

(c) Inlet valve switches buffers.

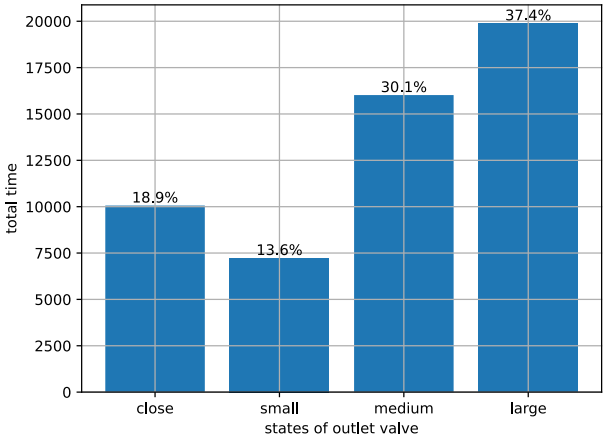

(d) Outlet valve switches buffers.

Figure 3.10 Simulation in S4 using LC-1.

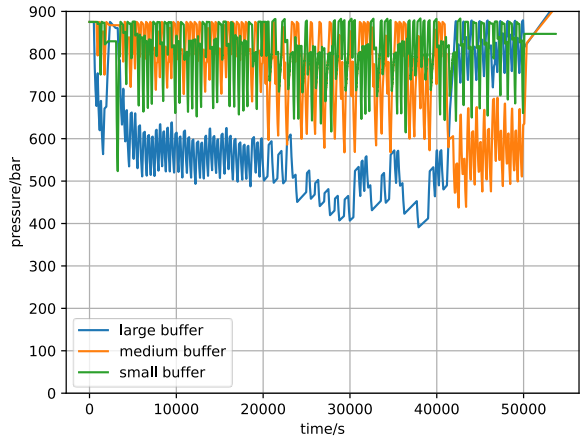

(a) Pressure changes of buffers.

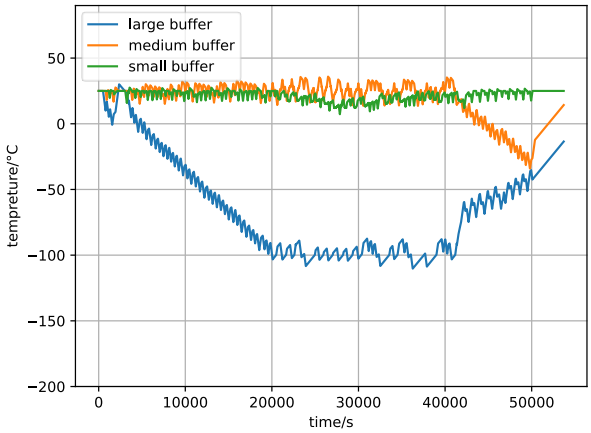

(b) Temperature changes of buffers.

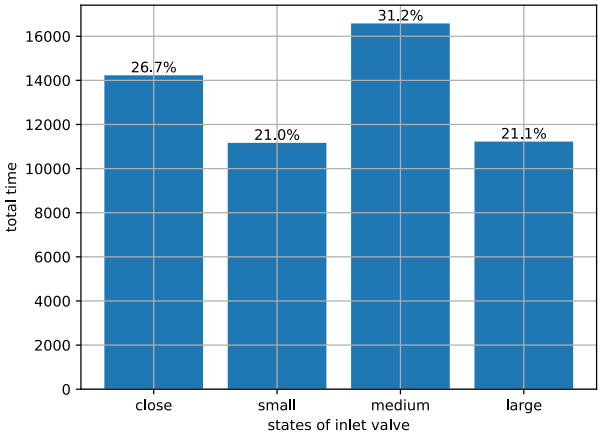

(c) Inlet valve switches buffers.

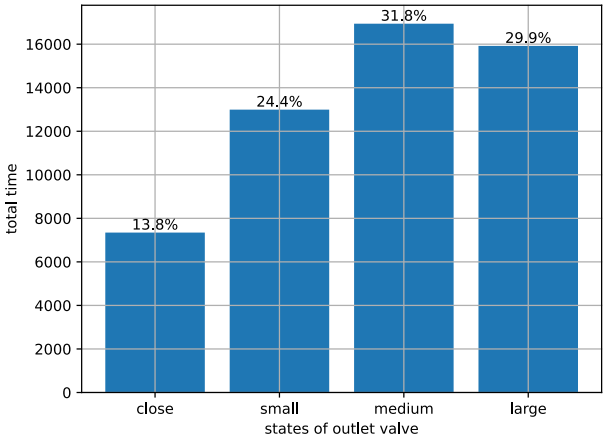

(d) Outlet valve switches buffers.

Figure 3.11 Simulation in S4 using LC-2.

In this simulation, a switching frequency diagram like those for S1 and S2 (subfigures (e) and (f) in Section 3.4.2) is not included. This is because the extended duration of S3 and S4 simulations would result in excessively dense vertical lines in such plots. At our 1 Hz sampling frequency, these lines would merge into a nearly solid blue rectangle, rendering the visualization uninformative. The 1 Hz control frequency implemented in our simulation represents a standard sampling rate for this type of analysis. Our comprehensive literature review confirmed that no established restrictions exist for this control frequency parameter.

Table 0.5 Performance of LC-1 and LC-2 with 96 vehicles per day.

Scenario		$t_{total}(s)$		$t_{avg}(s)$		$t_{comp}(s)$		$t_{dis}(s)$	
		Value	Change rate	Value	Change rate	Value	Change rate	Value	Change rate
S3	LC-1 ⇩ LC-2	**36701** ⇩ 45570	**24.17%**	**382** ⇩ 472	**23.56%**	40686 ⇩ **39215**	-3.62%	**42876** ⇩ 46948	**9.50%**
S4	LC-1 ⇩ LC-2	**43212** ⇩ 46427	**7.44%**	**450** ⇩ 483	**7.33%**	40560 ⇩ **38972**	-3.91%	**43140** ⇩ 45855	**6.29%**

The performance of LC-1 and LC-2 on scenarios S3 and S4 is shown in Table 3.5. In scenarios S3 and S4, vehicle entry times follow uniform and normal distributions, respectively. In these two scenarios, compared to LC-1, LC-2 causes longer vehicle waiting time and dispenser usage time but reduces compressor usage time. Compared with scenarios S1 and S2, the results in S3 and S4 demonstrate that LC-2's advantage in saving energy diminishes but takes more time from the vehicle in extended sparse scenarios.

The longer t_{dis} of the LC-2 dispenser is due to all buffers operating at lower pressure levels than those in LC-1, resulting in smaller pressure differentials with the vehicle and, consequently, slower flow rates, which extend the fuelling time. In contrast, the lower operating pressure of the buffers creates a larger pressure differential with the compressor, which increases the fuelling speed from the compressor side and shortens t_{comp}. As a result, this configuration improves the overall operational efficiency of the HRS. This phenomenon illustrates the fundamental trade-off in HRS systems between the dispenser and compressor runtime.

Considering the scenarios of short-term dense traffic flow (S1, S2), long-term uniformly distributed traffic (S3), and long-term random vehicle flow (S4), the control performance of the LC-1 and LC-2 controllers is summarized as follows. Compared with LC-1 under these four scenarios, LC-2 always reduces the compressor running time but has a higher waiting time for the vehicles. The small buffer usage is less in LC-1, while LC-2 uses buffers in a balanced way. In long-term simulations, LC-1 demonstrates lower dispenser operation time and vehicle waiting time, thereby exhibiting greater vehicle charging efficiency compared with LC-2.

In summary, LC-2 is energy efficient but time-consuming compared with LC-1, but the difference is minor. In real HRS control conditions, it is recommended to apply and test these two methods before usage, since their performance varies when the hardware setup changes.

Summary

This section validates the effectiveness of the HRSC simulator by comparing two logic control strategies: one based on priority and the other based on pressure-priority. The performance of these strategies is evaluated in managing HRSs under four scenarios simulating vehicle arrival patterns with varying distributions. The simulation results highlight differences in buffer utilization, energy consumption, and overall system efficiency for each control logic, demonstrating the simulator's capability to assess these factors.

Optimal Control for HRSs

This section presents an optimal control-based method for HRS control, addressing the limitations of logic control. Firstly, an overview of optimal control methods is provided. Next, an optimal control approach for HRSs is introduced, leveraging Mixed Integer Nonlinear Programming (MINLP) to optimize system performance. Finally, the effectiveness of the proposed method is demonstrated through the results obtained from the HRSC simulator.

Overview of Optimal Control

Optimal control is an advanced control method based on mathematical optimization, aimed at adjusting the control variables of dynamic systems to achieve optimal performance while meeting various constraints. Its fundamental principles include establishing a mathematical model of the system, defining an objective function, specifying constraints, and solving the optimization problem. In system modelling, differential or difference equations are commonly used to describe dynamic behavior, while the objective function measures system performance. To solve optimal control problems, methods such as calculus of variations, dynamic programming, or iterative numerical optimization algorithms like gradient descent or Lagrange multipliers are often employed. These approaches effectively handle complex multi-variable constraint problems, ensuring that the optimal control strategy is found under the given constraints.

In the application of HRSs, optimal control methods optimize hydrogen flow, operational modes of equipment, and the balancing of multi-objective demands to achieve comprehensive improvement of system performance. The core advantages lie in dynamic adaptability and achieving global optimal performance. Unlike logic control methods, optimal control dynamically adjusts strategies in real-time based on the system's state, enabling it to adapt to complex and variable refuelling demand. Furthermore, optimal control not only meets single objectives but also achieves global optimization across multiple objectives, such as reducing operational costs, shortening refuelling times, and enhancing equipment utilization. Therefore, optimal control methods may significantly improve the operational efficiency of HRSs and effectively reduce energy waste.

MINLP is well-suited to address the optimal control problem for the unique characteristics of HRSs. HRSs involve continuous variables (such as hydrogen flow rate and pressure) as well as discrete variables (such as the on/off states of compressors or valves). MINLP provides a robust framework capable of simultaneously optimizing these continuous and discrete variables while accounting for nonlinear dynamics and constraints. This capability is crucial for

accurately modelling the physical and operational complexities of HRS components while addressing practical constraints such as safety protocols, energy limits, and operational scheduling. By employing MINLP, the optimization process can capture the intricate interactions between variables, ensuring that the refuelling process is efficient and energy-saving while maintaining high safety standards.

Mixed Integer Nonlinear Programming

MINLP is an optimization method that integrates integer programming with nonlinear programming, enabling the solution of complex problems that involve both discrete and continuous variables. In the context of HRS control, MINLP provides a powerful framework to formulate and solve optimization challenges that arise from the interplay of various operational and physical constraints.

The variables in the model are divided into continuous variables, such as flow, pressure, and temperature, and discrete variables, such as the on/off state of equipment or operational modes. Constraints are used to represent physical limitations and operational standards, such as capacity limits, safety thresholds, and legal regulations. Assumptions are made to simplify the problem, such as linearizing complex dynamic processes or ignoring minor nonlinear effects that do not significantly impact the results.

A crucial component of the MINLP formulation is the objective function, which serves as the guiding criterion for optimization. This function, whether linear or nonlinear, is designed to align with key operational goals, such as minimizing energy consumption, maximizing overall efficiency. By defining a clear performance metric, the objective function steers the optimization process toward improved operational effectiveness and cost efficiency.

Finally, the MINLP approach for HRS control seeks to achieve a balanced solution by carefully managing the trade-offs between discrete decision-making, such as switching operations, and continuous process adjustments, like pressure or flow control. Through this systematic optimization, the HRS can operate more efficiently, ensuring a reliable and energy-saving hydrogen refuelling process. MINLP consists of several key parts as follows.

- Assumptions can simplify the complexity of practical problems and provide computability and theoretical support.
- Integer variables can only take on discrete integer values, often used to model yes/no decisions or to choose between a limited number of options. Continuous variables can take any value within a defined range, typically representing quantities that can vary continuously, such as time, temperature, or amount of a substance.

- Equality constraints require that expressions involving both integer and continuous variables equate to a specific value, defining strict conditions that the solution must satisfy. Inequality constraints allow for a range of values by specifying that an expression must be greater than or less than a certain value, providing flexibility in the modelling. Variable bounds are the upper and lower bounds of variables, which define the feasible range of values.
- The objective function in MINLP is a function (linear/nonlinear) that represents the goal of the optimization problem, such as minimizing costs, maximizing profits, or optimizing performance indicators.

These parts are combined with the control problem of HRSs in the following.

Assumptions

To optimize the energy consumption of HRSs, an optimal control problem will be formulated. Before this, the system process of the controller should be described mathematically. As seen in Figure 4.1, the main components of HRSs include a compressor, cascade high pressure buffers, a precooler, and a dispenser. Based on these, some assumptions are given first.

- Any of the buffers can either be fueled or emptied at any given time, but not both (i.e., both operations cannot be carried out on the same buffer simultaneously) [12].
- The energy consumption of the compressor and cooling are linear to the running time.
- Only one vehicle is fuelling at each time (one dispenser is working).
- The remaining gas (hydrogen in the cube) is enough.
- Suppose hydrogen is an ideal gas, which means when the temperature is stable, the pressure is proportional to the mass.
- The switching cost is not considered.

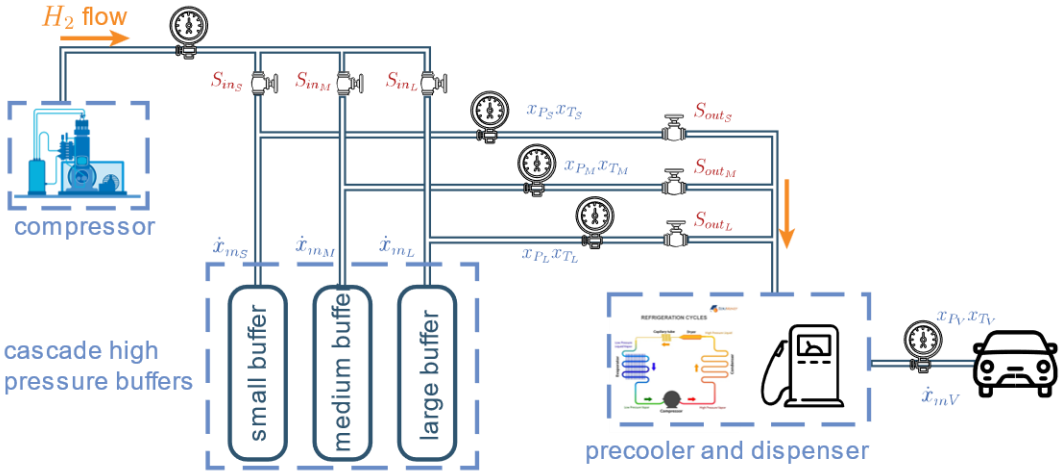

Figure 4.1 HRS system with defined variables.

Variables

To control HRSs more precisely, the transition of system states is considered to build the system model characterizing the operation of HRSs. The state variables are shown in Figure 4.1 as blue variables and defined in the following. For each buffer, the sensors report the real-time data to reflect the current state. The data used includes the pressure of buffers $x_{p_\#}$, temperature of buffers $x_{T_\#}$, and the flow rate of buffers $\dot{x}_{m_\#}$, where # represents S, M, or L which means small, medium, or large buffer. To illustrate the relationships of these data, some process variables are defined, which are the mass of gas $x_{m_\#}$ and the temperature change $\dot{x}_{T_\#}$. Similarly, the state variables for vehicles are also defined. However, sensors in HRSs may not always communicate with vehicle tanks in real-time. As a result, these values might not be available. The variables of system states are compiled in Table 4.1.

Table 0.1 System state variables.

	Unit	Small buffer	Medium buffer	Large buffer	Vehicle
Gas pressure	bar	x_{p_S}	x_{p_M}	x_{p_L}	x_{p_V}
Gas mass	g	x_{m_S}	x_{m_M}	x_{m_L}	x_{m_V}
Temperature	$\mathrm{°C}$	x_{T_S}	x_{T_M}	x_{T_L}	x_{T_V}
Flow rate	$\mathrm{g/s}$	$\dot{x}_{m_S}$	$\dot{x}_{m_M}$	$\dot{x}_{m_L}$	$\dot{x}_{m_V}$
Temperature changes	$\mathrm{°C/s}$	$\dot{x}_{T_S}$	$\dot{x}_{T_M}$	$\dot{x}_{T_L}$	$\dot{x}_{T_V}$

In this system, decision variables are defined as binary (binary variables, values of $0/1$), which can be reckoned as switches and are shown in Figure 4.1 as red valves. For each buffer, two channels are connected to them to control the inlet flow and outlet flow of hydrogen. As a result, decision variables are defined as the states of inlet and outlet valves on each buffer, namely, s_{in_S}, s_{out_S}, s_{in_M}, s_{out_M}, s_{in_L}, s_{out_L}.

Constraints

In Section 4.2.2, the variables involved in this problem have been defined, establishing a foundation for the optimization model. With the variables clearly identified, the next step is to introduce the constraints that govern the system's behavior and ensure feasible operation.

These constraints, which are crucial for accurately representing real-world limitations, are described in detail in the following sections.

(1) System dynamics

The constraints of system dynamics reveal the model of state evolution and relationships between different states, which are always described as differential equations.

1) Flow rate in buffers

The flow rate is the rate at which hydrogen passes through the buffer in a given time. When two containers (buffers, compressors, or vehicles) exchange gas, the flow rate between them is proportional to the difference in their pressure. Eqn. (1) is established with the term $c_{f_{in}}(p_{com} - x_{p_\#})s_{in_\#}$ describing the gas exchange between buffers and the compressor, as well as the term $c_{f_{out}}\left(x_{p_{S\#}} - x_{p_V}\right)s_{out_\#}$ describing the gas exchange between buffers and vehicles. Considering different conditions, two coefficients $c_{f_{in}}$ and $c_{f_{out}}$ are assigned to them.

$$\dot{\boldsymbol{x}}_{\boldsymbol{m_S}} = \boldsymbol{c_{f_{in}}}(\boldsymbol{p_{com}} - \boldsymbol{x_{p_S}})\boldsymbol{s_{in_S}} - \boldsymbol{c_{f_{out}}}\left(\boldsymbol{x_{p_S}} - \boldsymbol{x_{p_V}}\right)\boldsymbol{s_{out_S}}, \tag{1a}$$

$$\dot{x}_{m_M} = c_{f_{in}}(p_{com} - x_{p_M})s_{in_S} - c_{f_{out}}\left(x_{p_M} - x_{p_V}\right)s_{out_S}, \tag{1b}$$

$$\dot{x}_{m_L} = c_{f_{in}}(p_{com} - x_{p_L})s_{in_S} - c_{f_{out}}\left(x_{p_L} - x_{p_V}\right)s_{out_S}. \tag{1c}$$

However, when solving the MINLP problem, these constraints are too strict to find a feasible solution. As a result, Eqn. (1) is separated into two parts: Eqn. (2) and Eqn. (12). The equality constraints are separated into two parts of inequality constraints to clamp the value of the flow rate. It not only increases the flexibility of computation during compression and refuelling but also reduces the computational burden when there is no vehicle to be refueled.

Additionally, for safety considerations, the flow rate of the buffer has both upper and lower limits. A positive flow rate indicates that the buffer has a positive flow, meaning hydrogen is flowing in (the compressor is operating), while a negative flow rate indicates that the buffer has a negative flow, meaning hydrogen is flowing out (the dispenser is operating). There are 2 distinct circumstances:

1) Positive flow rate is determined by the compressor's flow capacity, or in other words, by the initial system design.

2) Negative flow rate is governed by the dispenser by the SAE J2601 refuelling protocol.

The maximum flow rate of the compressor is defined as a constant value v_{cmax}, and the maximum flow rate of the dispenser is defined as a constant value v_{dmax}.

$$-v_{dmax} \leq \dot{x}_{m_S} \leq c_{f_{in}}(p_{com} - x_{p_S})s_{in_S} \leq v_{cmax}, \tag{2a}$$

$$-v_{dmax} \leq \dot{x}_{m_M} \leq c_{f_{in}}(p_{com} - x_{p_M})s_{in_M} \leq v_{cmax}, \tag{2b}$$

$$-v_{dmax} \leq \dot{x}_{m_L} \leq c_{f_{in}}(p_{com} - x_{p_L})s_{in_L} \leq v_{cmax}. \tag{2c}$$

2) Ideal gas relationship of buffers

This is one of the assumptions of the HRSC simulator. In the simulation, the hydrogen is assumed to obey the ideal gas rule. In Eqn. (3), variable R is the gas constant equal to $8.3145\, J \cdot K^{-1} \cdot mol^{-1}$, where pressure is expressed in pascals, volume in cubic meters, and absolute temperature in kelvin. Variable M is the molar mass of hydrogen equal to 0.002016 in the simulator. Variables $V_{S/M/L}$ are the volume of three buffers.

$$x_{p_S}V_S = \frac{x_{m_S}Rx_{T_S}}{M}, \qquad x_{p_M}V_M = \frac{x_{m_M}Rx_{T_M}}{M}, \qquad x_{p_L}V_L = \frac{x_{m_L}Rx_{T_L}}{M}. \tag{3}$$

3) Temperature changes of buffers

In the HRSC simulator, the proper coefficients to describe different procedures of gas exchanges are obtained by assuming the temperature change of buffers is linear to the time, as presented in Eqn. (4). Variables $c_{T_{Sin}}$, $c_{T_{Sout}}$ and c_{T_n} are the coefficients of the input valve, output valve, and environmental heat exchange, respectively. In the simulator, the environmental temperature T_{env} is assumed to be a constant value of $25°C$.

$$\dot{x}_{T_S} = c_{T_{Sin}}s_{in_S} - c_{T_{Sout}}s_{out_S} + c_{T_n}(T_{env} - x_{T_S}), \tag{4a}$$

$$\dot{x}_{T_M} = c_{T_{Min}}s_{in_M} - c_{T_{Mout}}s_{out_M} + c_{T_n}(T_{env} - x_{T_M}), \tag{4b}$$

$$\dot{x}_{T_L} = c_{T_{Lin}}s_{in_L} - c_{T_{Lout}}s_{out_L} + c_{T_n}(T_{env} - x_{T_L}). \tag{4c}$$

4) Temperature evolution of buffers

The temperature of buffers evolves according to the rate calculated in Eqn. (4). The system is assumed to be a discrete-time system with a sampling period of one second. Then, the evolution of the temperature can be formulated as Eqn. (4a).

$$x_{T_S}(k+1) = x_{T_S}(k) + \dot{x}_{T_S}(k), \tag{5a}$$

$$x_{T_M}(k+1) = x_{T_M}(k) + \dot{x}_{T_M}(k), \tag{5b}$$

$$x_{T_L}(k+1) = x_{T_L}(k) + \dot{x}_{T_L}(k). \quad (5c)$$

(2) Condition dependent constraints

The refuelling process in HRSs is a time-varying optimization problem, meaning that constraints vary according to different conditions. Specifically, the system states depend on whether a vehicle is being refueled. If there is no vehicle, the system stays in a stable state, or the compressor refuels the buffers. When the vehicle is refuelling, system dynamics change with the dispensing process. These two conditions are considered. For each condition, constraints are different and presented as follows.

1) Condition 1: At least one vehicle

Under this condition, the states and dynamic equations of the vehicles refuelling, as well as their influence on the HRS, need to be considered.

- The flow rate of a vehicle represents that the flow rate of the vehicle is proportional to the pressure difference between vehicles and cascade high pressure buffers. It depends on whether the valve is open or close to the dispenser. $c_{f_{out}}$ is a flow rate constant.

$$\dot{x}_{m_V} = c_{f_{out}}\left(\left(x_{p_S} - x_{p_V}\right)s_{out_S} + \left(x_{p_M} - x_{p_V}\right)s_{out_M} + \left(x_{p_L} - x_{p_V}\right)s_{out_L}\right). \quad (6)$$

- The flow rate of each buffer. As mentioned in Eqn. (1), the second part of the buffer flow rate is only considered in Condition 1. For each buffer, if it is used to dispense, its flow rate is proportional to the difference of pressures and the value should be equal to the flow rate of the vehicle. $c_{f_{out}}$ is the same as the one in Eqn. (1).

$$\dot{x}_{m_S} \geq -c_{f_{out}}\left(x_{p_S} - x_{p_V}\right)s_{out_S}, \quad (7a)$$

$$\dot{x}_{m_M} \geq -c_{f_{out}}\left(x_{p_M} - x_{p_V}\right)s_{out_M}, \quad (7b)$$

$$\dot{x}_{m_L} \geq -c_{f_{out}}\left(x_{p_L} - x_{p_V}\right)s_{out_L}. \quad (7c)$$

- The relationship between the pressure and temperature of vehicles follows the ideal gas law, as shown in Eqn. (3). All the values of parameters are the same as in Eqn. (3).

$$x_{p_V}V_V = \frac{x_{m_V}Rx_{T_V}}{M}. \quad (8)$$

- Temperature changes of vehicles correspond to the state refuelling. If it is in the refuelling process, the temperature will increase; however, if it is pending, it will cool down due to the heat exchanges with the environment. c_{T_n} and T_{env} are the speed of temperature exchange and the environmental temperature, which are the same as in Eqn. (4). c_{T_V} is the speed of temperature exchange when a vehicle is refueled.

$$\dot{x}_{T_V} = c_{T_V}\left(s_{out_S} + s_{out_M} + s_{out_L}\right) + c_{T_n}\left(T_{env} - x_{T_V}\right). \quad (9)$$

Similar to Eqn.(5), the temperature of vehicles follows the same rule.

$$x_{T_V}(k+1) = x_{T_V}(k) + \dot{x}_{T_V}(k). \quad (10)$$

- Max/min flow rate of the dispenser. This is a bounded constraint of the flow rate, which is required in the SAE J2601 protocol [4]. This protocol also indicates that $v_{dmax} = 60g/s$ which is defined in Eqn. (2). The maximum flow rate of the compressor is assumed as $v_{cmax} = 60g/s$ accordingly.

$$0 \le \dot{x}_{m_V} \le 60\text{g/s} \quad (11)$$

- The flow rate of buffers is defined as follows. The threshold of the pressure difference between buffers and vehicles during the refuelling process should be greater than $p_{dref} = 100\ bar$.

$$\dot{x}_{m_S} \ge -c_{f_{out}}\left(x_{p_S} - x_{p_V}\right)s_{out_S} \quad (12a)$$

$$\dot{x}_{m_M} \ge -c_{f_{out}}\left(x_{p_M} - x_{p_V}\right)s_{out_M} \quad (12b)$$

$$\dot{x}_{m_L} \ge -c_{f_{out}}\left(x_{p_L} - x_{p_V}\right)s_{out_L} \quad (12c)$$

$$\left(x_{p_S} - x_{p_V} - p_{dref}\right)s_{out_S} \ge 0 \quad (12d)$$

$$\left(x_{p_M} - x_{p_V} - p_{dref}\right)s_{out_M} \ge 0 \quad (12e)$$

$$\left(x_{p_L} - x_{p_V} - p_{dref}\right)s_{out_L} \ge 0 \quad (12f)$$

- The maximum temperature of vehicles is set to follow safety restrictions. It is set as $T_{Vmax} = 80°\text{C}$ in the simulation.

$$x_{T_V} \le T_{Vmax}. \quad (13)$$

2) Condition 2: No vehicle

When there is no vehicle, the HRS returns to a setting state, and all dispenser valves are then closed.

$$s_{out_S} = 0, \qquad s_{out_M} = 0, \qquad s_{out_L} = 0. \quad (14)$$

(3) Limitations and requirements

The constraints represent the limitations of the system or the requirements of users. They can be revised based on different conditions when applying this method.

- The maximum temperature of buffers in the simulation is set as $T_{bmax} = T_{Vmax} = 80°\mathrm{C}$.

$$x_{T_S} \leq T_{bmax}, \qquad x_{T_M} \leq T_{bmax}, \qquad x_{T_L} \leq T_{bmax}. \tag{15}$$

- The threshold of the inlet valve is set to $800\ bars$. If the pressure of a buffer is greater than this threshold, this buffer is not in the refuelling process and will not be refueled by the compressor to optimize operational efficiency. The k in Eqn. (16 a, b, and c) represents the current time instant. The $s_{in_S}(k-1)$ represents the decision value in the last time instant, which is a constant value, $M \geq 0$ is a large enough real constant.

$$s_{in_S}(k) - 1 \leq s_{in_S}(k-1) - \frac{\left(x_{p_S}(k) - 800\right)}{M} \tag{16a}$$

$$s_{in_M}(k) - 1 \leq s_{in_M}(k-1) - \frac{\left(x_{p_M}(k) - 800\right)}{M} \tag{16b}$$

$$s_{in_L}(k) - 1 \leq s_{in_L}(k-1) - \frac{\left(x_{p_L}(k) - 800\right)}{M} \tag{16c}$$

- Inlet and outlet valves cannot open simultaneously for each buffer.

$$s_{in_S} + s_{out_S} \leq 1, \qquad s_{in_M} + s_{out_M} \leq 1, \qquad s_{in_L} + s_{out_L} \leq 1. \tag{17}$$

- The number of compressors could be one or more, which is set by a constant n_{com}. In the simulation, only the condition $n_{com} = 1$ is considered, which is the same as the condition of the real HRSs in Section 5.

$$s_{in_S} + s_{in_M} + s_{in_L} \leq n_{com}. \tag{18}$$

- The number of dispensers is set to one in a set of equipment in our simulation, so the sum of all buffers to the outlet valve should be less than one.

$$s_{out_S} + s_{out_M} + s_{out_L} \leq 1 \tag{19}$$

Objective Function

In this project, the following three objectives are considered.

- $J_1(k)$ is the sum of the energy consumption of all buffers and is defined as

$J_1(k)$ $$J_1(k) = e_S(k) + e_M(k) + e_L(k). \tag{20}$$

introduces the energy-saving optimization aspect. Each term is defined as follows.

where

$$e_S(k) = c_{e_{in}} s_{in_S}(k) + c_{e_{out}} s_{out_S}(k), \tag{21a}$$

c_{in} and

$$e_M(k) = c_{e_{in}} s_{in_M}(k) + c_{e_{out}} s_{out_M}(k), \tag{21b}$$

c_{out} are

$$e_L(k) = c_{e_{in}} s_{in_L}(k) + c_{e_{out}} s_{out_L}(k), \tag{21c}$$

the weights of cost from the compressor and precooler of the dispenser. Since the compressor costs more energy than the precooler in a time instant, $c_{in} : c_{out}$ is set to $2:1$ in the simulation.

As mentioned in Section 3.4.1, the ratio in the current literature is not a fixed value. In this simulation, a $2:1$ coefficient is adopted as an assumption to weigh their energy consumption in the objective function. This parameter is adjustable based on practical requirements.

- $J_2(k)$, which prioritizes refuelling efficiency, represents the effort to replenish buffers, defined as

$$J_2(k) = \left(x_{p_S}(k) - p_{max}\right)^2 + \left(x_{p_M}(k) - p_{max}\right)^2 + \left(x_{p_L}(k) - p_{max}\right)^2. \tag{22}$$

p_{max} is the maximum pressure of each buffer and is defined as 875 *bars*.

- $J_3(k)$ considers vehicle refuelling as the objective, which serves as the foundational requirement to maintain basic HRS operations, defined as

The

$$J_3(k) = \left(x_{p_V}(k) - x_{p_{vmax}}\right)^2. \tag{23}$$

squared difference between the current pressure of the vehicle and the maximum pressure $x_{p_{vmax}}$ represents the effort required to refuel the vehicle, where $x_{p_{vmax}}$ is 700 *bars*. As a result, $J_3(k)$ is an essential component of the objective function.

Consider these three aspects, the objective function of the MINLP at time instant k with a prediction horizon t is formulated as:

where c_{eng}, c_b and c_v

$$J(k) = \sum_{i=0}^{t} \left(c_{eng} J_1(k+i) + c_b J_2(k+i) + c_v J_3(k+i)\right) \tag{24}$$

are the coefficients of J_1, J_2, and J_3, respectively. Meanwhile, the prediction horizon t means the length of the time-period or time step that is considered when predicting the behavior of the system in the future. The controller performance will be better if the prediction horizon t is longer, but the computational load will also increase dramatically.

After constructing all components of the optimization problem, the MINLP is given as:

To

$$\begin{aligned} &\min && \text{Eqn. (24)} \\ &\text{s.t.} && \text{Eqn. (1) to Eqn. (19)} \end{aligned} \tag{25}$$

analyze the impact of the coefficients in the objective function, three different coefficient setups are adopted to illustrate the trade-off in the MINLP algorithm between energy savings and refuelling efficiency. The coefficient setups and corresponding objective functions are listed in Table 4.2.

Table 0.2 MINLP control methods with three sets of objective function coefficients.

	Coefficients	Objective function
MINLP 1	$c_{eng} = c_b = c_v = 1$	$J(k) = \sum_{k=0}^{t}(J_1 + J_2 + J_3)$
MINLP 2	$c_{eng} = c_b = 0,$ $c_v = 1$	$J(k) = \sum_{k=0}^{t}\left(x_{p_V} - x_{p_{vmax}}\right)^2$
MINLP 3	$c_b = 0,$ $c_{eng} = c_v = 1$	$J(k) = \sum_{k=0}^{t}\left(e_S(k) + e_M(k) + e_L(k) + \left(x_{p_V} - x_{p_{vmax}}\right)^2\right)$

(1) MINLP 1

This setup regards the minimization of J_1, J_2, and J_3 as equally important. MINLP 1 is more efficient and aggressive in refuelling vehicles since buffers can be replenished in the refuelling process to maintain a higher buffer pressure. This strategy tries to replenish buffers and vehicles as fast as possible to satisfy the objective. This approach results in higher buffer pressures on average, which:

1. Reduces refuelling time for FCEVs (due to stronger pressure differentials)
2. Increases compressor runtime (t_{comp}) to maintain high buffer pressures, resulting in higher energy consumption.

(2) MINLP 2

This setup focuses solely on the objective of refuelling vehicles, without considering the energy consumption of HRSs or the effort to replenish buffers as optimization factors. The primary goal of MINLP 2 is to refuel the vehicles. Although the MINLP 2 uses refuelling the vehicles as the unique objective, the efficiency of refuelling may not be the highest compared to other methods, as the buffers operate continuously at low pressure in scenarios with high demand.

(3) MINLP 3:

This condition focuses solely on the energy required to refuel the vehicles and does not account for the energy consumption for buffer replenishment. The strategy aims to minimize the use of the compressor, which in turn reduces energy consumption. As a

result, this method should be the most energy-saving strategy, as it minimizes compressor usage as much as possible.

Unlike logic controllers, in optimal controllers, the dispenser does not inherently hold a higher priority than the compressor. The prioritization between these components is determined by our selected control objectives.

Simulation Results

To compare the MINLP control methods with the logic controllers in Section 3 and confirm whether the performance of MINLP matches our design, the simulation results of MINLP under S1-S4 are discussed in this section. The HRS setup in this section is the same as in Table 2.1.

In the simulation, the performance of three objective functions is compared with the prediction horizon fixed at $t = 1$. This means it can compute one step of control input and predict the system states of the HRS one step ahead. The primary reason for this choice is the computational limitations of the hardware. The sampling period of the HRS varies in different conditions, and the minimum sampling period is one second during refuelling. The MINLP problem must be solved within one second.

MINLP under S1 and S2

The simulation results of the MINLP controller in scenario S1 are shown in Figures 4.2, 4.3, and 4.4. Subfigures (a) and (b) in these figures illustrate the differences in control execution between MINLP 1, MINLP 2, and MINLP 3.

By comparing the inlet valve switching results of MINLP 1, MINLP 2, and MINLP 3, it can be observed that MINLP 1 acts like a single buffer, and the compressor does not shut down until the entire refuelling session is completed. This behavior arises because MINLP 1 simultaneously optimizes all three objective functions, J1, J2, and J3, aiming to achieve a balanced trade-off among them. As a result, MINLP 1 frequently switches among the three buffers. This rapid switching is an outcome of the optimization process, which yields relatively uniform utilization across all buffers. It is worth noting that although the switching is frequent, it still complies with all timing constraints.

By observing Figures 4.3(e) and 4.4(e), it can be found that the compressor is activated beyond 4000s while the pressure of buffers is higher than 800 bars. This phenomenon may happen because 800 bars is a singular value of the pressure in Eqn. (16 a, b, and c). Since M is a large enough constant, $(x_{p\#} - 800)/M$ is very small with an undefined sign (determined by the value of $x_{p\#}$). Assuming this value is δ, then when $s_{in}(k-1) = 0$ and $x_{p\#} \geq 800$, the

$s_{in}(k) \leq 1 - \delta < 1$, which means $s_{in}(k)$ must be 0 (close). On the contrary, if $x_{p\#} < 800$, $s_{in}(k) \leq 1 + \delta < 2$, which means $s_{in}(k)$ can be 0 or 1 (close/open). However, when the optimizer (Python-based Gurobi optimizer) solves this complex MINLP problem with nonlinear and joint parameters, there may be some problems with computational accuracy and slight oscillations around the singular value (800 bars), leading to the phenomenon in Figures 4.3(e) and 4.4(e).

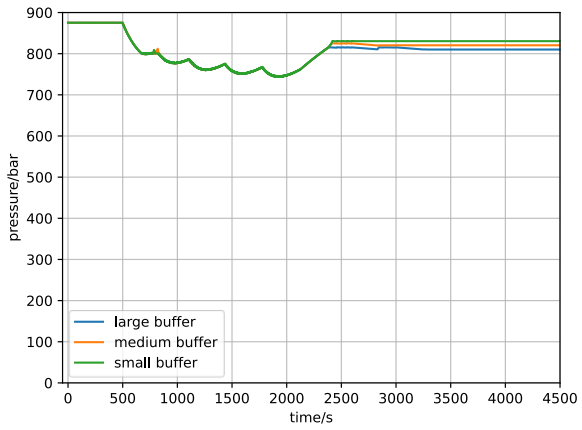

(a) Pressure changes of buffers.

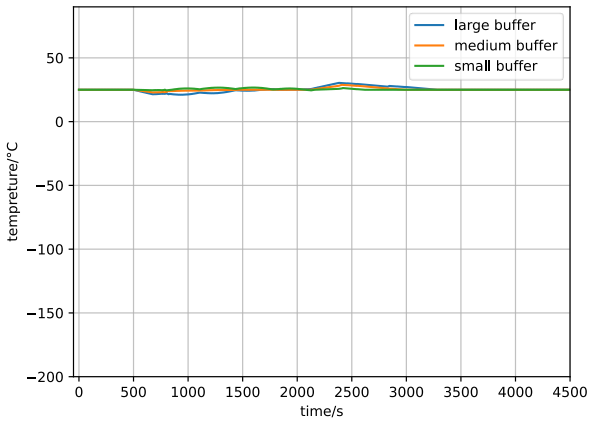

(b) Temperature changes of buffers.

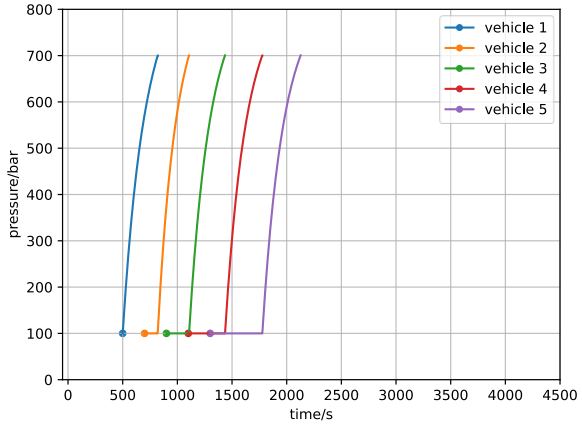

(c) Pressure changes of vehicles. Each color represents one vehicle.

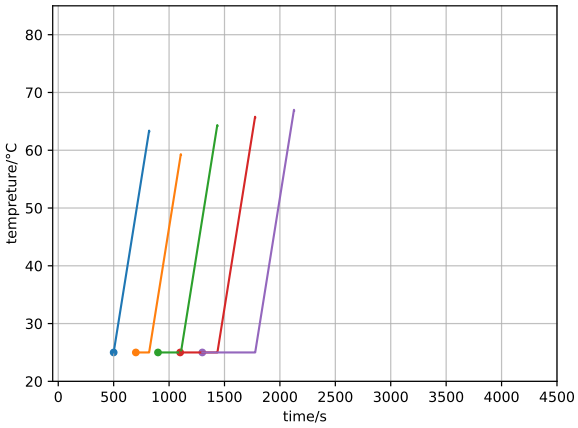

(d) Temperature changes of vehicles. Each color represents one vehicle.

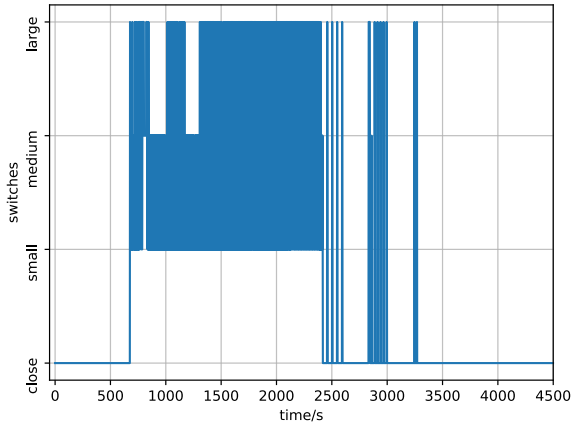

(e) Inlet valve switches buffers.

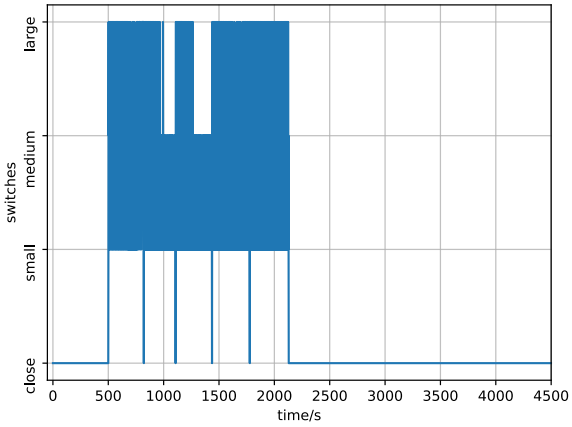

(f) Outlet valve switches buffers.

Figure 4.1 Simulation in S1 using MINLP 1.

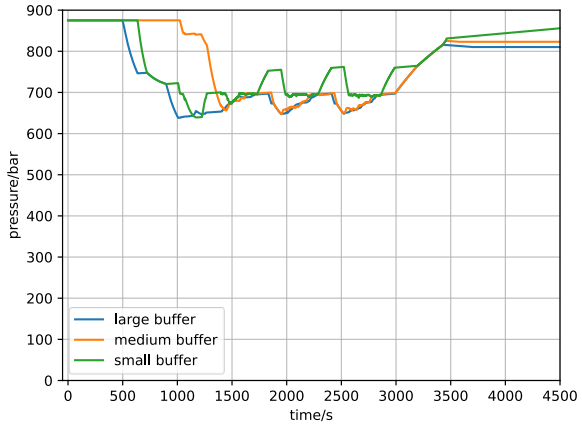

(a) Pressure changes of buffers.

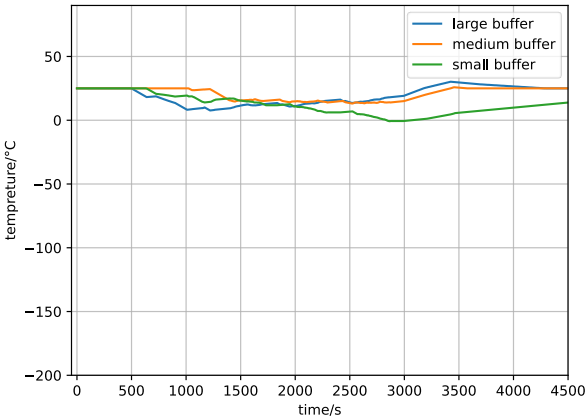

(b) Temperature changes of buffers.

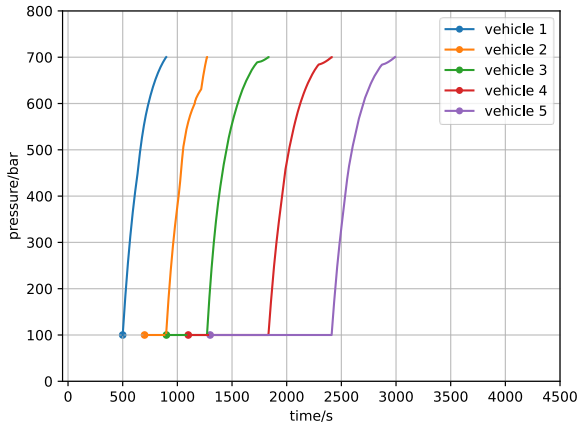

(c) Pressure changes of vehicles.
Each color represents one vehicle.

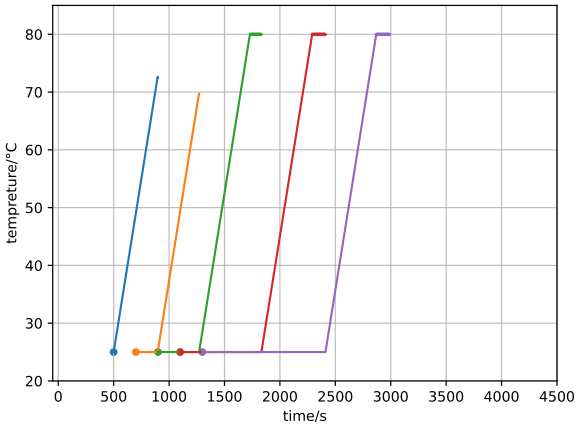

(d) Temperature changes of vehicles.
Each color represents one vehicle.

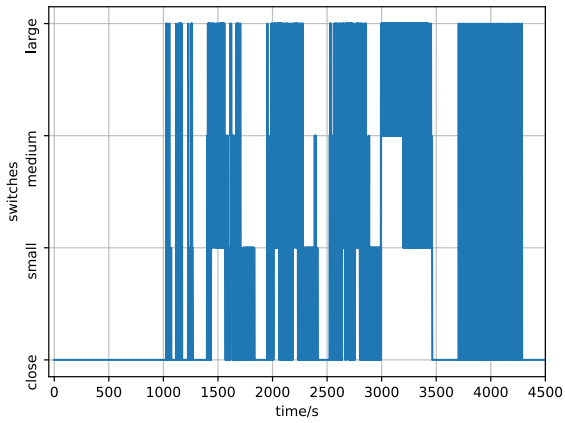

(e) Inlet valve switches buffers.

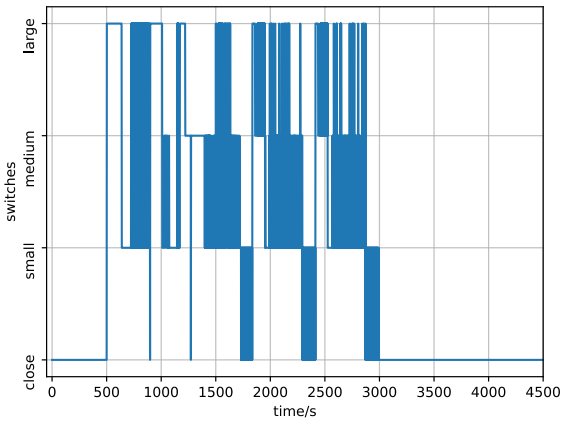

(f) Outlet valve switches buffers.

Figure 4.2 Simulation in S1 using MINLP 2.

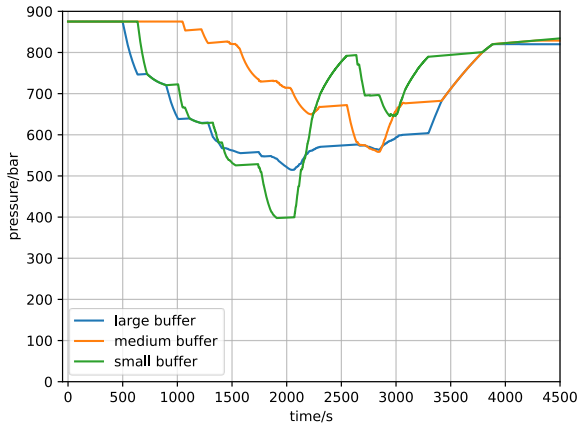

(a) Pressure changes of buffers.

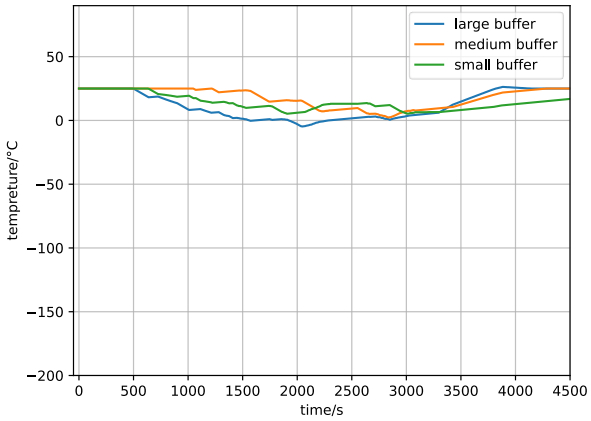

(b) Temperature changes of buffers.

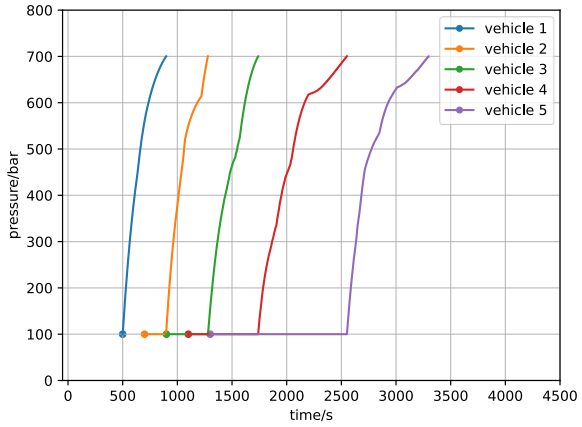

(c) Pressure changes of vehicles. Each color represents one vehicle.

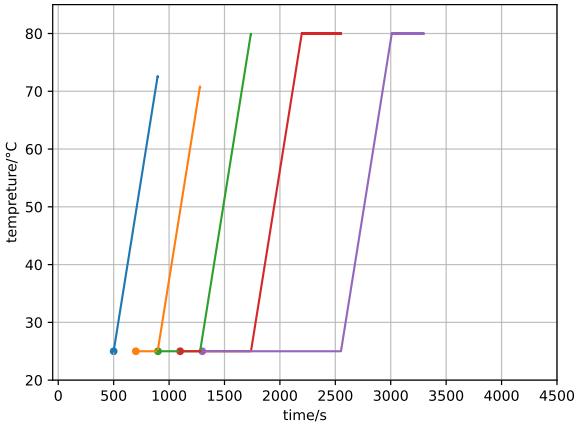

(d) Temperature changes of vehicles. Each color represents one vehicle.

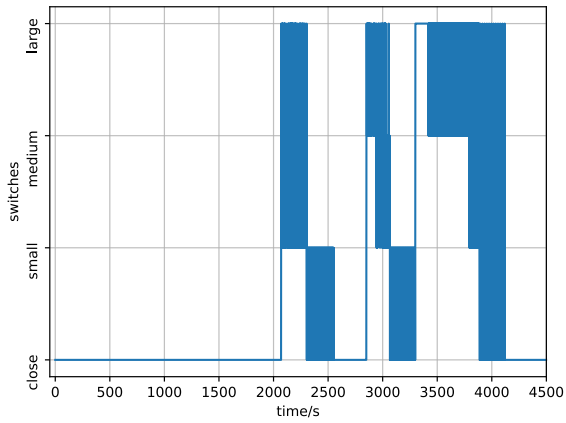

(e) Inlet valve switches buffers.

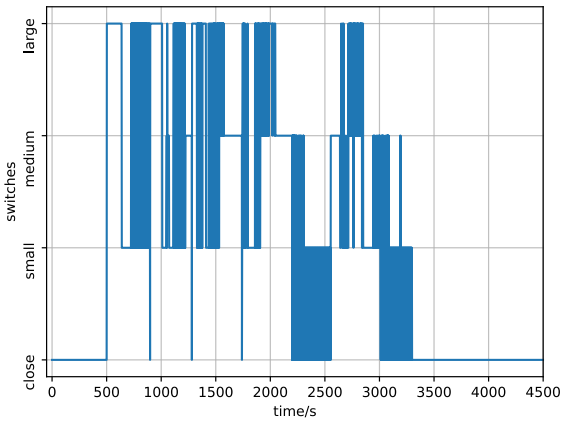

(f) Outlet valve switches buffers.

Figure 4.3 Simulation in S1 using MINLP 3.

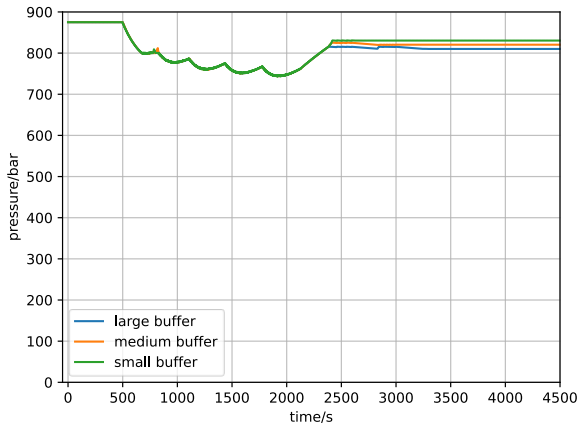

(a) Pressure changes of buffers.

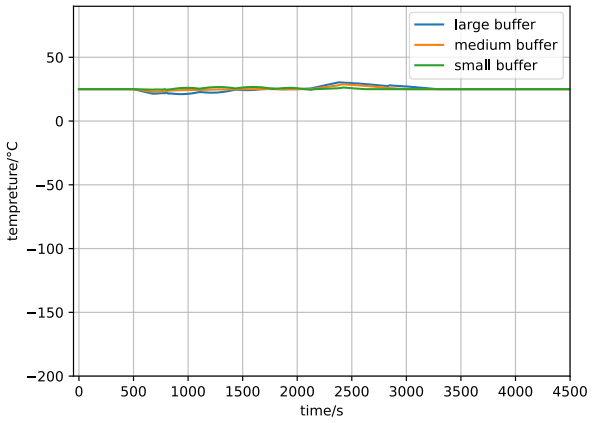

(b) Temperature changes of buffers.

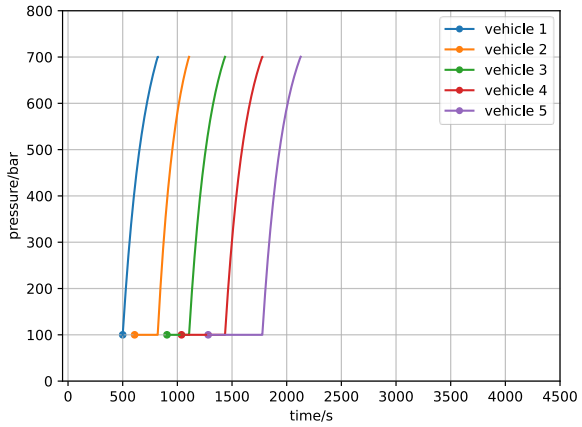

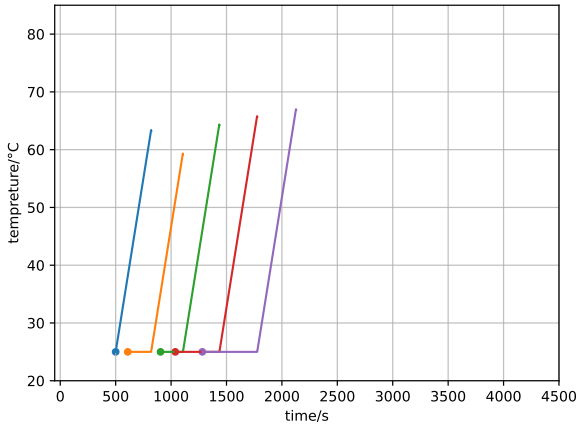

(c) Pressure changes of vehicles. Each color represents one vehicle.

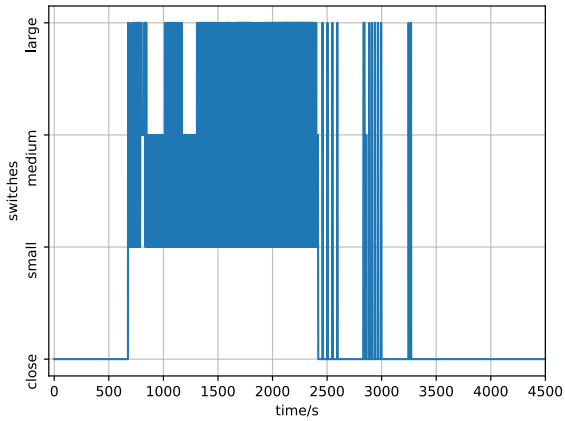

(d) Temperature changes of vehicles. Each color represents one vehicle.

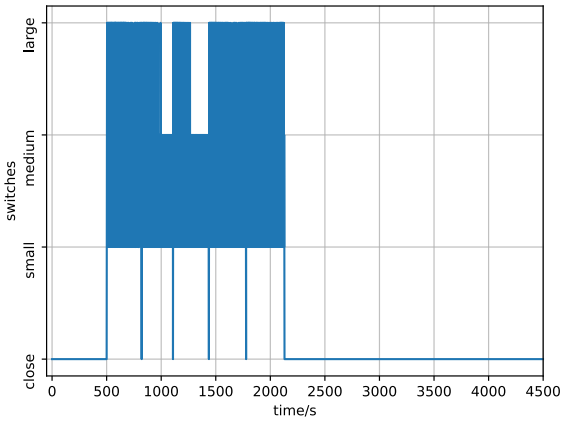

(e) Inlet valve switches buffers.

(f) Outlet valve switches buffers.

Figure 4.4 Simulation in S2 using MINLP 1.

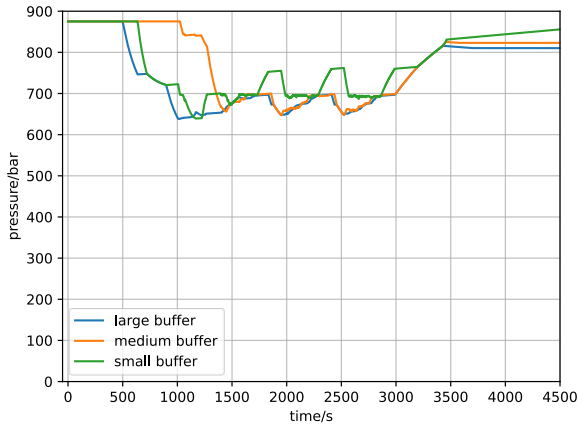

(a) Pressure changes of buffers.

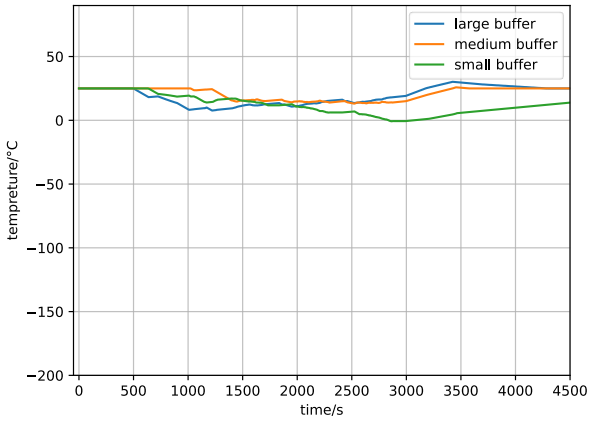

(b) Temperature changes of buffers.

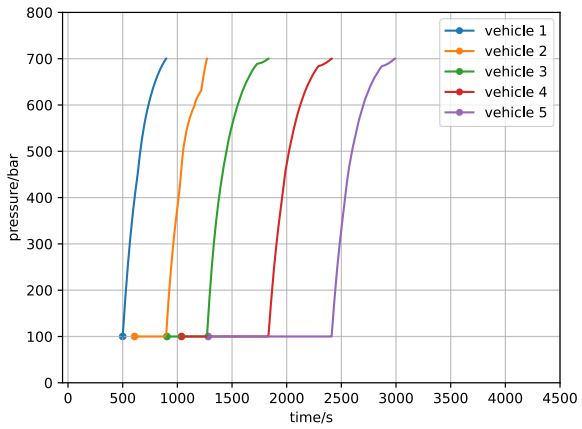

(c) Pressure changes of vehicles. Each color represents one vehicle.

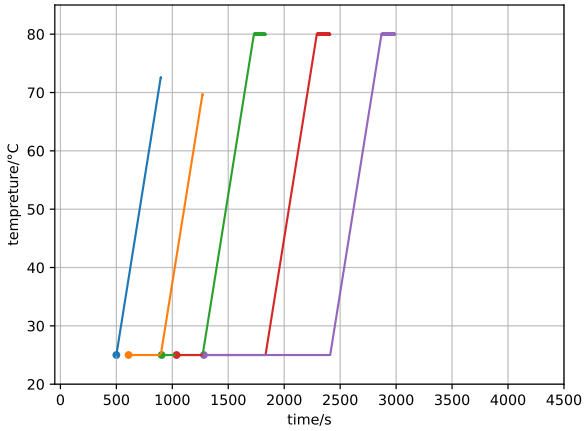

(d) Temperature changes of vehicles. Each color represents one vehicle.

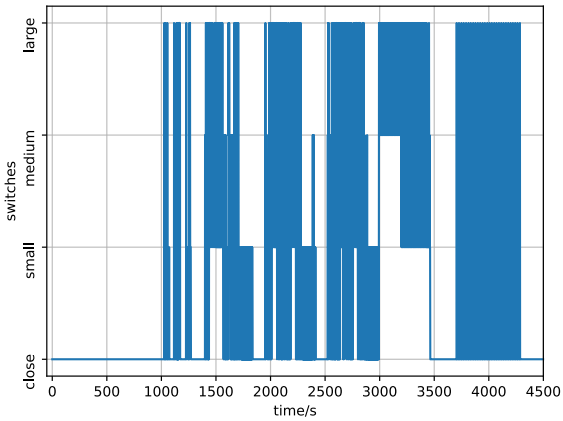

(e) Inlet valve switches buffers.

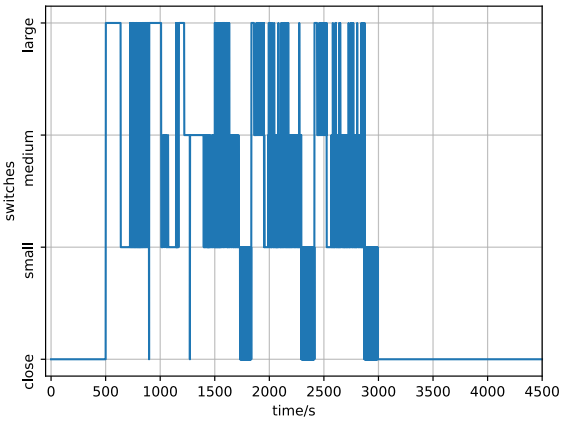

(f) Outlet valve switches buffers.

Figure 4.5 Simulation in S2 using MINLP 2.

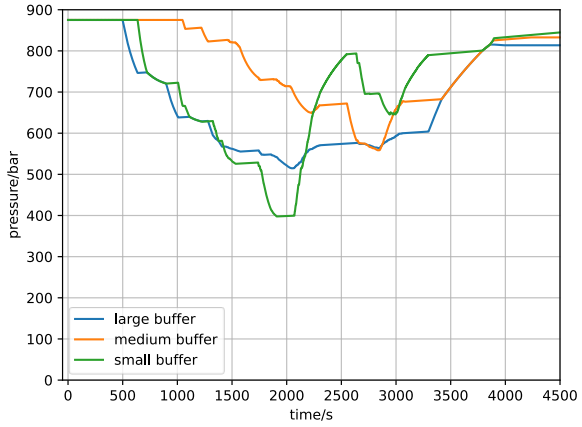

(a) Pressure changes of buffers.

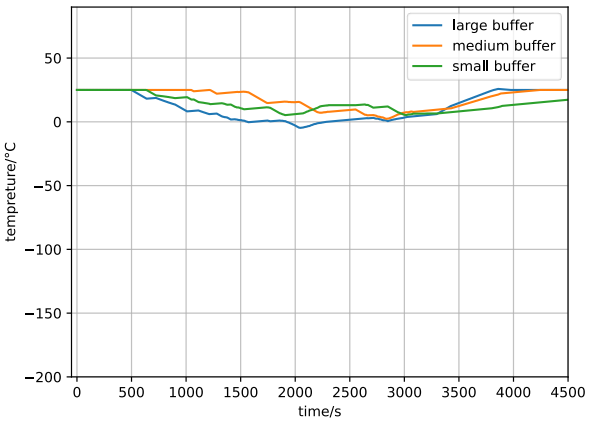

(b) Temperature changes of buffers.

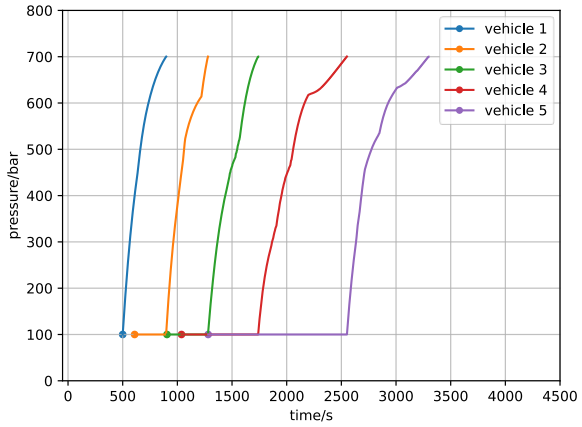

(c) Pressure changes of vehicles. Each color represents one vehicle.

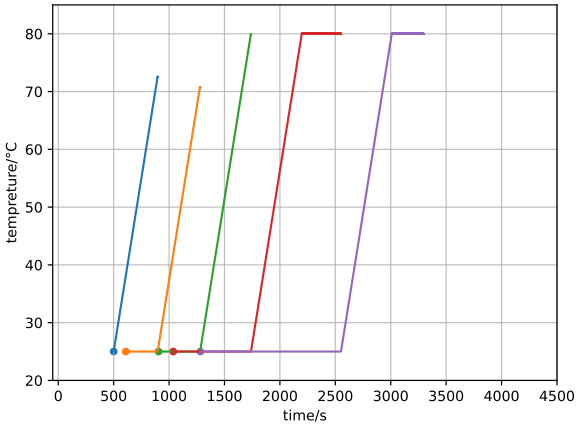

(d) Temperature changes of vehicles. Each color represents one vehicle.

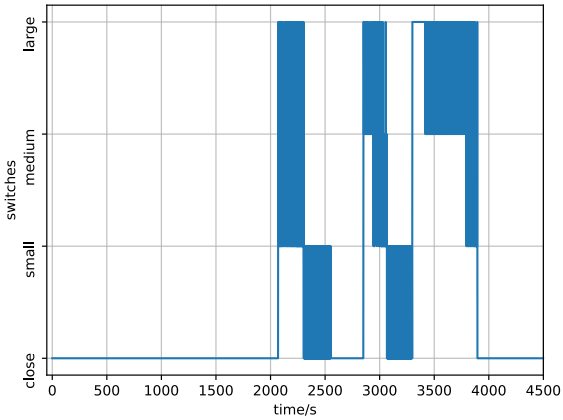

(e) Inlet valve switches buffers.

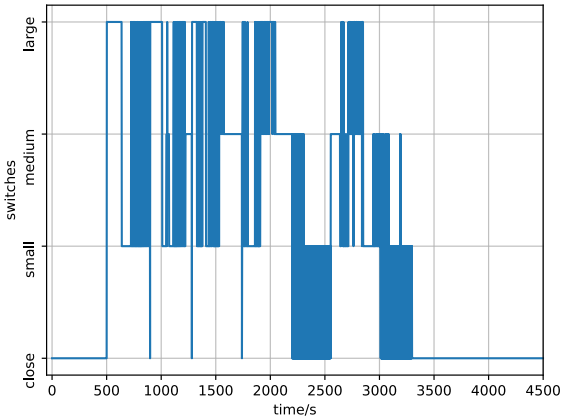

(f) Outlet valve switches buffers.

Figure 4.6 Simulation in S2 using MINLP 3.

The refuelling time for each MINLP method varies (Subfigures (c) and (d) in Figures 4.2, 4.3, and 4.4). The MINLP 1 method has the shortest refuelling time of $2200\ s$. In comparison, the refuelling times for MINLP 2 and MINLP 3 are $3000\ s$ and $3300\ s$, which are 36.4% and 50% longer than that of MINLP 1, respectively. Whenever the vehicle tank temperature reaches the safety threshold of 80°C, the hydrogen flow rate will be reduced to allow the vehicle tank temperature to stay at or below the threshold. Hence, this would lead to an extend refuelling time. This process extends the total refueling time for the vehicle. Subfigures (e) and (f) show that MINLP 1 has the most frequent buffer switches between the compressor and buffers and between buffers and the dispenser. Figures 4.5, 4.6, and 4.7 show the simulation results of the MINLP controllers for scenario S2. Similar to scenario S1, the results of the three MINLP controllers under S2 conditions lead to the same conclusions. It can be observed that the MINLP 2 controller strikes a balance between MINLP 1 and MINLP 3, representing a trade-off that integrates the advantages of both approaches. This balance highlights the system's effort

to distribute buffer utilization more evenly, thereby optimizing operational dynamics and enhancing overall system efficiency.

Table 0.1 Performance of controllers under S1 dense traffic flow.

Scenario		$t_{total}(s)$		$t_{avg}(s)$		$t_{comp}(s)$		$t_{dis}(s)$	
S1	LC-1	1140	\	228	\	1788	\	1763	\
	LC-2	1156	1.40%	231	1.32%	1741	-2.63%	1789	1.47%
	MINLP 1	**993**	**-12.89%**	**198**	**-13.16%**	1790	0.11%	**1624**	**-7.88%**
	MINLP 2	1704	49.47%	340	49.12%	1405	-21.42%	2317	31.42%
	MINLP 3	1844	61.75%	368	61.40%	**1288**	**-27.96%**	2474	40.33%

Table 0.2 Performance of controllers under S2 dense traffic flow.

Scenario		$t_{total}(s)$		$t_{avg}(s)$		$t_{comp}(s)$		$t_{dis}(s)$	
S2	LC-1	1226	\	245	\	1788	\	1763	\
	LC-2	1242	1.31%	248	1.22%	1741	-2.63%	1789	1.47%
	MINLP 1	**1079**	**-11.99%**	**215**	**-12.24%**	1790	0.11%	**1624**	**-7.88%**
	MINLP 2	1790	46.00%	358	46.12%	1405	-21.42%	2317	31.42%
	MINLP 3	1930	57.42%	386	57.55%	**1288**	**-27.96%**	2474	40.33%

The performance of MINLP controllers in S1 (Table 4.3) and S2 (Table 4.4) is summarized above. Observations from these two tables reveal that under scenarios with a high density of vehicles waiting to refuel in short durations, the results are consistent. Compared to LC-1, MINLP 1 significantly reduces both the waiting and refuelling time for vehicles. MINLP 3 reduces the running time of the compressor, but it increases the waiting time for vehicles. MINLP 2 exhibits effects similar to MINLP 3, but the results of MINLP 3 are more extreme.

In contrast, MINLP 1 simultaneously considers J_1, J_2, and J_3, comprehensively optimizing energy consumption, replenishing buffer performance, and vehicle refuelling efficiency, reducing the total waiting time (t_{total}) of all vehicles. Although t_{comp} increases slightly, MINLP 1 achieves an overall optimized performance compared to other algorithms, demonstrating the effectiveness of the optimized control strategy. Furthermore, results from MINLP 2 and MINLP 3 show that optimizing buffer replenishment performance J_2, can effectively reduce compressor running time. Moreover, compared to MINLP 2, MINLP 3 also optimizes J_1, reducing energy consumption and further decreasing t_{comp}. However, the drawback is evident: Other control

methods complete refuelling more quickly than MINLP 2 and MINLP 3, which requires additional time to finish the process. Therefore, when vehicle density is low, MINLP 2 and MINLP 3 can be used to reduce the running time of the compressor and extend the compressor lifespan. Conversely, when vehicle density is high, MINLP 1 can be employed to improve the overall operational efficiency of the HRS.

Finally, this project aims to address the critical trade-off in vehicle refuelling time. As shown in Table 4.3 and Table 4.4, control methods that reduce energy consumption often lead to longer vehicle waiting times. This correlation stems from their operational approach of maintaining the buffer at a lower average pressure, which reduces the dispenser flow rate and extends refuelling time. This outcome represents an inevitable compromise in achieving higher energy efficiency. The most evident example is the MNLP 3 method in S1, which, compared to LC-1, reduces compressor operating time by 27.96% but increases vehicle waiting time by 61.4%. Therefore, in actual HRS operation, the control objective weights can be adjusted based on real-time traffic conditions to balance compressor running time and vehicle waiting time.

MINLP under S3 and S4

The simulation results for longer time periods are also discussed in this section. The results of scenario S3 are shown in Figure 4.8, Figure 4.9, and Figure 4.10. The subfigures (c) and (d) show the total duration and the corresponding percentage that the inlet and outlet valves of buffers are in throughout the entire simulation process from these three strategies. For S3, MINLP 2 and 3 use medium and small pressure buffers more frequently (Figures 4.9(c)(d) and 4.10(c)(d)), resulting in buffer temperatures significantly lower than those observed in MINLP 1. The simulation results also show that the pressure and temperature of the vehicles are within the safety range. Overall, MINLP 2 has a balanced usage of these three buffers. MINLP 2 and 3 are similar in buffer utilization ratios. Compared to MINLP 1 and 3, MINLP 2 has a moderate control strategy.

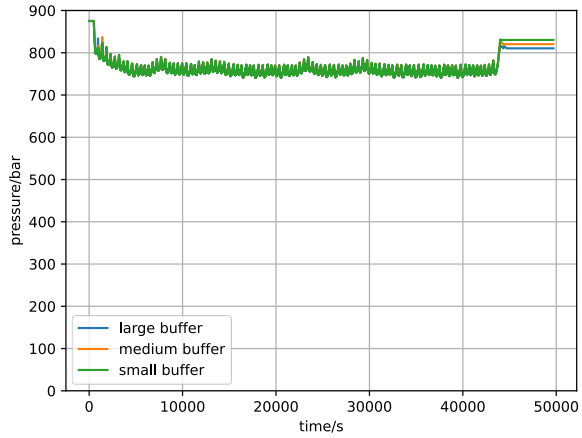

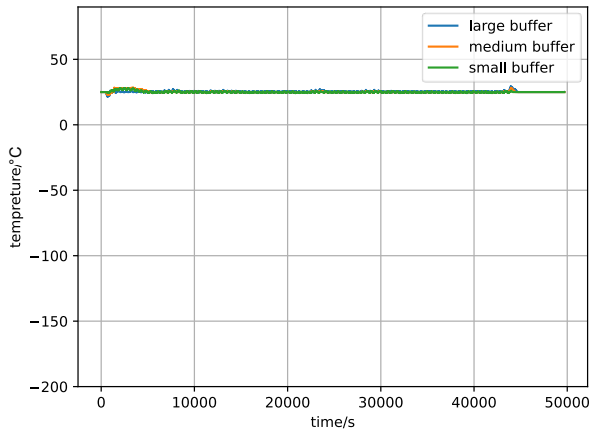

(a) Pressure changes of buffers.

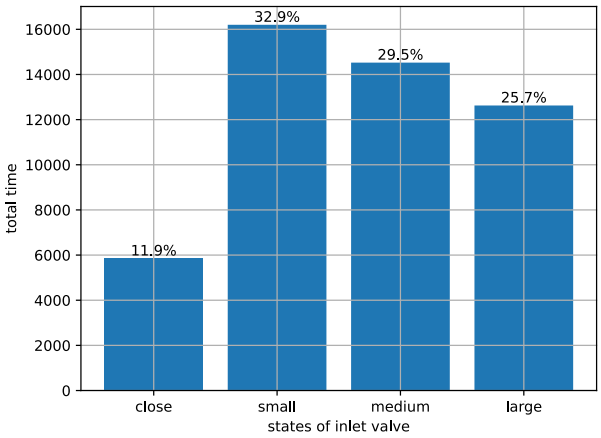

(b) Temperature changes of buffers.

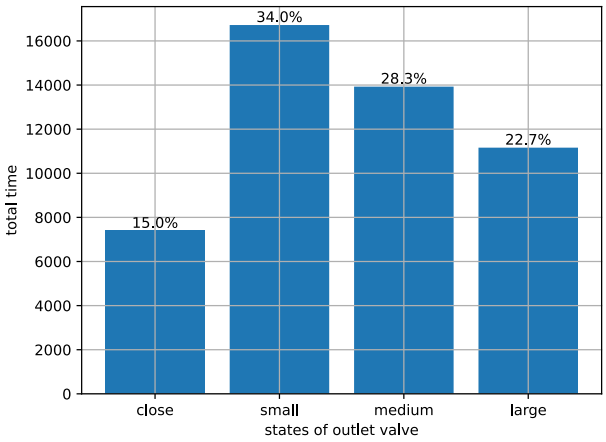

(c) Inlet valve switches buffers.

(d) Outlet valve switches buffers.

Figure 4.7 Simulation in S3 using MINLP 1.

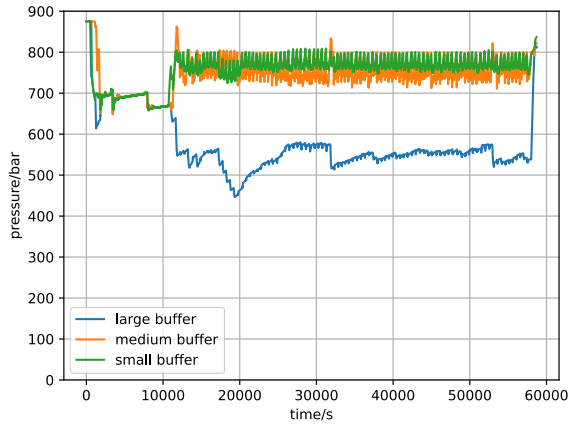

(a) Pressure changes of buffers.

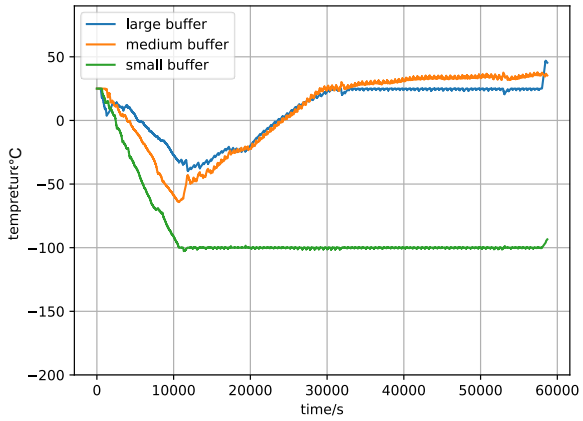

(b) Temperature changes of buffers.

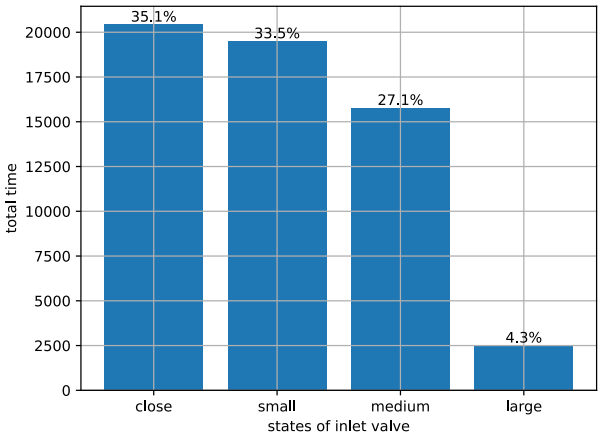

(c) Inlet valve switches buffers.

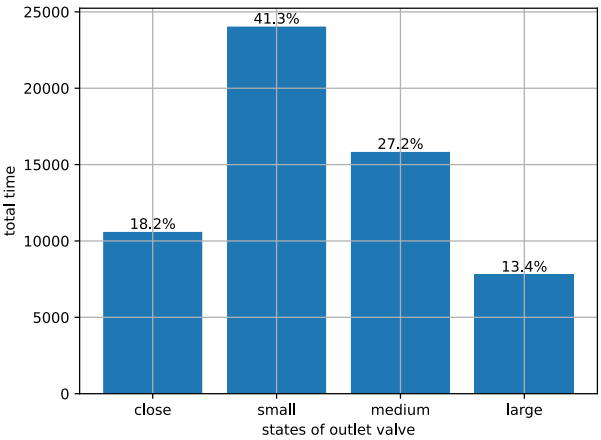

(d) Outlet valve switches buffers.

Figure 4.8 Simulation in S3 using MINLP 2.

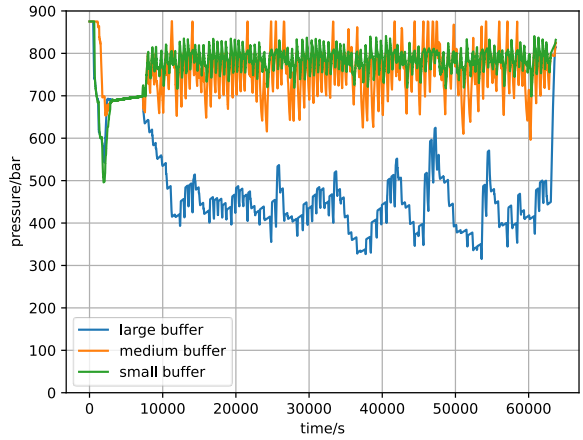

(a) Pressure changes of buffers.

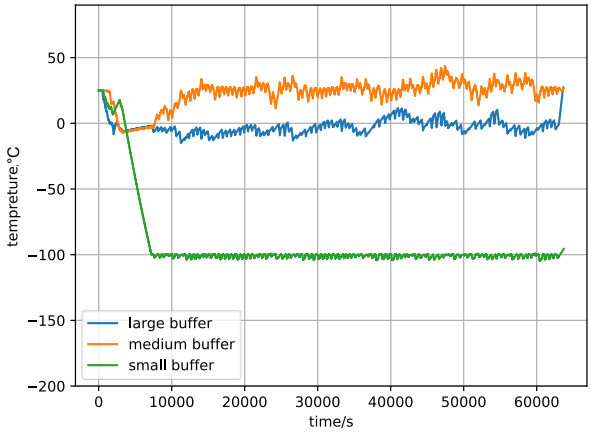

(b) Temperature changes of buffers.

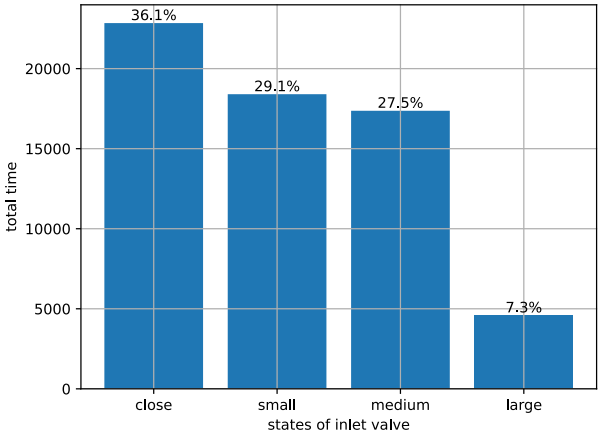

(c) Inlet valve switches buffers.

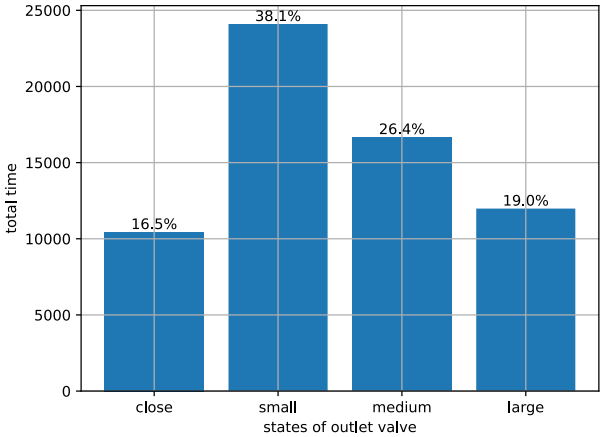

(d) Outlet valve switches buffers.

Figure 4.9 Simulation in S3 using MINLP 3.

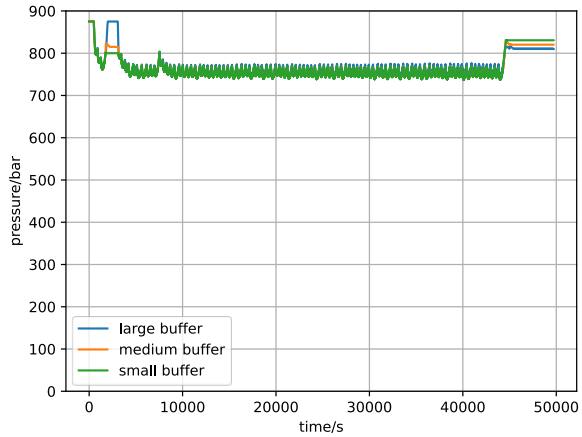

(a) Pressure changes of buffers.

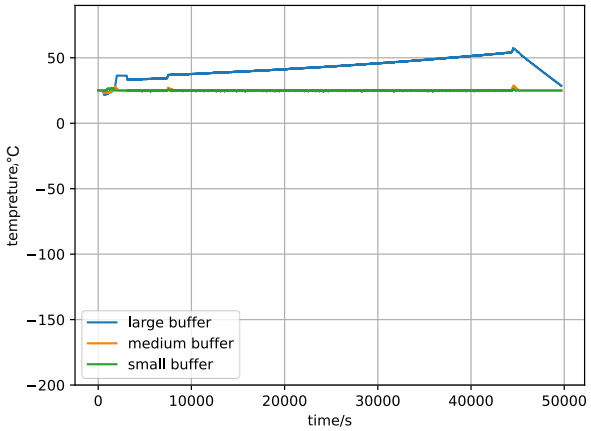

(b) Temperature changes of buffers.

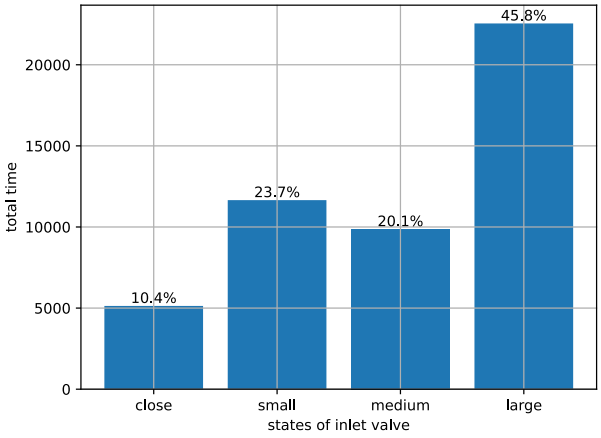

(c) Inlet valve switches buffers.

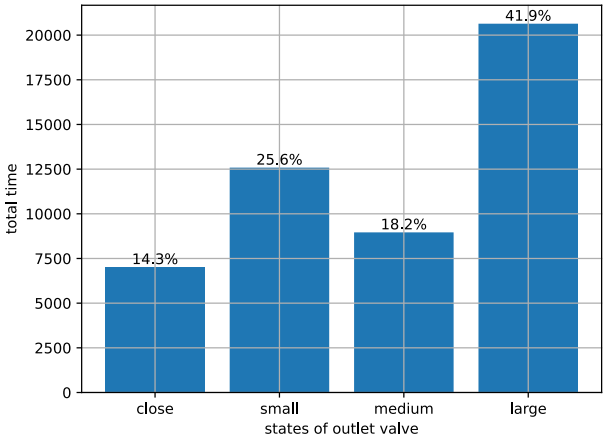

(d) Outlet valve switches buffers.

Figure 4.10 Simulation in S4 using MINLP 1.

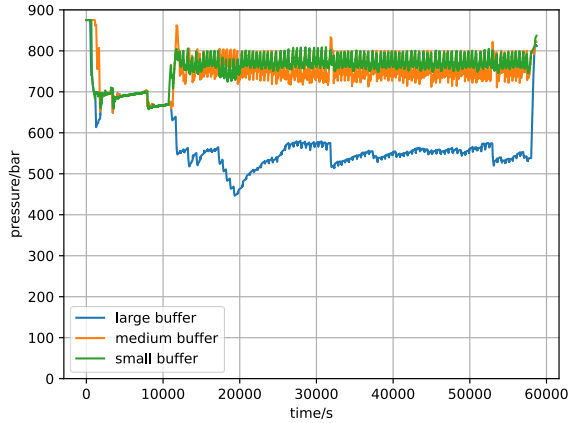

(a) Pressure changes of buffers.

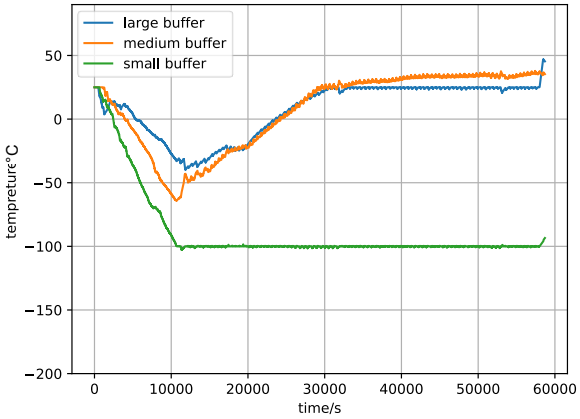

(b) Temperature changes of buffers.

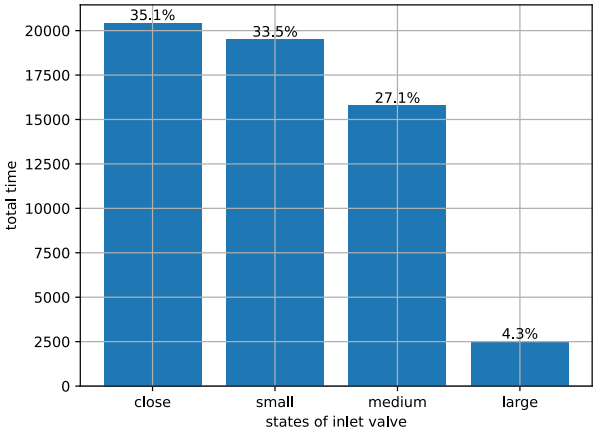

(c) Inlet valve switches buffers.

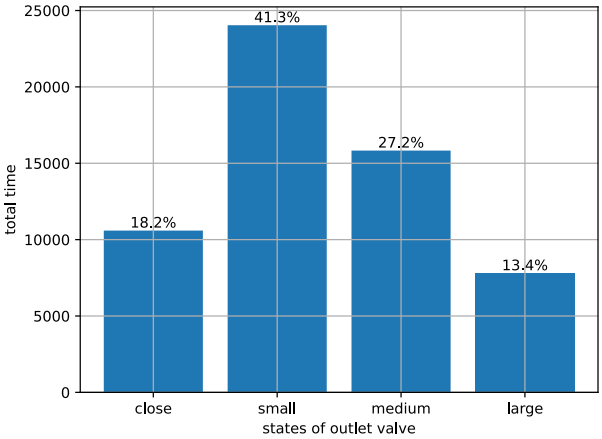

(d) Outlet valve switches buffers.

Figure 4.11 Simulation in S4 using MINLP 2.

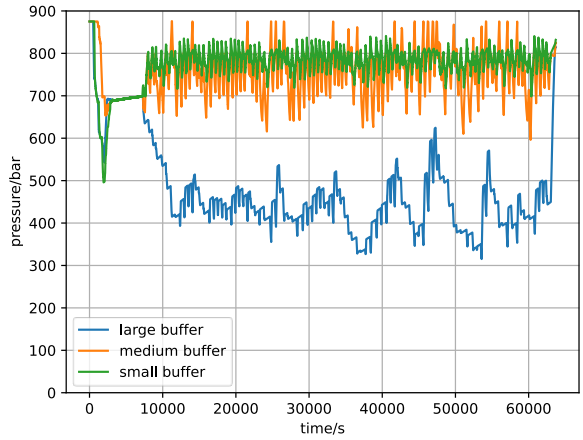

(a) Pressure changes of buffers.

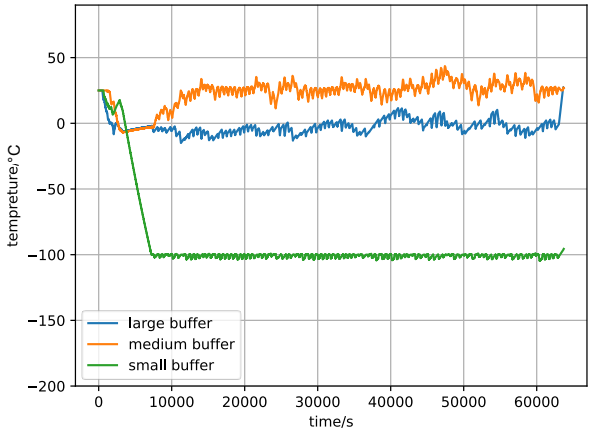

(b) Temperature changes of buffers.

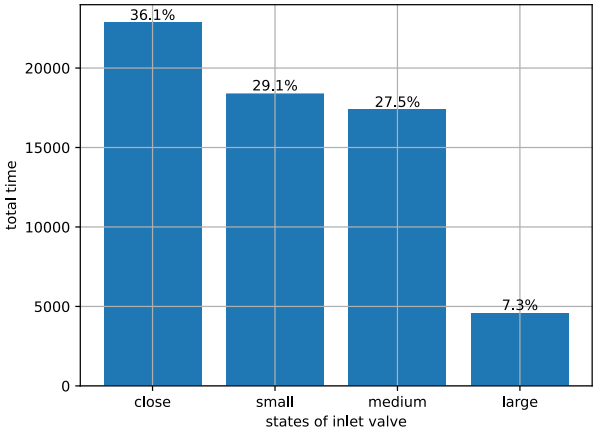

(c) Inlet valve switches buffers.

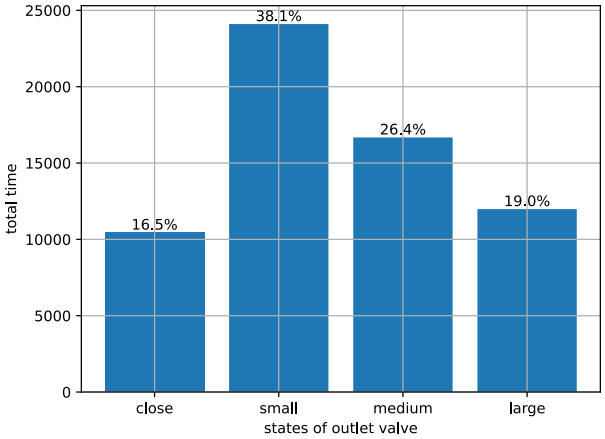

(d) Outlet valve switches buffers.

Figure 4.12 Simulation in S4 using MINLP 3.

The simulation results for scenario S4, as depicted in Figures 4.11, 4.12, and 4.13, exhibit a similar trend. As S4 is a large-scale scenario with a normal distribution, uncertainties in vehicle entry times affect control performance. The pressure and temperature profiles for MINLP 1, MINLP 2, and MINLP 3 in S4 are consistent with those in S3. Additionally, the buffer utilization in subfigures (c) and (d) follows the same pattern observed in S3.

Table 0.3 Performance of controllers under S3 with 96 vehicles.

Scenario		$t_{total}(s)$		$t_{avg}(s)$		$t_{comp}(s)$		$t_{dis}(s)$	
S3	LC-1	36701	\	382	\	40686	\	42876	\
	LC-2	45570	24.16%	472	23.56%	39215	-3.62%	46948	9.50%
	MINLP 1	**4799**	**-86.92%**	**49**	**-87.17%**	43352	6.55%	**41810**	**-2.49%**

	MINLP 2	48239	31.43%	502	31.41%	**37786**	**-7.13%**	47680	11.20%
	MINLP 3	47058	28.22%	490	28.27%	40357	-0.81%	52759	23.05%

Table 0.4 Performance of controllers under S4 with 96 vehicles.

Scenario		$t_{total}(s)$		$t_{avg}(s)$		$t_{comp}(s)$		$t_{dis}(s)$	
S4	LC-1	43212	\	450	\	40560	\	43140	\
	LC-2	46427	7.44%	483	7.33%	38972	-3.92%	45855	6.29%
	MINLP 1	**40021**	**-7.38%**	**416**	**-7.56%**	44068	8.65%	**42184**	**-2.21%**
	MINLP 2	51304	18.73%	534	18.67%	**37786**	**-6.84%**	47680	10.52%
	MINLP 3	48124	11.37%	501	11.33%	40357	-0.50%	52759	22.30%

The simulation results for S3 and S4 are summarized in Table 4.5 and Table 4.6. Under these conditions, MINLP 1 has a shorter refuelling time ($t_{dis}(s)$) for vehicles, while MINLP 2 significantly reduces energy consumption. Therefore, in scenarios with infrequent vehicle presence like S3, it is advised to use the more energy-saving control strategy, MINLP 2.

The results in Table 4.5 and Table 4.6 indicate that MINLP 1 significantly reduces vehicle waiting time but also increases energy consumption. On the other hand, MINLP 2 and MINLP 3 reduce energy consumption but drastically increase both the waiting and refuelling time for vehicles. The simulation results for S3 and S4 are identical under both MINLP 2 and MINLP 3. This is due to the addition of multiple constraints, from 96 vehicles/24h to 96 vehicles/12h, which made the vehicle scheduling in S3 and S4 too dense for both control methods. As a result, all arriving vehicles had to wait regardless of the scenario, preventing any observable distinction between the two methods. This issue could be resolved by adjusting the number of cylinders on each level buffer or reducing the vehicle count in S3/S4 (e.g., from 96 to 48). Such modifications would enable a meaningful comparison of the control performance between the two methods for the vehicle arriving time with different distributions. These topics will be discussed in future work.

In summary, this section presents the simulation results of three optimized control methods of MINLP 1, 2, and 3 across four scenarios (S1-S4) and their comparison with the performance of LC-1 and LC-2. The various MINLP methods facilitate a balance between minimizing customer waiting time and reducing the system energy consumption. In practical control applications, the appropriate controller can be selected based on different vehicle traffic conditions and station requirements. For instance, when vehicles arrive in rapid succession, MINLP 1 can be employed to reduce waiting time. MINLP 2 is better for energy conservation over a long-term low-traffic scenario (S3 & S4), and MINLP 3 is better for energy conservation over a short time

span with high traffic (S1 & S2). Meanwhile, LC-2 may also be a viable alternative in this scenario (S3 & S4).

Energy Consumption Comparison under Four Scenarios

This section presents a quantified comparison of the energy consumption associated with different algorithms proposed in this project. In the optimization algorithms, a weighting ratio of 2:1 between the compressor and precooler is used in the design. However, as previously mentioned, this ratio is adjustable in practical systems. To ensure generality, Table 4.7 also provides energy consumption results based on both 2:1 and 5:1 weighting ratios.

Table 0.5 Energy consumption comparison of different controllers in four scenarios.

Method	S1		S2		S3		S4	
	2: 1	**5: 1**	**2: 1**	**5: 1**	**2: 1**	**5: 1**	**2: 1**	**5: 1**
LC-1	\	\	\	\	\	\	\	\
LC-2	-1.27%	-1.95%	-1.27%	-1.95%	0.91%	-1.33%	-0.37%	-2.12%
MINLP 1	-2.53%	-1.21%	-2.53%	-1.21%	3.43%	4.98%	4.88%	6.74%
MINLP 2	-3.97%	-12.72%	-3.97%	-12.72%	**-0.80%**	**-3.94%**	**-0.81%**	**-3.79%**
MINLP 3	**-5.41%**	**-16.71%**	**-5.41%**	**-16.71%**	7.42%	3.34%	7.41%	3.50%

The results indicate that MINLP 2 and MINLP 3 demonstrate superior performance across different scenarios. In high-traffic conditions, as represented by scenarios S1 and S2, MINLP 3 exhibits a clear advantage over the other four methods. This superiority comes from its ability to simultaneously optimize the energy consumption of all buffers and vehicle refuelling processes. Under high traffic density (S1 and S2), this integrated optimization leads to a more energy-saving operation, effectively minimizing overall energy consumption.

This comparison demonstrates that the MINLP approaches achieve energy savings to a certain extent compared to the LC-1 method. Specifically, the MINLP 2 method consistently outperforms both logic-based control strategies across all scenarios. In contrast, its effectiveness significantly deteriorates in long-duration and low-density scenarios (S3/S4), whereas the MINLP 2 method remains effective under these conditions.

This outcome may be attributed to the fact that in short and high-density cases (S1 and S2), the energy demand (energy density) on the refuelling station is high. As a result, energy

consumption is concentrated, allowing the energy-saving-oriented MINLP 3 method to reduce energy consumption while still meeting demand. However, in long-duration and low-density cases (S3 and S4), the MINLP 3 method’s aggressive approach to shutting off valves for energy savings leads to buffer pressure operating at low levels. This, in turn, increases the operating time of the dispenser, thereby reducing energy efficiency. In such cases, the MINLP 2 method achieves optimal energy performance.

Regarding different vehicle distribution patterns, the current simulation did not yield a systematic conclusion in terms of energy efficiency. Therefore, future work should focus on designing more realistic simulation scenarios to evaluate the controllers' adaptability, particularly their disturbance rejection capability, when handling varying vehicle arrival distributions. Some unresolved issues remain in this experiment. For example, the differences observed between the results of S1/S2 and S3/S4 scenarios require further investigation to determine whether they are caused primarily by simulation duration or vehicle arrival density. Identifying the dominant factor will be an important topic for future work.

Summary

This section introduces an optimal control-based HRS control method, solving the problem that logic control cannot adapt to dynamic conditions and is difficult to achieve optimal performance for multiple objectives. The four essential parts of MINLP, assumptions, variables, constraints, and objective functions, are elaborated in detail. Based on this, the optimal control problem is defined. The simulation results demonstrate that MINLP methods effectively balance energy consumption and vehicle waiting time. If the primary goal is to minimize waiting time and enhance user experience, MINLP 1 is the most effective approach, as it significantly reduces the overall waiting time for all vehicles. However, if energy efficiency is prioritized, MINLP 2 and MINLP 3 are preferable in high-traffic scenarios, as they effectively reduce compressor runtime, thereby extending compressor lifespan. In low-traffic conditions, the benefits of optimal control become less pronounced, and logic control can serve as a fundamental backup to ensure basic system operation.

Comparative Results of Controllers in Real HRSs

To further demonstrate the effectiveness of MINLP, this section compares the performance of above five controllers through the data from the real HRSs. The setup of simulations is presented first. Then, the results and analysis are given, followed by a summary of this section.

Setup

In the simulations of this section, the data from the real HRSs is used as the parameters of HRSC simulator. Meanwhile, all controllers are performed on HRSC simulator to compare the performance.

Specifically, the number of refuelling events from January to June 2023 in HRS-01, HRS-02, HRS-03, and HRS-04 are extracted from the database. Figure 5.1 shows the daily statistics over the past six months, counting the total number of vehicles refueled at each HRS per day. It is evident that stations HRS-01 and HRS-02 are used more frequently, while HRS-03 and HRS-04 are less utilized. Given that differences in controller performance are not obvious and the potential for energy savings is limited during the periods of sparse vehicle visits, the data on March 1st, 2023, in HRS-02 with highest daily vehicle traffic is selected as the basis for simulations. This data ensures that the simulations reflect realistic, high-traffic conditions, allowing for a more accurate assessment of the controllers' effectiveness and the overall system's efficiency during peak usage. Furthermore, this would be more representative of the technology as it grows in popularity.

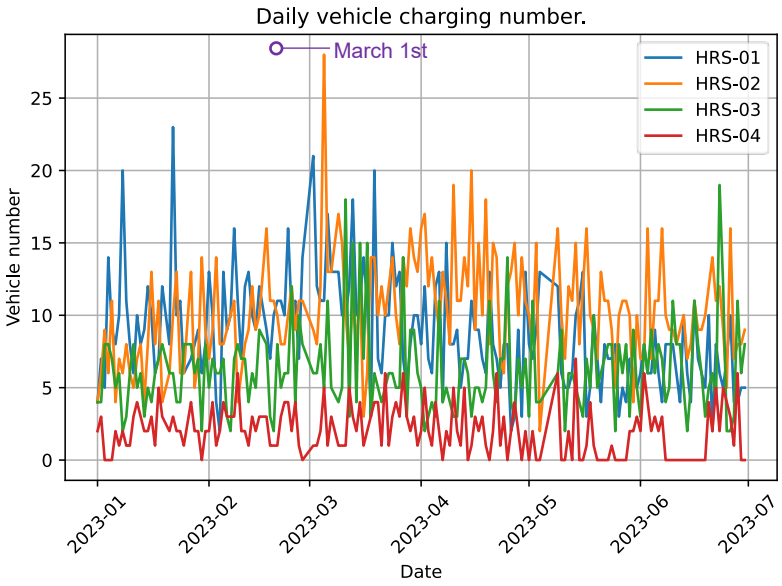

Figure 5.1 HRS-01 utilisation from January 1st to June 30th, 2023.

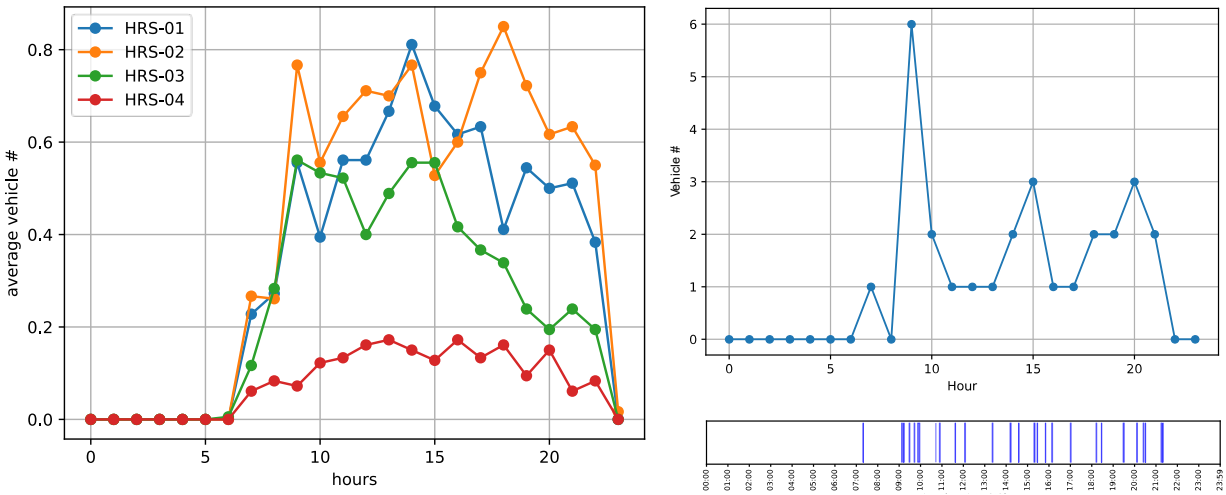

(a) The average number of vehicles per hour over six

(b) The number of vehicles hourly on March 1st, 2023, in

Figure 5.2 The distribution of daily arriving vehicles.

Figure 5.2 shows the distribution of vehicles arriving within 24 hours per day at each HRS. Due to the low vehicle traffic at all HRSs, the hourly distribution of vehicle refuelling times for each day over six months is summarized. Specifically, the total number of vehicles visits per hour for each HRS throughout the half-year period is displayed in Figure 5.2(a). This visualization provides a clear overview of peak and off-peak usage hours, aiding in the evaluation of operational efficiency and the planning of resource allocation. From this figure, it is observable

that for all HRSs, there are vehicles arriving only between 7:00 AM and 10:00 PM daily. The distribution of vehicle visits during this period follows a normal distribution, with a higher frequency of arriving vehicles between 9:00 AM and 6:00 PM. In Figure 5.2(b), the distribution of arriving vehicles within 24 hours at HRS-02 on March 1st, 2023, is presented. There are a total of 28 vehicles that arrived in 10 hours, which is very sparse. It is also evident that the most intense period of arriving vehicles occurred at 9:00 AM, with at least six vehicles arriving at HRS-02 within this hour. Since the database only records the time when vehicles begin refuelling, it cannot exclude the possibility of vehicles waiting and consequently starting their refuelling at 10:00 AM. However, in the simulations, these more complex scenarios are not considered. The arrival times of each vehicle are represented by vertical lines in the lower part of Figure 5.2(b).

Compared to scenarios S3 and S4 in Section 4, where 96 vehicles arrived over 12 hours under a similar daytime simulation setting, the vehicle arrival and departure distribution in this section is significantly sparser. Five control methods were applied to the scenario on March 1st, 2023, at HRS-02, including two logic control and three optimal control methods.

Results and Analysis

In this section, the simulation results and the analysis of the real HRS station condition are presented. Five control methods are applied: LC-1 (Figure 5.3), LC-2 (Figure 5.4), MINLP 1 (Figure 5.5), MINLP 2 (Figure 5.6), and MINLP 3 (Figure 5.7) to the scenario on March 1st 2023, in HRS-02.

By comparing the buffer pressure profiles in MINLP 1, MINLP 2, and MINLP 3 (see subfigure (a)), it can be observed that the buffer pressure occasionally exhibits unexpectedly high values above 800 bars. This phenomenon can be attributed to two distinct scenarios. First, during pressure decrease, the buffer pressure may drop and then stabilize at an elevated level slightly above 800 bars. This is due to a system constraint: The compressor cannot be activated until the buffer pressure falls below 800 bars. As a result, the pressure may remain constant at an elevated level just above 800 bars. Second, during pressure increase, the system is designed to stop replenishment only when the pressure reaches 875 bars. However, the MINLP algorithm determines which buffer to replenish based on the optimization outcome and may switch between buffers in a non-sequential manner. As a result, it is possible that one buffer is partially replenished to a pressure above 800 bars but below 875 bars. At this point, the algorithm might switch to replenishing another buffer, leaving the previous one at a high pressure. Even if the algorithm returns to this buffer later, it will no longer be selected for replenishment because its pressure is already above 800 bars.

Comparing Figures 5.3(a), (b) and Figures 5.4(a), (b), it can be observed that the LC-1 method relies more on the LB, while LC-2 has a balanced usage among three buffers. This observation is quantitatively confirmed in subfigures (c) and (d). However, even with LC-2's more balanced distribution, the LB still maintains a higher utilization frequency compared to the other buffers.

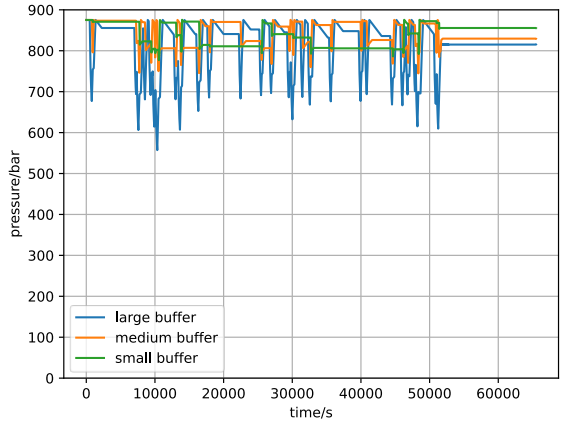

(a) Pressure changes of buffers.

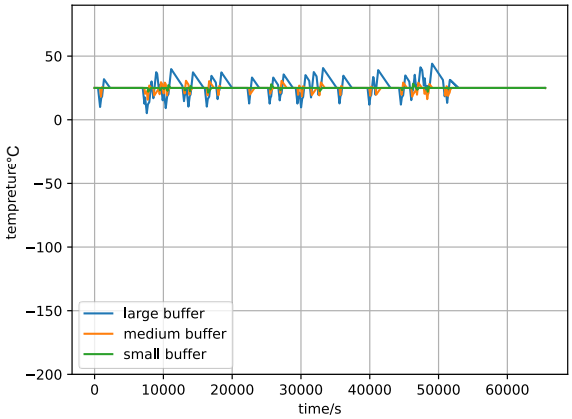

(b) Temperature changes of buffers.

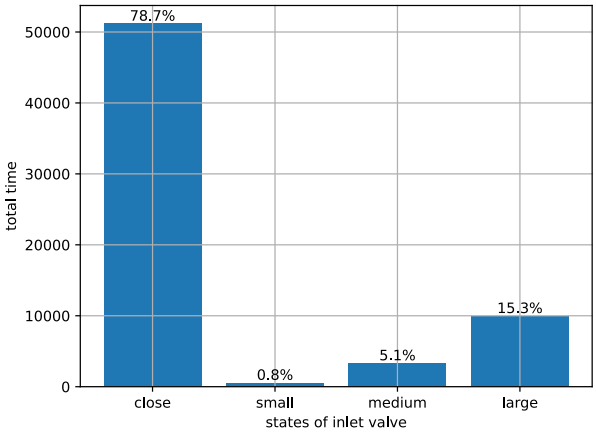

(c) Inlet valve switches buffers.

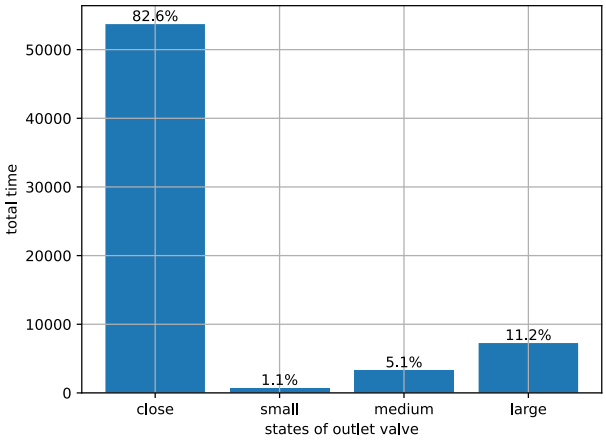

(d) Outlet valve switches buffers.

Figure 5.1 Simulation results for LC-1 controller on March 1st, 2023, in HRS-02.

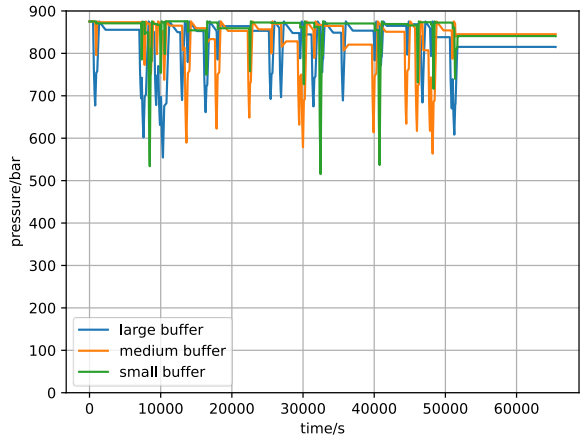

(a) Pressure changes of buffers.

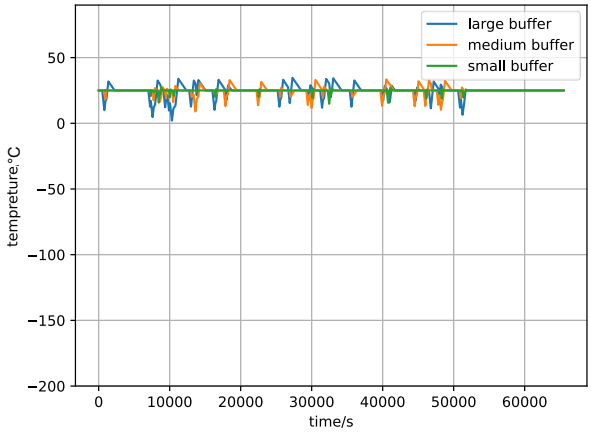

(b) Temperature changes of buffers.

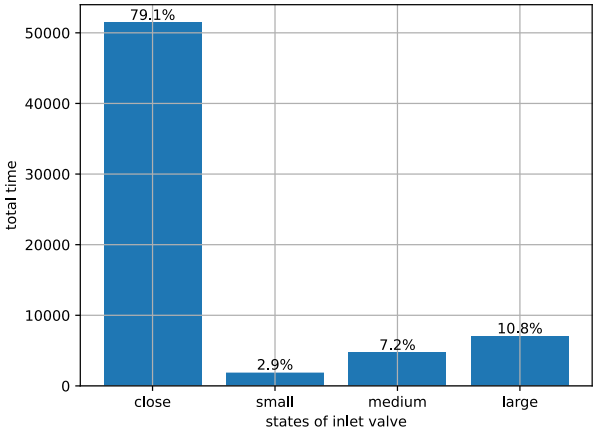

(c) Inlet valve switches buffers.

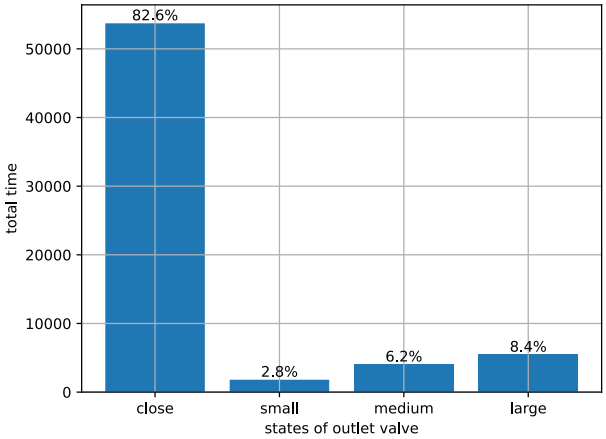

(d) Outlet valve switches buffers.

Figure 5.2 Simulation results for LC-2 controller on March 1st, 2023, in HRS-02.

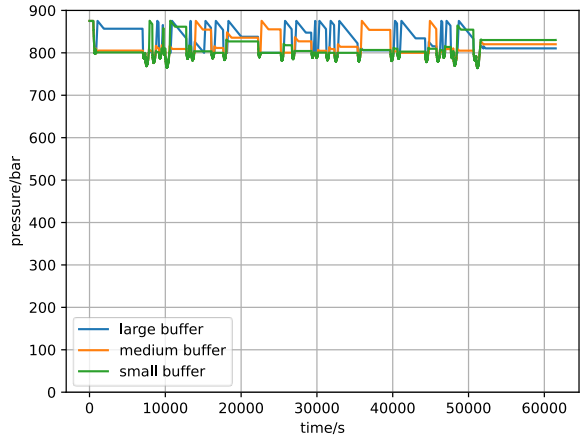

(a) Pressure changes of buffers.

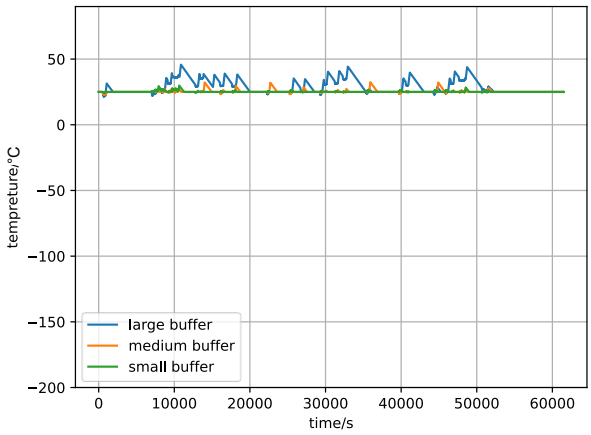

(b) Temperature changes of buffers.

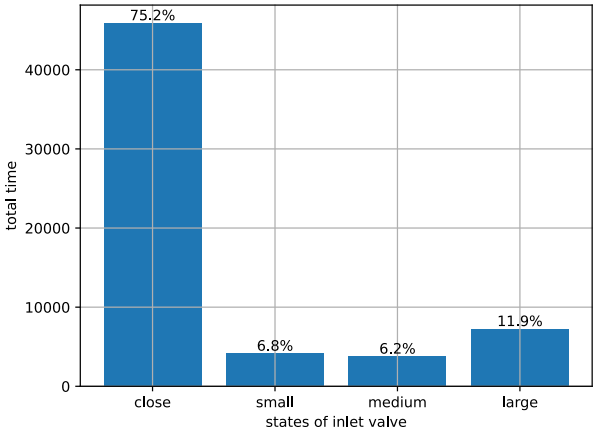

(c) Inlet valve switches buffers.

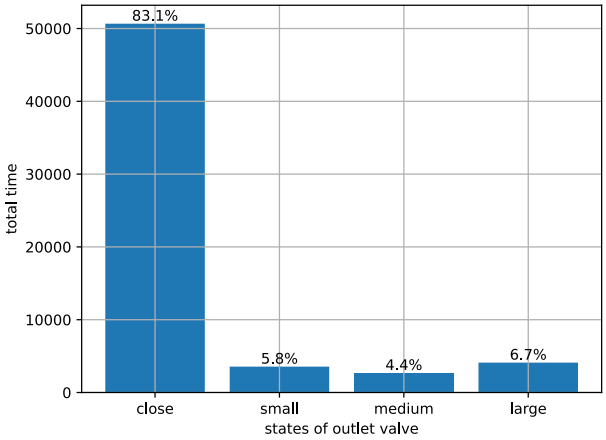

(d) Outlet valve switches buffers.

Figure 5.3 Simulation results for MINLP 1 controller on March 1st, 2023, in HRS-02.

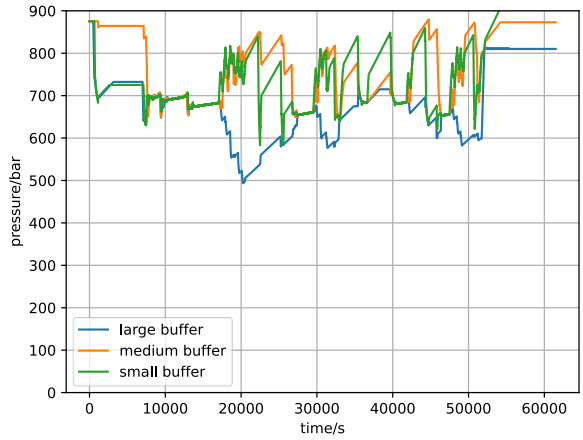

(a) Pressure changes of buffers.

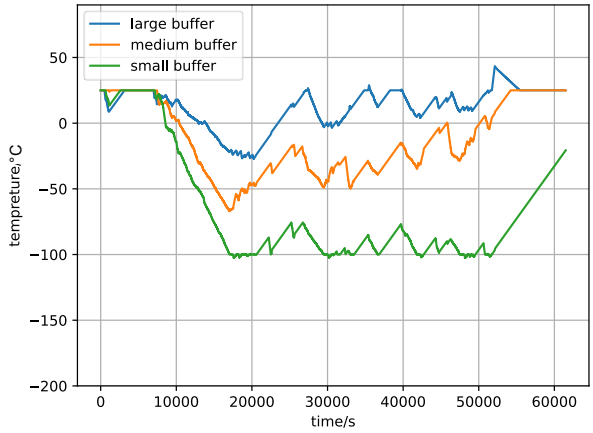

(b) Temperature changes of buffers.

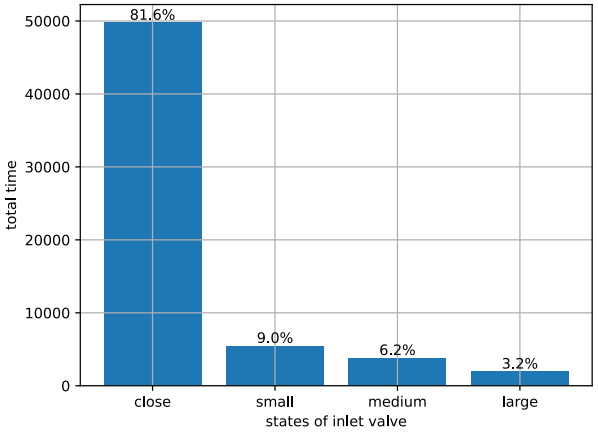

(c) Inlet valve switches buffers.

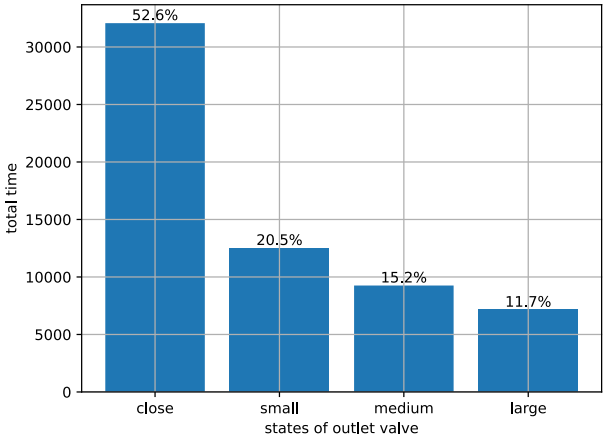

(d) Outlet valve switches buffers.

Figure 5.4 Simulation results for MINLP 2 controller on March 1st, 2023, in HRS-02.

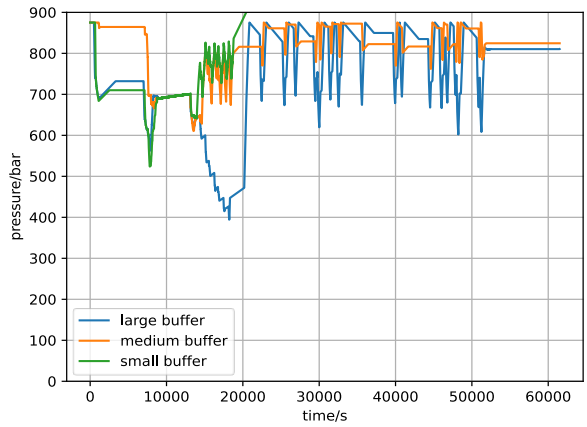

(a) Pressure changes of buffers.

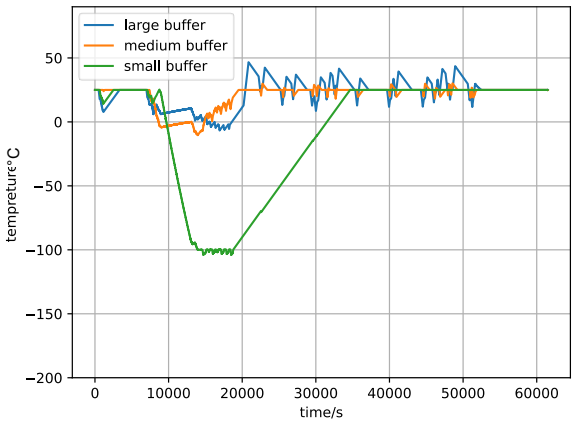

(b) Temperature changes of buffers.

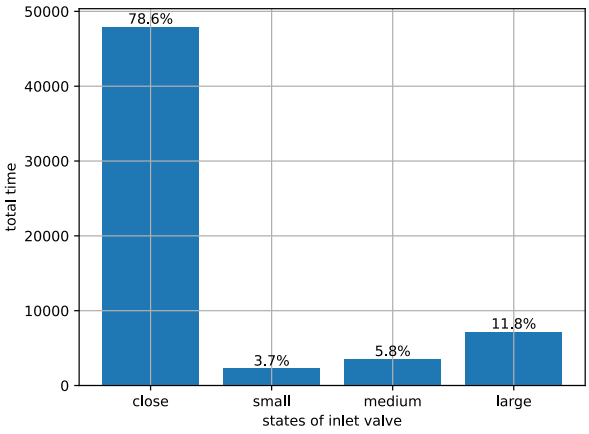

(c) Inlet valve switches buffers.

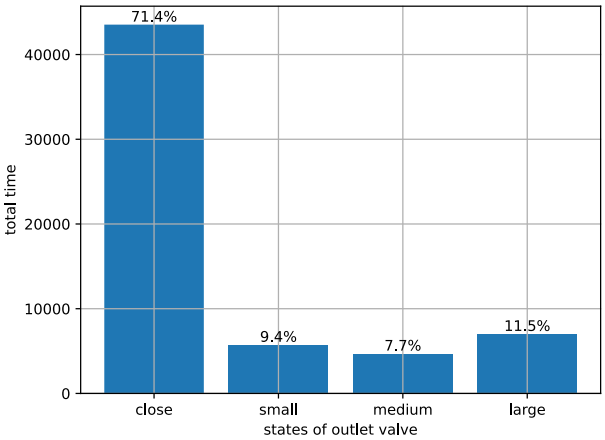

(d) Outlet valve switches buffers.

Figure 5.5 Simulation results for MINLP 3 controller on March 1st, 2023, in HRS-02.

Comparing subfigures (a) and (b) from Figure 5.3 to Figure 5.7, it is evident that MINLP 1 maintains the most stable and highest buffer pressure, leading to high efficiency in vehicle refuelling and reduced waiting times. However, this performance comes at the cost of higher energy consumption compared to all other controllers. Observing the subfigures (c) and (d) among them, it is evident that different controller has different preferences for using buffers.

Moreover, from the observation of the pressure changes in Figure 5.7 (a), the small buffer is out of utilization after around 2000s. This is because in this simulator, the threshold of pressure is set to be under 875 bars ($p_{buffer} \leq 875\ \text{bar}$) as a constraint for the optimization algorithm. However, for MINLP 3 in HRS-02, the pressure buffer does increase beyond 875 bars because of the environmental heating exchange. As a result of this constraint violation, the small buffer is not used for the remainder of the simulation, and the potential energy gains from the thermal exchange with the environment are lost. This flaw should be revised in the future version of the simulator.

Although this simulation selected the busiest operational scenario among the four refuelling stations (HRS01-04), the vehicle arrival density (28 vehicles/10h) remains significantly lower compared to the four scenarios in Section 3 (96 vehicles/12h). This sparse vehicle distribution pattern fundamentally alters the system dynamics, leading to divergent simulation results from those presented in Section 4. The statistical simulation results of five controllers are summarized in Table 5.1.

The result of LC-1 is used as the baseline, as it represents the control strategy utilized in most HRSs. In comparison to LC-1, LC-2 reduces vehicle waiting time and energy consumption a little bit, which has the best performance among them in the sparse condition.

Table 0.1 Performance of controllers under real-world conditions.

	$t_{total}(s)$		$t_{avg}(s)$		$t_{comp}(s)$		$t_{dis}(s)$		Energy consumption 2:1	Energy consumption 5:1
LC-1	499	/	17.8	/	13823	/	11283	/		
LC-2	491	-1.6%	17.5	-1.7%	13587	-1.7%	11279	-0.04%	**-1.23%**	**-1.47%**
MINLP 1	**392**	**-21.4%**	**14**	**-21.3%**	15118	9.3%	**10338**	**-8.4%**	4.22%	6.87%
MINLP 2	1724	245.4%	61.5	245.5%	**11235**	**-18.7%**	28929	156.4%	32.0%	5.85%
MINLP 3	996	99.6%	33.5	88.2%	13039	-5.6%	17471	54.8%	11.86%	2.82%

The MINLP 1 method reduces waiting time but increases overall system energy consumption. However, in this simulation's sparse vehicle distribution scenario (with long inter-arrival intervals), all methods demonstrate small waiting times (all less than 1 minute on average for each vehicle), diminishing MINLP 1's relative advantage. While MINLP 2 and MINLP 3 can moderately reduce compressor runtime, they proportionally extend dispenser operation duration. Although MINLP 2 and MINLP 3 can moderately reduce compressor running time, they proportionally extend dispenser operation duration. While compressors bear significantly higher weighting in actual systems, both MINLP approaches demonstrate higher total energy consumption than the LC-2 method when considering comprehensive energy consumption, as shown in Table 5.1. Consequently, under HRS-02 scenarios, LC-2 proves to be the superior choice.

Consequently, LC-2 emerges as a more rational control strategy for scenarios with sparse vehicle distributions. When vehicle density is low, as shown in our 28 vehicles/10 h case, the differences in vehicle waiting times become negligible. Under these conditions, LC-2 ensures full refuelling of buffers between refuelling events, enabling efficient service for each vehicle. However, MINLP 2 and MINLP 3 avoid full refuelling of idle buffers even when time permits

since they prioritize reducing compressor runtime. This results in longer operating durations for dispensers under MINLP control, particularly in sparse traffic scenarios. Therefore, LC-2 achieves comparable service quality without the energy trade-offs characteristic of MINLP approaches, which makes it more practical for low-traffic conditions.

Summary

This section shows simulation results based on data from real HRSs, demonstrating the effectiveness of the designed optimal controller. The station utilization rates for the four HRSs from January to June 2023 are first analyzed, from which the data used for simulation are selected. After that, two logic controllers and three MINLP controllers are compared in the HRSC simulator. Based on the simulation results, the characteristics of each controller are analyzed, and recommendations are provided to optimize both energy efficiency and refuelling performance.

Conclusion and Future Work

In this project, the goal is to drive the transition to hydrogen-powered transport by controlling HRSs, thereby reducing carbon emissions. Through the analysis of the key components of HRSs and the challenges they face, the importance of advanced modelling and optimization techniques to improve refuelling efficiency and reduce operating costs is highlighted. Therefore, the goal of the project is to develop a customized simulator for HRSs, testing and evaluating different control methods, and designing an optimal controller to optimize energy consumption.

Section 2 introduces the HRSC simulator, focusing on its design and validation. It first reviews two existing HRS simulators: a general HRS simulator and H2FillS, both developed in MATLAB. The HRSC simulator, developed in Python, is then presented with its modular design, offering features such as offline data processing, hardware simulation, and a flexible environment for testing control methods. The section also includes a comparison between the HRSC simulator and the existing simulators, demonstrating its effectiveness in replicating real-world HRS dynamics while providing greater flexibility and scalability.

Section 3 validates the HRSC simulator by comparing two control methods: LC-1 and LC-2. These methods are tested under four scenarios with varying vehicle arrival patterns, assessing their performance in buffer utilization, energy consumption, and overall system efficiency. LC-1 fuels buffers in a fixed priority order, while LC-2 adjusts the fuelling sequence based on buffer pressures. The simulation results demonstrate that the HRSC simulator can effectively be used to test and compare different control methods, confirming its adaptability in evaluating various methods for optimizing HRS operations.

Section 4 introduces the optimal control method MINLP for HRSs, achieving a balance between energy consumption and waiting time. This study formulates the optimal control problem by defining key components, including assumptions, variables, constraints, and objective functions. Simulation results demonstrate that MINLP 1 minimizes overall vehicle waiting time, making it the best choice for enhancing user experience. In high-traffic scenarios, MINLP 2 and MINLP 3 effectively reduce compressor runtime, extending its lifespan. However, in low-traffic conditions, the advantages of optimal control diminish, and logic control can serve as a reliable alternative to ensure stable system operation.

Section 5 evaluates five controllers (LC-1, LC-2, MINLP 1, MINLP 2, and MINLP 3) using real-world data from four hydrogen refuelling stations. Simulations based on peak usage data from HRS-02 reveal that LC-2 balances buffer utilization and slightly reduces waiting times, while

MINLP 1 minimizes waiting times at a high energy cost. MINLP 2 and MINLP 3 save compressor runtime but lead to longer waiting times. Since the simulation environment represents a sparse traffic scenario with noticeable gaps between vehicle arrivals, especially compared to S3 and S4 (yet representative of “high” traffic at a real HRS), the findings reinforce the conclusion in Section 4. In low-traffic conditions, LC-2 is recommended as an alternative strategy, as the benefits of optimal control strategy may be less significant.

Based on the characteristics of all methods, these control strategies can be selected according to different vehicle traffic patterns and specific station requirements. For instance, MINLP 1 is well-suited for scenarios with a sudden surge in vehicle arrivals, as it effectively minimizes waiting times. If energy efficiency is the primary objective for HRS management, MINLP 2 and MINLP 3 are more appropriate for high-traffic conditions, as they optimize the balance between vehicle refuelling and compressor operation. In low-traffic scenarios, LC-2 is recommended as an alternative strategy to ensure basic control effectiveness.

In the future, this project can be further improved and enhanced in the following aspects.

- For HRSC simulator, the mathematical model of HRSs can be further refined to include thermodynamic processes of gases and other aspects that have been overlooked.
- For MINLP, accuracy can be improved by extending the prediction horizon to optimize for multiple future steps. In this project, due to limited computational power, predictions are only made for the one step ahead. Therefore, there is room for enhancing the performance of the optimization control.
- The traffic flow can be predicted based on historical data, including the distribution of vehicles for different HRSs at various time. This will allow for the selection of appropriate control strategies, achieving the best energy-saving effects and user experience.
- In future work or practical applications, if the hardware system imposes a specific limit on the control frequency, constraints can be incorporated to regulate the switching frequency. If reducing the control frequency is necessary to minimize system wear, this can be achieved by modifying the optimization objective function—such as adding a penalty term for switching frequency in the objective function of the optimal control algorithm. Therefore, this issue has also been included in our future research agenda.
- After the compressor stops operating, the natural temperature recovery in the buffer tank leads to a pressure increase beyond 900 bars. To address this, future research could explore adaptive control strategies that dynamically adjust the maximum refuelling pressure based on real-time buffer temperature measurements.
- In the future, increasing and adjusting the settings of the simulation scenarios, such as evaluating the relationship between the number of vehicles, interval times, and buffer capacities, could be beneficial to better compare the effects of various control algorithms.

References

[1] J.-Q. Li, Y. Chen, Y. B. Ma, J.-T. Kwon, H. Xu, and J.-C. Li, “A study on the Joule-Thomson effect of during filling hydrogen in high pressure tank,” *Case Studies in Thermal Engineering*, vol. 41, p. 102678, Jan. 2023, doi: 10.1016/j.csite.2022.102678.

[2] K. Reddi, A. Elgowainy, N. Rustagi, and E. Gupta, “Impact of hydrogen SAE J2601 fueling methods on fueling time of light-duty fuel cell electric vehicles,” *International Journal of Hydrogen Energy*, vol. 42, no. 26, pp. 16675–16685, June 2017, doi: 10.1016/j.ijhydene.2017.04.233.

[3] M. Genovese and P. Fragiacomo, “Hydrogen refueling station: Overview of the technological status and research enhancement,” *Journal of Energy Storage*, vol. 61, p. 106758, May 2023, doi: 10.1016/j.est.2023.106758.

[4] Society of Automotive Engineers, “Fueling Protocols for Light Duty Gaseous Hydrogen Surface Vehicles (SAE J2601).” SAE International, 2016.

[5] MATLAB, “Hydrogen Refueling Station.” Accessed: Mar. 27, 2025. [Online]. Available: https://www.mathworks.com/help/hydro/ug/hydrogen-refueling-station.html

[6] “Stateflow.” Accessed: May 14, 2024. [Online]. Available: https://www.mathworks.com/products/stateflow.html

[7] T. Kuroki *et al.*, “Thermodynamic modeling of hydrogen fueling process from high-pressure storage tank to vehicle tank,” *International Journal of Hydrogen Energy*, vol. 46, no. 42, pp. 22004–22017, June 2021, doi: 10.1016/j.ijhydene.2021.04.037.

[8] HTEC, “Powercube H2 Distribution System.” Accessed: Mar. 27, 2025. [Online]. Available: https://www.htec.ca/wp-content/uploads/2021/09/HTEC_FactSheet4_POWERCUBE_F.pdf

[9] T. Q. Hua, H.-S. Roh, and R. K. Ahluwalia, “Performance assessment of 700-bar compressed hydrogen storage for light duty fuel cell vehicles,” *International Journal of Hydrogen Energy*, vol. 42, no. 40, pp. 25121–25129, Oct. 2017, doi: 10.1016/j.ijhydene.2017.08.123.

[10] Z. Xu, W. Dong, K. Yang, Y. Zhao, and G. He, “Development of efficient hydrogen refueling station by process optimization and control,” *International Journal of Hydrogen Energy*, vol. 47, no. 56, pp. 23721–23730, July 2022, doi: 10.1016/j.ijhydene.2022.05.158.

[11] M. Li *et al.*, “Experimental and numerical study of the temperature evolution in hydrogen cylinder under fast-refueling process,” *International Journal of Heat and Mass Transfer*, vol. 211, p. 124220, Sept. 2023, doi: 10.1016/j.ijheatmasstransfer.2023.124220.

[12] A. Elgowainy, K. Reddi, E. Sutherland, and F. Joseck, “Tube-trailer consolidation strategy for reducing hydrogen refueling station costs,” *International Journal of Hydrogen Energy*, vol. 39, no. 35, pp. 20197–20206, Dec. 2014, doi: 10.1016/j.ijhydene.2014.10.030.